UNIVERSITY OF HAMBURG

DOCTORAL THESIS

Mass Spectrometry Performed Under Ultrafast Stress-Confinement Conditions

Cornelius L. PIETERSE

Cumulative dissertation submitted in partial fulfillment of the requirements for the degree of Doctor of Philosophy at the

Faculty of Mathematics, Informatics and Natural Sciences
Department of Physics at University of Hamburg

May 2018

Cornelius L. PIETERSE
Mass Spectrometry Performed Under Ultrafast Stress-Confinement Conditions

Gutachter der Dissertation:
Prof. Dr. R.J. Dwayne Miller
Prof. Dr. Arwen Pearson

Zusammensetzung der Prüfungskommission:
Prof. Dr. R.J. Dwayne Miller
Prof. Dr. Arwen Pearson
Prof. Dr. Daniela Pfannkuche
Prof. Dr. Robert Blick
Dr. Sadia Bari

Vorsitzender der Prüfungskommission:
Prof. Dr. Daniela Pfannkuche

Datum der Disputation:
16 Juli 2018

Vorsitzender Fach-Promotionsausschusses PHYSIK:
Prof. Dr. Wolfgang Hansen

Leiter des Fachbereichs PHYSIK:
Prof. Dr. Michael Potthoff

Dekander Fakultät MIN:
Prof. Dr. Heinrich Graener

*"It is my ambition to say in ten sentences what everyone else says in a whole book — what everyone else does **not** say in a whole book."*

Friedrich Nietzsche

Declaration of Authorship

I, Cornelius L. PIETERSE, declare that this thesis and the work presented in it are my own. I confirm that:

- This work was done wholly or mainly while in candidature for a research degree at this University.

- Where I have consulted the published work of others, this is always clearly attributed.

- I have acknowledged all main sources of help.

- Where the thesis is based on work done by myself jointly with others, I have made clear what was done by others and what I have contributed.

Signed:

_____

Date:

_____

Hiermit versichere ich an Eides statt, die vorliegende Dissertationsschrift selbst verfasst und keine anderen als die angegebenen Hilfsmittel und Quellen benutzt zu haben.

Signed:

_____

Date:

_____

UNIVERSITY OF HAMBURG

Abstract

Faculty of Mathematics, Informatics and Natural Sciences
Department of Physics

Doctor of Philosophy

Mass Spectrometry Performed Under Ultrafast Stress-Confinement Conditions

by Cornelius L. PIETERSE

The subject of this dissertation was to demonstrate the advantages of performing mass spectrometry measurements under the conditions of stress-confinement. To be in a position to discuss such measurements, there was the need to develop a high-performance time-of-flight mass spectrometer in-house, since commercially available instruments do not allow the scientist the freedom to adequately study the underlying physical mechanisms. Furthermore, due to the high complexity of the datasets generated by these studies, there was a definite need for novel data analysis routines to improve the quality of the available information.

Laser desorption mass spectrometry is an established, but not yet adequately quantitative analytical technique. One of the primary reasons for this unfortunate limitation is because the desorption and ionisation processes are highly coupled. Consequently, this does not allow the ionisation efficiency to be varied without varying the amount of material desorbed and vice versa. The only way to get past this inherent deadlock is to separate these two processes. Interestingly, molecular dynamics simulations have suggested that when performing mass spectrometry measurements under stress-confinement conditions the desorption and ionisation processes would become separable. It is for this reason why there was a basic need to understand the desorption and ionisation mechanisms under these conditions since an appropriate understanding could potentially facilitate laser desorption mass spectrometry to become more quantitative.

Within this thesis, it has been established that there are numerous advantages to performing mass spectrometry studies under conditions of stress-confinement. The practicality of this concept was demonstrated both at atmospheric conditions by using a picosecond infrared laser for studying bulk water samples and under high-vacuum by utilising a femtosecond ultraviolet laser with standard matrices. The atmospheric studies indicated that the infrared laser produces mass spectra which qualitatively compares well to that of electrospray ionisation, but enjoyed the benefits of laser control. Importantly, it was shown that no source of secondary ionisation is required. To my knowledge, the vacuum experiments demonstrated for the first time that desorption and ionisation processes are separable with the application of ultrashort pulses. This observation was made by studying survival yields (intensity of the fragment ions relative to a parent ion) of thermometer ions for a range of laser pulse energies. Moreover, a Bayesian deconvolution algorithm was developed to improve the quantification of these fragmentation channels. By decoupling the desorption and ionisation processes, I believe that laser desorption mass spectrometry measurements can genuinely be made quantitative.

UNIVERSITÄT HAMBURG

Zusammenfassung

Fakultät für Mathematik, Informatik und Naturwissenschaften
Fachbereich Physik

Doktor der Naturwissenschaften

Das Thema vorliegender Dissertation war die Durchführung von Massenspektrometrie-Messungen im Hinblick auf die Analyse der vorteilhaften Bedingungen des sogenanten "stress-confinement". Hierfür war es nötig eine leistungsstarkes Massenspektrometer zu konstruieren und in Betrieb zu nehmen, da kommerziell verfügbare Instrumente den Blick auf die zugrunde liegenden Mechanismen erschweren. Auf Grund der hohen Komplexität der generierten Datensätze gab es Bedarf an neuartigen Auswertungsansätzen, um die Qualität der extrahierbaren Informationen zu verbessern.

Die Laserdesorption-Massenspektrometrie ist zwar eine etablierte, jedoch noch nicht vollständig quantitative Analysetechnik. Einer der Hauptgründe für diese Begrenzung liegt darin, dass die Desorptions- und Ionisationsprozesse stark gekoppelt sind. Dies führt dazu, dass die Ionisationseffizienz nicht unabhängig von der Menge des desertierten Materials variiert werden kann und umgekehrt. Um diese Begrenzung zu überwinden müssen die beiden Prozesse getrennt werden. Molekulare Dynamiksimulationen haben gezeigt, dass bei der Durchführung von Massenspektrometrie unter "stress-confinement" Bedingungen die Prozesse trennbar werden. Aus diesem Grund ist ein Verständnis um die Desorptions- und Ionisationsprozesse unter diesen speziellen Bedingungen von großer Bedeutung, da unter Umständen der Schritt zu einem qualitativen Verfahren möglich wird. Im Rahmen dieser Arbeit wurde festgestellt, dass es zahlreiche Vorteile massenspektrometrische Untersuchungen unter "stress-confinement" Bedingungen durchzuführen. Die Praxistauglichkeit dieses Konzepts wurde sowohl bei atmosphärischen Bedingungen, unter Einsatz eines Pikosekunden-Infrarotlasers zur Untersuchung wässriger Proben, als auch unter Hochvakuum bei gleichzeitigem Einsatz eines ultravioletten Femtosekunden-Lasers appliziert auf Standardmatrizen, validiert.

Die atmosphärischen Studien zeigten ferner, dass sich die Massenspektren mittels Infrarotlaser qualitativ gut mit jenen der Elektrospray-Ionisation vergleichen lassen, jedoch ist die verbesserte experimentelle Kontrolle der Ionisation mittels Laser von Vorteil. Bei diesem Verfahren ist also keine sekundäre Ionisation mehr erforderlich. Meiner Kenntnis nach konnten die Vakuumexperimente erstmals zeigen, dass Desorptions- und Ionisationsprozesse unter Anwendung von ultrakurzen Laserpulsen voneinander trennbar sind. Diese Beobachtung konnte durch die Analyse der Ausbeuten (Intensität der Fragment-Ionen relativ zu einem Hauption) von Thermometer-Ionen für eine Reihe von Laserpulsenergien gemacht werden. Schließlich ist ein Bayesscher Entfaltungsalgorithmus entwickelt worden, um die Quantifizierung der vorhandenen Fragmentierungskanäle zu verbessern. Über die Entkopplung der Desorptions- und Ionisationsprozesse wird die Laserdesorption-Massenspektrometrie letztlich, so scheint es, quantitativ durchführbar.

Contributions

In this section, I list my contributions with regards to developing the presented instrumentation and deduced results. The section is concluded with a list of the papers which were written as a result of this research and, therefore, represents the core of this cumulative dissertation.

Atmospheric investigations

The atmospheric investigations were part of the research project of my co-worker Yinfei Lu. She was responsible for leading this project, while I was collaborating closely with her. My main contributions were with regards to the sampling conditions and the interpretation of the ionisation mechanisms. Further contributions from myself included programming of the control software and synchronisation of the beam delivery for the chip measurements.

Vacuum investigations

The vacuum instrumentation development formed part of my primary research projects. I was responsible for leading these projects. It was entirely my concept to employ femtosecond, ultraviolet pulses to study the desorption process using the thermometer probe ions. I, together with a set of co-workers, commissioned and tested the vast majority of the individual components, followed by the associated characterisation and optimisation. My primary responsibilities were the electrical and electronic components, such as the implementation and characterisation of the high-voltage systems and ion detection schemes. Another student and myself contributed equally to the laser beam delivery and beam characterisation.

Bayesian data analysis

The development of a novel Bayesian data analysis framework was my secondary research project. I took the initiative to develop and characterise this data analysis framework to improve the quantification of our time-of-flight mass spectra. In order to realise this project, the collaboration with the University of Stellenbosch was initiated and maintained by myself.

I performed both the initial literature reviews and conceptual brainstorming, having the aim of increasing quantification of these low-resolution mass spectra. Michiel de Kock was integral to the development of the deconvolution algorithm, as he was responsible for the lengthy mathematical derivations. It was my main responsibility for implementing this algorithm within the data analysis pipeline (which I have also developed) while assisting Michiel in improving the algorithm further. In addition, after the algorithm was successfully implemented and tested, I was responsible for analysing and interpreting the experimental data.

Soft Picosecond Infrared Laser Extraction of Highly Charged Proteins and Peptides from Bulk Liquid Water for Mass Spectrometry

Yinfei Lu, <u>Cornelius L. Pieterse</u>, Wesley D. Robertson, and R. J. Dwayne Miller
Analytical Chemistry, **90**(7), 4422–4428 (2018)

Yinfei Lu and I conducted the experiments. Yinfei processed and analysed the data. I performed the initial literature reviews regarding the sampling conditions and ionisation mechanisms. Yinfei prepared the initial manuscript and all other co-authors provided suggestions and proof-reading to finalise the manuscript.

Direct Laser Sampling of Aqueous Solutions from Lab-on-a-Chip Devices for Mass Spectrometry

Yinfei Lu, <u>Cornelius L. Pieterse</u>, Dennis Eggert, Candice Ip, Frederik Busse, Sercan Keskin, Wesley D. Robertson, and R. J. Dwayne Miller
Under revision at Lab on a Chip.

Yinfei Lu and I conducted the experiments. Yinfei processed and analysed the data. I was also responsible for the control software and synchronisation. Candice Ip developed an initial version of chip wetting, and Dennis Eggert performed the confocal microscope imaging. Yinfei prepared the initial manuscript and all other co-authors provided suggestions and proof-reading to finalise the manuscript.

Femtosecond Pumping Rate Dependence of Fragmentation Mechanisms in Matrix-Assisted Laser Desorption Ionization

<u>Cornelius L. Pieterse</u>, Frederik Busse, Friedjof Tellkamp, Wesley D. Robertson, and R. J. Dwayne Miller
Prepared to submit to the Journal of Physical Chemistry.

I developed the overall concept to employ femtosecond, ultraviolet laser pulses to study the desorption process using thermometer ions. I, therefore, determined the sample preparation protocols with Susanne Meier, performed the experiments, and analysed the data. Furthermore, I prepared the initial manuscript, which was edited by Frederik Busse. All of the other co-authors have provided suggestions and proof-reading to finalise the manuscript.

Rapid Deconvolution of Low-Resolution Time-of-Flight Data using Bayesian Inference

<u>Cornelius L. Pieterse</u>, Michiel B. de Kock, Wesley D. Robertson, Hans C. Eggers, and R. J. Dwayne Miller
Prepared to submit to Analytical Chemistry.

I developed the overall concept to investigate a Bayesian inference framework to improve the quantification of our time-of-flight mass spectra. Michiel de Kock performed the mathematical derivations and programming. I implemented this algorithm within our data analysis pipeline and assisted Michiel in improving the algorithm. I subsequently also analysed and interpreted the experimental data. I prepared the initial manuscript, which was edited by Michiel and Hans. All other co-authors provided suggestions and proof-reading to finalise the manuscript.

Contents

Chapter 1

Introduction

Mass spectrometry dates back almost a century and is one of the oldest and most developed analytical techniques within the physical sciences.[1–4] Surprisingly, some important details on the forming of the ions are still scarcely understood,[1] which therefore hampers quantitative measurements. Consequently, for the vast majority of applications, the underlying mechanisms are still very much debated and far from being disentangled.[5] Mass spectrometry is one of the fields with a vast number of different techniques available for consideration. One of the major breakthroughs in this field has been the demonstration that liable biomolecules can be routinely introduced into the gas-phase.[6–8]

Presently, the most widely employed techniques are electrospray ionisation (ESI)[8] and matrix-assisted laser desorption/ionisation (MALDI)[7]. Comparing these two techniques, ESI (an atmospheric interface) tends to be easier to perform in regards to the sample preparation and the instrument operation (transferring samples into a vacuum is more challenging than performing the same procedure at atmospheric conditions). The main disadvantages associated with atmospheric conditions are a reduction in sensitivity and facing more complicated ionisation mechanisms. Vice versa, MALDI (vacuum-based technique) tends to facilitate an improved sensitivity since there are no atmospheric interactions which reduce the overall collection efficiency. The ionisation processes are also better understood due to the reduced total number of underlying processes. Nevertheless, operating under vacuum conditions are both challenging and costly.

For the remainder of this thesis, the focus is on ESI and MALDI-MS, because currently, these are the two most commonly employed techniques. It is, therefore, only appropriate to have a brief introduction of each method and also a discussion on the underlying ionisation mechanisms. Attention will further be placed on novel approaches to overcome the current challenges associated with both atmospheric and vacuum ionisation techniques. In addition, by performing measurements under the conditions of stress-confinement using ultrashort laser pulses, both of these techniques can be rendered more quantitative. The overall structure of this thesis is segmented into atmospheric and vacuum-based sections to improve the coherence and ease of reading.

1.1   Atmospheric pressure ionisation techniques

The use of atmospheric ionisation techniques such as electrospray ionisation (ESI) has revolutionised analytical chemistry.[8] These techniques are typically soft and capable of producing highly charged states of biomolecules.[9–11] For example, peptides and proteins are known to have about two and twenty charges present, respectively. The ability to generate such states is particularly attractive since it allows the usage of mass analysers with low mass-to-charge ratio (m/z) ranges.

However, this comes at the expense of producing complicated and overlapping mass spectra. One of the main disadvantages of these techniques are that they do not facilitate the sampling flexibility and control, which is inherently provided by the laser-based techniques.[12] It is for this reason that MALDI is overall the most popular technique for performing mass spectrometry imaging,[13] even though it is known to be considerably less soft than the atmospheric techniques.[5] Due to the collisional cooling of ions, the latter techniques are generally softer than their vacuum counterparts, where cooling is very challenging to implement.

In the attempt to enjoy a similar level of control, while retaining the advantage of performing measurements at atmospheric conditions, various novel techniques were developed for coupling lasers to the liquid interface. This led to techniques such as atmospheric pressure MALDI, which displayed promise, but came with the challenge of predominantly producing singly charged states.[14, 15] Hence, supplementary techniques were investigated to overcome the problem to increase the charging states by usage of a secondary ionisation source.[16–18] A novel and well-established implementation of such an approach is inlet ionisation where the matrix is ablated into the heated transfer capillary, with the favourable outcome of producing both highly charged peptides and proteins.[19] All of these techniques, however, still rely on the matrix, which is undesirable and presumably the most significant drawback when compared to other atmospheric methods.

The first approach to address the matrix frustration was to use infrared lasers to produce highly charged biomolecules from bulk liquid water.[20–22] Although using continuous wave lasers requires large volumes of sample, this method has several advantages compared to ESI.[21] It is novel in regards to the sample being thermally ablated into a capillary held at high voltage, and thereupon producing highly charged ions. The natural extension of this technique was the introduction of pulsed infrared lasers, which produced low charged ion states from both pure water solutions, ice, and also IR-MALDI matrices.[23–25] Nevertheless, all of the pulsed laser methods still had the necessity for secondary electrospray ionisation, which is difficult to align with the laser beam and introduces instabilities within the ion signals (images have been shown difficult to reproduce).[26]

To appreciate how the secondary ionisation predicament could be addressed, a discussion regarding these ablation dynamics is in order. It is well-established that liquid water ablated by using pulsed infrared lasers result in plumes which have velocities several times the speed of sound.[27–29] Studies have indicated that these ablation processes can be constrained to the conditions of both stress and thermal confinement,[30] which will ensure that all of the deposited surplus energy is converted into the translation energy of the water molecules.[28–30] The application of such a technique appears perfect for softly extracting labile water-soluble biomolecules into the gas-phase. The picosecond infrared laser (PIRL) has demonstrated extraction of biomolecules both from tissue and liquid solutions, while conserving their structures, and further preserving enzymes, proteins and even viruses.[31, 32] These extractions were facilitated by resonantly exciting the stretching mode of water molecules, resulting in a translation expansion which leads to the cold and soft ejection of water constituents into the gas-phase.[28–30] Furthermore, molecular dynamics studies indicated that during this process the water molecules are stripped from the constituent analytes due to a conservation of momentum.[33] It is only logical that by using such an approach, the ionisation efficiency could be improved compared to current techniques.

All systems which introduce liquids in a bulk fashion, including methods such as ESI and laser spray, suffer from cross-contamination and large sample volume requirements. These challenges have been addressed in part by the lab-on-a-chip (LOC) technologies since they provide unique advantages with regards to sample localisation and sorting.[34, 35] It is for this reason that serious efforts have been made to interface such LOC device to ESI and MALDI systems.[34–39] Given that MALDI is a laser-based technique, it offers improved geometrical flexibility and sampling precision than its atmospheric counterparts, which resulted in various successful interfacing of LOC devices for both online and offline analyses.[36, 37] The biggest challenge faced by MALDI techniques is the mandatory application of the matrix, which can quickly complicate the entire LOC process. Even though ESI is usually considered to be both simpler and more cost-effective than MALDI, especially with regards to producing highly charged states which are appropriate for fragmentation based studies, it lacks laser flexibility and usually requires high voltages and/or pressures to be applied directly to samples.[34–39] It is, therefore, difficult to couple a LOC device to an ESI system, especially since there are almost always leakages and/or dead volumes present. Another avenue to explore is the direct integration of an ESI nebuliser into the LOC device, but this comes with the challenge of requiring control over both flow rates and pressures.[40–43] Having complete control over these parameters is unique, but it comes at the expense of complicating the reproducibility since the ionisation efficiency strongly depends on both of these parameters (they can easily destabilise the electrospray process). Regardless, all of these methods still lack the flexibility of laser techniques.

In this thesis, picosecond infrared pulses are used to extract small molecules and highly charged biomolecules. This technique is demonstrated to be soft and produce mass spectra similar to those generated using standard ESI techniques. Most importantly, it is fairly stable over long periods of time without requiring a secondary ionisation source. In addition, it is further shown that no high voltage or curtain gas is required, while having a capability of extracting volumes within the picolitre range (27 pL). The sampling flexibility facilitated by the laser-based approach is beneficial in the sense that fragmentation studies could be performed on a cost-effective atmospheric instrument with minimum effort. The technique was extended with the addition of an optically transparent, self-localisation chip, which was optimised for aqueous solutions. A proof-of-principle study indicated that this system could localise small sample volumes, which could be individually analysed, therefore laying the groundwork towards a system free of cross-contamination and offering improved quantification.

1.2   Vacuum laser desorption and ionisation

The MALDI imaging of biological samples is an established technique and heavily relied upon in various scientific disciplines, including the rapidly evolving field of drug tailoring.[44–47] One of the factors which primarily prohibits the adequate lateral resolution is the spatial restrictions imposed by optical focusing elements. Given that a finite distance is required for ion extraction, it tends to be a difficult task to interface the laser beam to the front surface of the sample. Depending on the separation distance between the sample surface and the ion extraction region, the problem becomes apparent for small separations when considering the angle of the laser beam relative to the surface.[48–52] As the angle decreases, due to a decrease in separation, the shape of the beam on the surface becomes elliptical,

which has undesirable effects on the images obtained.[48] One possible approach to circumvent this challenge is to implement a transmission geometry, which is characterised by a laser beam being aligned collinearly with ion extraction optics. Application of such an arrangement lifts the geometrical optical restrictions since it is possible to collinearly manipulate the beam from behind the samples, which inherently allows a more symmetrical laser beam profile and the usage of shorter focal length lenses. The main disadvantage of this configuration is that the sample thickness needs consideration, which is problematic for thick tissue sections.

The use of a transmission geometry was introduced during the infant days of MALDI,[53–56] but was regrettably never popularised within the community until rather recently when the highest lateral resolution was reported with it.[57] For this reason, there was an obvious necessity to further investigate whether such a configuration poses any unknown disadvantages over the reflection geometry, because it is difficult to foresee another approach which would be as cost-efficient and straightforward to implement, yet promise an improvement with regards to the currently available lateral resolutions. An initial study already indicated that the mass spectra obtained for both of the transmission and reflection geometries are qualitatively comparable for common biomolecules, particularly with regards to the mass resolution and fragmentation.[55]

One of the main reasons why MALDI is not yet adequately quantitative is due to the desorption and ionisation processes being highly coupled, which inherently translates into the fact that the ionisation efficiencies cannot be increased without increasing the amount of material desorbed and vice versa.[5] There are several examples of this deadlock, but only the challenge surrounding asphaltenes will be discussed here, as it is the extreme manifestation of this reality. The asphaltenes are central to the understanding of petroleum, but unexpectedly, until rather recently, very little has been known about these molecules.[58] The main reason for this void in our knowledge was because it was not possible to determine their molecular masses accurately, with the initial estimates spanning several orders of magnitude.[58] It was merely with the advent of laser post-ionisation, which have facilitated the decoupling of both desorption and ionisation processes, that this problem was addressed.[59] By improving the ionisation efficiency, and therefore allowing a decrease in the desorption fluence, the plume is remarkably less dense, which results in the reduction of the gas-phase aggregation, and, therefore, comprehensible data.[60] Post-ionisation, therefore, allows the predominantly neutral plume to be ionised, without the undesirable addition of further energy.

The complexity mentioned earlier of the desorption and ionisation processes being inherently coupled was recognised during the initial molecular dynamics studies.[30] Subsequent work has built on these results and showed that by using ultrashort pulses, the desorption process proceeds under both stress and thermal confinement conditions.[33] A vast majority of mass spectrometry measurements are performed under thermal confinement conditions, but only when operating under stress-confinement conditions are the desorption and ionisation processes decoupled. It is perceivable from this study that the usage of ultrashort pulses could improve the degree of quantification offered by mass spectrometry, because even though laser post-ionisation does enhance the quality of the mass spectra, a transfer of internal energy to the neutral molecules still occurs.[61] Regardless, there exists no comprehensive body of data regarding the use of ultrashort pulses.

Not long after the introduction of MALDI by Karas and Hillenkamp, a brief discussion appeared on the usage of femtosecond pulses for this purpose.[62] These authors demonstrated that ultrashort pulses could be used similarly to that

of nanosecond pulses, but at the expense of facing a mass upper-limit (5000 Da), something which was not initially observed for nanosecond experiments. Most importantly, this was the first study to show that the MALDI process is primarily dependent on the laser fluence (expressing energy per area) and not the irradiance (related to the peak intensity of the pulse duration).[62] At the time, this was not understood, but it was illustrated that for an 560 fs pulse, the heaviest biomolecule which could be routinely measured was insulin (~5000 Da). Nonetheless, it was explicitly highlighted that the intensity of these insulin ions relative to the ferulic acid matrix ions was significantly reduced in the case of using ultrashort pulses. Somewhat disappointingly, following this study, there have only been a handful of similar studies which investigated the effect of using ultrashort pulses for mass spectrometry purposes.[63–66] Although 500 ps pulses are usually not considered to be ultrashort, not much later it was shown that the only difference between the use of picosecond and nanosecond (3 ns) pulses is a small difference in threshold fluences.[63] Per contra, unlike for the scenario of the femtosecond pulses, it was possible to measure proteins, such as cytochrome c and bovine serum albumin, both through direct desorption and post-ionisation of the neutrals.

The first real comparison between nanosecond and femtosecond pulses was conducted when a detailed study was performed to improve the understanding of laser desorption/ionisation mechanisms.[64] For this objective, the mass spectra produced by a nitrogen, Nd:YAG and Ti:Sapphire laser were carefully examined. The most intriguing result from this study was the fact that the spectra appeared almost identical for all of the laser systems investigated, with the exception of the analyte-to-matrix signal ratio being somewhat reduced for femtosecond pulses. It is important to mention that for these measurements, the matrix-to-analyte molar ratios were quite low (less than 100:1) in comparison to other studies. In general, this ratio is substantially in the excess of 1000:1 for analytes investigated because matrix suppression is common for such a low matrix-to-analyte molar ratio.[67] Regardless, it was still illustrated that for the femtosecond pulses there was an increase in the magnitude of the matrix peaks relative to the analytes.

Chen and Vertes performed the first true quantitative comparison for the mass spectra generated by using nanosecond and picosecond laser pulses.[65] Although the central objective of this investigation was to shed light on morphology effects associated with the most commonly used MALDI matrices (DHB, SA and CHCA), fundamental observations with regards to the underlying ionisation mechanisms were also made. These results supported the earlier observations that the fluence threshold is only marginally dependent on the pulse duration. Moreover, for all of the matrices investigated, fragmentation was considerably more pronounced for the longer pulse durations. Interestingly, similar to the study by Demirev *et al.* a mass upper-limit at the mass of insulin was observed. Their interpretation was that when considering the high optical pumping rates achievable by picosecond pulses, the temporal overlap between the neutral biomolecules and matrix ions within the plume was too small for sufficient ionisation to occur.[65]

Given that all of the biomolecules studied are relatively robust and that these results were qualitative, the exercise which remained was to measure the softness for the different laser pulse durations quantitatively.[5] The most straightforward method to demonstrate the softness of a given ionisation method is to determine the internal energy imparted onto a thermometer ion because the internal energy defines the conceivable fragmentation pathways thereof.[61] On these grounds, a study was formulated to estimate the amount of energy transferred from several matrices to the benzyltriphenylphosphonium (BTP) thermometer ions due to the

collisions within the desorption plume.[66] The simple structure of BTP, and also other benzylpyridinium species, render it the optimal model system for studying the transfer of internal energy, especially because they have known fragmentation channels and are present in the solid phase as preformed ions.[68] It would have been considerably more challenging to use biomolecules for this purpose since an additional ionisation step would have been required.[66] It was demonstrated that the picosecond pulses resulted in the reduced transfer of energy for the BTP, which was apparent from the reduction in fragmentation.[66] The explanation for this result was based on the premise that the picosecond desorption occurs under stress-confinement conditions, whereas the nanosecond desorption will only be thermally confined, which agrees with earlier molecular dynamics studies which suggested that under stress-confinement conditions a reduced amount of internal energy will be transferred.[30]

Furthermore, studying a fragmentation pathway, such as that of BTP, is not trivial. Although the underlying fragmentation channels are simple and generally well-established, both interpretation and accurate quantification of the data can be challenging.[69] The frustration of facing complex datasets is often attributed to the signals which originate from the underlying ion sources not being constant within time. Such signal variabilities result in correlations and will consequently conceal the true underlying signal generating processes. It should be empathised that the time coordinate can also refer to the laser shot sequence, and is thus not restricted to an absolute time scale. As an example, when performing atmospheric measurements where laser pulses irradiate a liquid interface,[70] the fluctuating interface results in a highly transient signal due to the change in optical fluence. The straightforward approach would be to choose shorter experimental runs, but this comes at the expense of reducing the signal-to-noise ratio. Fortunately, these problems were encountered and addressed before in the fields of particle physics and cosmology with considerable success using Bayesian inference.[71–73] It was therefore only logical to pursue this concept for transient mass spectrometry in an attempt to improve the degree of quantification.

Within this thesis, the first attempt was made to determine whether it is indeed possible to separate both desorption and ionisation processes by performing UV, ultrafast desorption of the popular thermometer ion BTP. The internal energy of BTP thermometer ions was qualitatively investigated to determine whether the desorption process is appropriately soft. The results indicated that the magnitude of fragmentation of BTP is independent of the pulse energies for the laser fluence values studied, which was the first indirect confirmation of the ionisation process being decoupled from desorption. More importantly, these measurements were performed in a transmission geometry to establish whether it poses unknown disadvantages over the standard reflection geometry. The presented results indicate that the transmission geometry, combined with ultrashort pulses, could be used similarly to nanosecond pulses in the reflection geometry. Moreover, a Bayesian deconvolution framework was implemented to improve the quality of the mass spectra, which added a more quantitative aspect to the interpretation thereof. The increase in mass resolution facilitated by this deconvolution method enabled the BTP fragments to be identified with a more substantial degree of confidence. The higher quality mass spectra allowed the identification of further fragmentation channels, which was not initially possible, due to the mediocre data quality. These channels were minor but in agreement with earlier dissociation studies.

Chapter 2

Experimental

2.1 Atmospheric pressure ionisation techniques

Experiments under atmospheric conditions were performed on a commercial ion trap mass spectrometer (Esquire 3000, Bruker, Bremen, Germany), which included a modified ambient-vacuum interface to optimise the ion collection efficiency. As this setup has been discussed before, here the main emphasis will be on advances made regarding other commercially available systems.[70] In summary, the most innovative feature of this system is that picosecond infrared laser (PIRL) pulses are used for soft extraction of small and biomolecules from liquid water solutions without a secondary ionisation source. Similar interfaces have been reported for nanosecond infrared lasers, but this was always performed in a conjunction with secondary electrospray ionisation. The current system, as illustrated in Figure 2.1, was further advanced with the incorporation of an optically transparent sample sorting chip.[74] The optical chip, in combination with infrared ablation, showed that it is possible to localise and extract individual picolitre volumes.
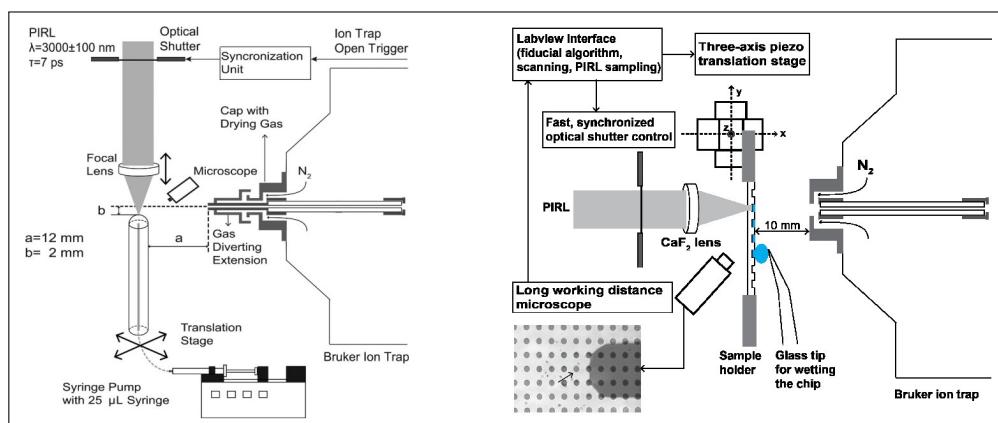
FIGURE 2.1: Experiments were performed on a modified commercial ion trap mass spectrometer. A schematic representation is given for both the (left) bulk and (right) chip localised (transmission geometry) measurements. These figures also appeared in the thesis of Yinfei Lu. Reproduced with permission.[70, 74]

For all of these measurements, a microscope with a long working distance was used to monitor the position of the air/water interface to keep it within the laser focal plane. Using a diode synchronised shutter, which was computer controlled, it was possible to select the desired pulse train from the picosecond infrared laser ($\lambda = 3$ μm, $\tau = 7$ ps, PIRL-APLQ-3000, Attodyne, Canada). The pulses (a single pulse to the 1 kHz fundamental) were synchronised with the ion trap for optimal collection efficiency. The laser beam was focused to $\sim$140 μm ($1/e^2$ spot diameter

definition) using an $L = 25$ mm lens, which resulted in a fluence of 0.3 J/cm^2 for the maximum energy (40 μJ). The in-house designed transfer capillary facilitated unique control of the sample temperature and applied voltages. For the capillary measurements, the aqueous solutions were delivered by using a syringe pump. Between the different measurements the tubing was appropriately flushed with no observable sample contamination. For the control measurements, mass spectra were acquired by mounting the ESI nebuliser perpendicular to the ion collection interface. All samples were prepared according to established protocols.[75]

2.2 Vacuum laser desorption and ionisation

The mass spectrometer schematically illustrated in Figure 2.2 has been described elsewhere.[76] Here focus will be on advances this instrument made compared to systems currently described in the literature. In summary, the most novel feature of this system is the combination of the transmission geometry with femtosecond pulses for desorption. Only a very small quantity of these transmission geometry instruments have been discussed since the introduction of laser-based vacuum desorption, even though such a geometry provides multiple advantages over the almost exclusively used reflection geometry.
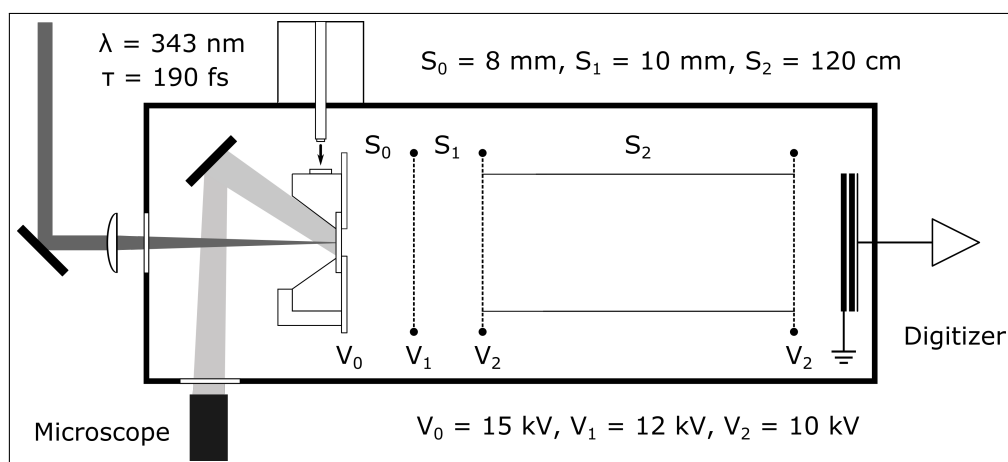
FIGURE 2.2: Experiments were performed in a transmission geometry of an in-house designed linear time-of-flight mass spectrometer (the laser impinges the backside of a substrate collinearly with the ion extraction axis). Reproduced with permission.[76]

Experiments were performed using an in-house designed linear time-of-flight mass spectrometer using the third harmonic output ($\lambda = 343$ nm, $\tau = 190$ fs) of an amplified Yb:KGW oscillator (Pharos SP 1.5mJ, Light Conversion, Vilnius, Lithuania). The beam was focused to 225 ± 7 μm (1/e^2 diameter definition) by using an $L = 750$ mm lens. The laser pulse energy could be set between 2 and 10 μJ, which resulted in peak fluence values between $\sim$100 and 500 J/m^2 at the sample surface. Desorbed ions were accelerated to an 5 keV positive kinetic energy within a static, two-stage extraction region, which was supplemented with an additional 10 keV post-acceleration stage, resulting in a total energy of 15 keV. A dual-stage chevron microchannel plate detector (F9890, Hamamatsu, Bridgewater, USA) measured positive ions with the help of an 8-bit digitiser (DC211, Acquiris, Plan-les-Ouates, Switzerland). Vacuum pressure varied from 2.0×10^{-7} mbar at the beginning of the measurements to better than 8.0×10^{-8} mbar on the completion thereof.

The matrix and analyte solutions were prepared to a matrix-to-analyte ratio of $\sim 3000 : 1$ per established protocols.[61, 65] Only those single shot mass spectra for which the largest peak was above a defined threshold were averaged, resulting in about 500 spectra averaged per sample. The fluence ($126\,\mathrm{J/m^2}$) of about 1.5 times that of the DHB matrix fragmentation threshold was the minimum value studied. The survival yields were calculated as $\alpha = \sum I_M / (\sum I_M + \sum I_F)$, where $\sum I_M$ and $\sum I_F$ are the integrated abundances of the parent and fragment ions.[61, 66, 77] It should be empathised that this approach assumes both identical collection and detection efficiencies for all of these ions, especially within the limit of overall low collection efficiencies. Although it is not required for these small molecules, in the case of larger molecules (in excess of 1000 Da), it would be necessary to account for the mass-limited detector efficiencies.[78, 79]

2.3   Bayesian deconvolution

Given the lengthy derivation of this Bayesian deconvolution algorithm, only the most important steps thereof will be introduced and discussed in this thesis.[80] The method was designed to extract the underlying signals from low-resolution time-of-flight spectra and was for this reason based on the well-established Lucy-Richardson algorithm.[81, 82] The most challenging steps were the incorporation and characterisation of several Bayesian prior distributions, which significantly improved the convergence rates and the quality of extracted signals.

The mass spectra are considered to be the set of discrete counts n_b, with one for each m/z interval b where the joint intervals of bins $b = 1, 2, \ldots, B$ cover the entire m/z range. Importantly, the individual events counted in each bin during the measurement are considered to be exchangeable, which suggests that the total discrete counts n_b follow a Poisson distribution

$$p(n_b \mid \lambda_b) = e^{-\lambda_b} \lambda_b^{n_b} / n_b! \qquad n_b = 0, 1, 2, \ldots, \infty \qquad b = 1, 2, \ldots, B. \qquad (2.1)$$

The parameter $\lambda_b > 0$ is proportional to the acquisition time and represents the underlying signals. The counts n_b are assumed to be mutually independent, which means that the likelihood (joint probability of all counts) is given by

$$p(\boldsymbol{n} \mid \boldsymbol{\lambda}) = \prod_{b=1}^{B} p(n_b \mid \lambda_b). \qquad (2.2)$$

The vector $\boldsymbol{n} = \{n_b\}_{b=1}^{B}$ represents the familiar averaged data of the experiment. As a result, the vector $\boldsymbol{n}$ is the sum of counts originating from the underlying, but broadened, narrow peaks: each n_b is the convolution of these narrow peaks. The exercise of deconvolution is to reverse that convolution and to successfully separate the low-resolution data into high-resolution peaks using where possible other appropriate information such as isotopic signatures and detector responses. The objective is therefore to find a set of parameters $\boldsymbol{s}^* = \{s_b^*\}_{b=1}^{B}$ which represent the best estimates of the amplitudes of the possibly narrow peak for each bin b, interpreting any small s_b^* as noise rather than a true signal.

Convolution and deconvolution are considered to be linear. Let s_c be the true peak amplitude of a bin c and let $\mathbb{A}$ (a point spread function) be the $B \times B$ square matrix whose components $\mathbb{A}_{bc}$ constitute the peak broadened contribution which transforms s_c into data in the nearby bins b. As a result, the Poisson parameter in bin b is, in component and vector-matrix notation respectively, given by

$$\lambda_b = \sum_c \mathbb{A}_{bc} s_c \qquad \text{or} \qquad \boldsymbol{\lambda} = \mathbb{A}\boldsymbol{s}. \tag{2.3}$$

After applying the Stirling approximation to all the counts n_b and also enforcing normalisation of the matrix $\mathbf{1}^\mathsf{T}\mathbb{A} = \mathbf{1}^\mathsf{T}$, appropriate for convolutions, the negative logarithm of the likelihood simplifies to

$$L[\boldsymbol{s}] = I[\boldsymbol{n} \,|\, \mathbb{A}\boldsymbol{s}] = \mathbf{1}^\mathsf{T} (\boldsymbol{s} - \boldsymbol{n}) + \boldsymbol{n}^\mathsf{T} \log \frac{\boldsymbol{n}}{\mathbb{A}\boldsymbol{s}}. \tag{2.4}$$

Here a relative entropy L replaces the metric distance that appears in the familiar least-squares method. It is convex, non-negative and coercive on the non-negative orthant, implying that a minimum exists which is global and unique.

To solve the equations, the $\boldsymbol{s}^*$ will be employed to minimise the I-divergence. The linearity of the divergence implies that the solution must obey

$$\sum_b s_b^* = \sum_b n_b. \tag{2.5}$$

Further, a logarithm requires that $s_b^* > 0$ for all b. However, convolution is a linear operation, meaning that the perfect reconstruction of the data would require both negative and positive parameter values, which complicates matters considerably. As a result, the I-divergence minimisers are constrained to be sparse. Should the underlying signals contain extended objects (objects which span several bins), this attribute will conflict with the sparsity, and the algorithm should, therefore, be stopped when an appropriate solution is found. For these reasons, this algorithm is considered semi-convergent. In addition, since the likelihood does not contain all of the relevant information, there is no point in running it for more extended periods of time, since this will only generate less plausible solutions.

So far the algorithm has followed the generic tale of Lucy-Richardson closely. To integrate it into a Bayesian framework, an appropriate prior must be defined. The exercise, therefore, becomes the maximisation of the joint probability, which is the product of the likelihood and source prior $p(\boldsymbol{n}, \boldsymbol{s}) = p(\boldsymbol{n} \,|\, \mathbb{A}, \boldsymbol{s})\, p(\boldsymbol{s})$,

$$J[\boldsymbol{s}] = L[\boldsymbol{s}] + \beta P[\boldsymbol{s}], \tag{2.6}$$

where the regularisation parameter β will negotiate the strength of the likelihood L relative to the prior P. For mathematical simplicity, the regularisation parameter is grouped with the prior instead of the likelihood.[83] To iteratively solve this system, the gradient descent method can be used

$$s_{j+1}^* = s_j^* \left\{ \mathbb{A}^\mathsf{T} \left(\frac{\boldsymbol{n}}{\mathbb{A}\boldsymbol{s}^*} \right) + \beta v_j^* \right\} \Big/ \left(1 + \beta u_j^* \right). \tag{2.7}$$

This algorithm is the split-gradient method, which in the multiplicative form, is not always convergent due to the prior influence.[84, 85] Should this happen, then the regularization parameter β needs to be reduced to change the behaviour thereof such that it is more aligned to that of the Lucy-Richardson algorithm.

The Gaussian distribution, with the appropriate choice of a Toeplitz matrix $\mathbb{B}_j$ and a scale parameter Λ, is a computationally modest prior distribution[83]

$$p(s \mid \Lambda, \mathbb{B}_j) = \left(\frac{\Lambda}{2\pi}\right)^{B/2} e^{-\Lambda s^\mathsf{T} \mathbb{B}_j^\mathsf{T} \mathbb{B}_j s / 2}. \tag{2.8}$$

The candidate $\mathbb{B}_j$ matrices express the underlying generic knowledge as follows. Prior knowledge might suggest that the prior distribution depends either on the signals itself, or it may be known that it might depend on the discrete differences between signals, or even on higher-order differences. The choice $\mathbb{B}_0 = 0$ therefore reflects the desire to have no prior at all, while the dependence on the signal itself would motivate usage of $\mathbb{B}_1 = \mathbb{I}$, or if a constant function is preferred, the first differences of the signal

$$\mathbb{B}_2 = \begin{bmatrix} -1 & 1 & 0 & 0 & 0 & 0 & \dots & 0 \\ 0 & -1 & 1 & 0 & 0 & 0 & \dots & 0 \\ \vdots & & & \ddots & & & & \vdots \\ 0 & \dots & 0 & 0 & 0 & -1 & 1 & 0 \\ 0 & \dots & 0 & 0 & 0 & 0 & -1 & 1 \end{bmatrix}. \tag{2.9}$$

The decision to apply higher-order signal differences are reflected in the matching second-order difference matrix

$$\mathbb{B}_3 = \begin{bmatrix} -1 & 2 & -1 & 0 & 0 & 0 & \dots & 0 \\ 0 & -1 & 2 & -1 & 0 & 0 & \dots & 0 \\ \vdots & & & \ddots & & & & \vdots \\ 0 & \dots & 0 & 0 & -1 & 2 & -1 & 0 \\ 0 & \dots & 0 & 0 & 0 & -1 & 2 & -1 \end{bmatrix}, \tag{2.10}$$

or, by preference, even a third-order difference can be considered

$$\mathbb{B}_4 = \begin{bmatrix} 1 & -4 & 6 & -4 & 1 & 0 & \dots & 0 \\ 0 & 1 & -4 & 6 & 4 & 1 & \dots & 0 \\ \vdots & & & \ddots & & & & \vdots \\ 0 & \dots & 1 & -4 & 6 & -4 & 1 & 0 \\ 0 & \dots & 0 & 1 & -4 & 6 & -4 & 1 \end{bmatrix}. \tag{2.11}$$

Chapter 3

Results and discussion

3.1 Atmospheric pressure ionisation techniques

The infrared ablation at the water/air interface was monitored for stability using a long working distance microscope and, when required, executing the appropriate adjustments to either the sample delivery or the laser systems. The system was characterised using phosphazene salt variants from the ESI tuning mix, dissolved in pure water, before performing further measurements with biomolecules. The direct ablation of such samples resulted in several of these singly charged species, such as; the hexamethoxy (m/z = 322), hexakis(2,2-difluoroethoxy) (m/z = 622), hexakis(1H,1H,3Htetrafluoropropoxy) (m/z = 922), and also hexakis(1H,1H,5H-octafluoropropoxy) phosphazene (m/z = 1522) ions. Extraction of the small drug molecules caffeine and acetaminophen demonstrated the softness of PIRL, since no signs of extensive fragmentation regarding thermal or hydrolytic degradation were observed, in comparison to ESI, for which this is common.[86]

Figure 3.1 shows a representative mass spectrum of the phosphazene species. The volume of sample extracted per laser shot was determined by synchronising the sample flow rate to the number of laser shots in a given pulse train. From the gradient of the parameters, an extraction volume of 27 pL/shot was determined, corresponding to an extraction depth of $\sim$1.5 μm. With regards to the sensitivity of this method, when considering the concentration of hexamethoxyphosphazene and the amount of sample extracted, an approximate value of 220 amol was found when averaging for 5 seconds (reduced to less than 100 amol for shorter averaging times). Figure 3.1 further indicates that the signal intensity is within one order of magnitude of what is routine using ESI and stable over a reasonable time period. The effect of the laser extraction were also demonstrated using low duty cycles to illustrate that the signal did originates from ablation and not evaporation.
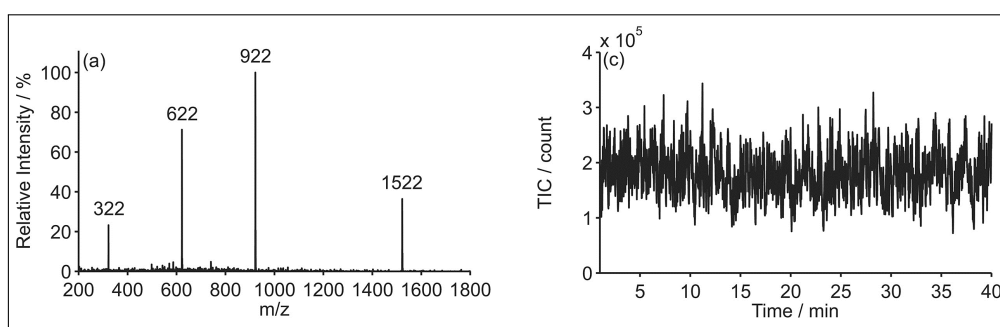
FIGURE 3.1: Infrared ablation was characterised using phosphazene salt variants. (a) Mass spectrum of these salts and the associated (c) total ion current versus time. This figure also appeared in the thesis of Yinfei Lu. Reproduced with permission.[70]

The next logical step was to perform similar measurements for biomolecules. The mass spectrum obtained from a solution of the peptide angiotensin I (10 μM) in water with 0.1 % formic acid is shown in Figure 3.2. The ion charge states (and signal-to-noise ratios) observed from the PIRL extraction were very similar to those produced using ESI. It is important to mention that a constant flow rate of 167 nL/min^{-1} was used for these measurements, which is comparable to that of nanoESI (for the ESI the flow rate was about an order of magnitude larger). It was possible to generate MS/MS spectra by isolating the second charged state of this peptide using fragmentation by collisionally induced dissociation. These results were almost identical to those produced by ESI, which indicates that the signal intensity and stability thereof is sufficient to perform tandem mass spectrometry. Similar sensitivities to that of the phosphazene salts were obtained.
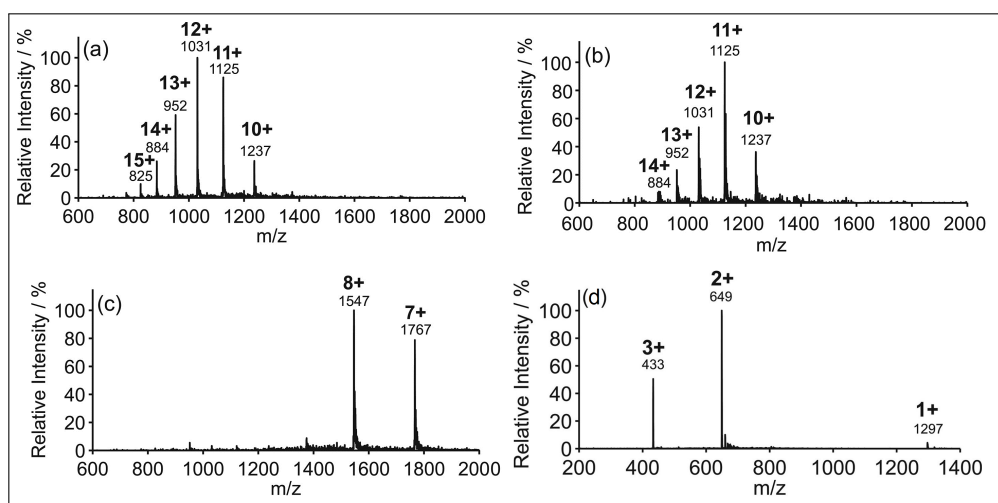
FIGURE 3.2: Mass spectrum of the protein cytochrome c prepared in (a) water with 0.1 % formic acid, (b) acid-free water, and in also (c) 10 mM ammonium acetate buffer. In addition, the (d) peptide angiotensin I prepared in 0.1 % formic acid is shown. Figures appeared in the thesis of Yinfei Lu. Reproduced with permission.[70]

Moving then on to the proteins, a mass spectrum measured from a solution of cytochrome c (10 μM) in water with 0.1 % formic acid is also shown in Figure 3.2. Similar to an earlier study performed with ESI, a highly charged distribution was centred at the 12+ charge state, which is indicative of an unfolded protein.[87] A similar outcome was obtained with the pure water solution, with the exception that the distribution was shifted slightly to the lower end. It was found that the position of the charge states could be shifted further by changing the sampling conditions (such as a transfer capillary temperature or sample acidity). A protein solution was also prepared according to the sampling conditions for native mass spectrometry.[88] When analysing this solution, a narrow distribution located at the 8+ charge state was obtained, which is consistent with a folded protein. This result is comparable to what is obtained with ESI techniques and is indicative of the soft nature by which the biomolecules are extracted. A large distribution of highly charged states were observed for the protein lysozyme, which is indicative of a mixture of the folded and unfolded states, which is probably due to the sampling conditions employed.

Molecular dynamics studies have indicated that by using an ultrashort pulsed infrared laser, it is possible to extract a biomolecule from water in vacuum causing minimal damage.[33] However, by performing measurements under atmospheric conditions, the supersonic plume will most possibly condense into liquid droplets due to atmospheric collisions. Furthermore, if these droplets are not desolvated completely, or be directly ejected from the bulk liquid water,[29] then charging and ionisation can proceed according to mechanisms similar to that of ESI.[89] A temperature dependence study showed no change in the distribution of charged states for cytochrome c, but there was an increase in the total ion signal. Such an observation suggests that some molecules were initially not completely stripped of the water. Nevertheless, a voltage dependence study indicated that these ions formed before reaching the transfer capillary, which rules out a mechanism such as that of inlet ionisation.[19] Further studies are required to better understand the underlying ionisation mechanisms.

The concept of interfacing a lab-on-a-chip (LOC) device was born when it was realised that it is possible to use single laser pulses to extract small volumes. The LOC device fabricated for this purpose can localise ∼10 pL liquid volumes, which corresponds to a meniscus height of 1.5 μm. With the comfort of automated well registration and scanning, the same phosphazene salt solutions were successfully analysed to produce the mass spectra shown in Figure 3.3. The employed loading method resulted in approximately 500 amol of sample loaded per well, which was extracted using a pulse train of 100 pulses. Each row on the sorting device resulted in an intense signal for which the mass spectra was easily recognisable. There was variation in the signal intensity for each row because there was a synchronisation mismatch between the ion trap collection time and laser ablation. Similar results have been obtained for biomolecules. Nevertheless, these results do indicate that the discussed picosecond infrared laser is capable of extracting small amounts of aqueous solution at ambient conditions with adequate sensitivity.
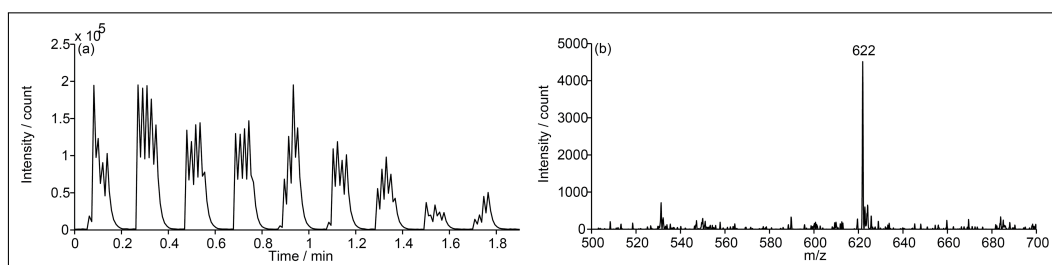
FIGURE 3.3: Total ion current (a) when scanning an entire row and the corresponding (b) mass spectrum. The variation in the ion current for each row (a) is attributed to a synchronisation mismatch between the ion trap collection time and laser ablation. The figure appeared in the thesis of Yinfei Lu. Reproduced with permission.[74]

3.2   Vacuum laser desorption and ionisation

A molecular dynamics investigation suggested that the desorption and ionisation processes will become separable under the conditions of stress-confinement,[33] which motivated the measurement of the survival yields for both the DHB matrix and the BTP thermometer ions as a function of the laser fluence. If these processes are indeed decoupled, then a larger fluence would result in an increased number of photons absorbed by the matrix, but without the additional transfer of energy to the thermometer ions. Due to the increase in the number of photons absorbed, the matrix is expected to fragment more noticeably.[5] A representative spectrum for such a measurement is shown in Figure 3.4. The DHB matrix (m/z 154), the dehydroxylated DHB matrix (m/z 137), and the BTP thermometer (m/z 353) ion peaks are easily identifiable. However, it does appear as if the BTP is only slightly fragmented, given that the peaks of both the benzyl (m/z 91, fragment F1) and the triphenylphosphine radicals (m/z 262, fragment F2) are barely visible.
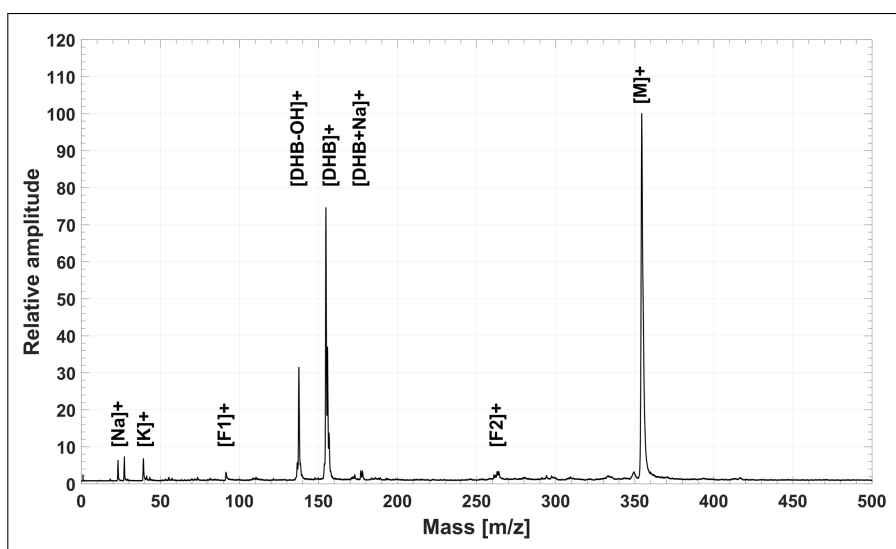
FIGURE 3.4: A mass spectrum for the low fluence (126 J/m^2) measurement showing the DHB matrix ion (m/z 154), the dehydroxylated DHB matrix ion (m/z 137), and the BTP thermometer (m/z 353), as well as numerous ion fragments. Reproduced with permission from the ACS.[76]

A major premise made here was the decision to define the investigated fluence range relative to the DHB fragmentation fluence threshold (84 J/m^2). The BTP did not fragment sufficiently enough to correctly identify such a threshold. However, it was noticed that the DHB fragmentation does escalate with the fluence, which is in agreement with an earlier study.[65] From these studies, it is also observable that for the case of picosecond pulse durations the fragmentation thresholds of the DHB and BTP are comparable.[65, 66] It was for this reason that fluence values between ~1.5 and 2.7 times the DHB fragmentation threshold were studied. From this study, it was observed that the survival yields of BTP (~0.95) is independent of the pulse energies studied. Figure 3.5 shows that in contrast to the BTP, DHB is highly sensitive to a fluence increase, which is in agreement with the assumption of it absorbing further photons. Unfortunately, due to challenging crystallisation conditions, it was not possible to increase the total number of fluence data points (reproducibility was, however, high within a given sample batch).
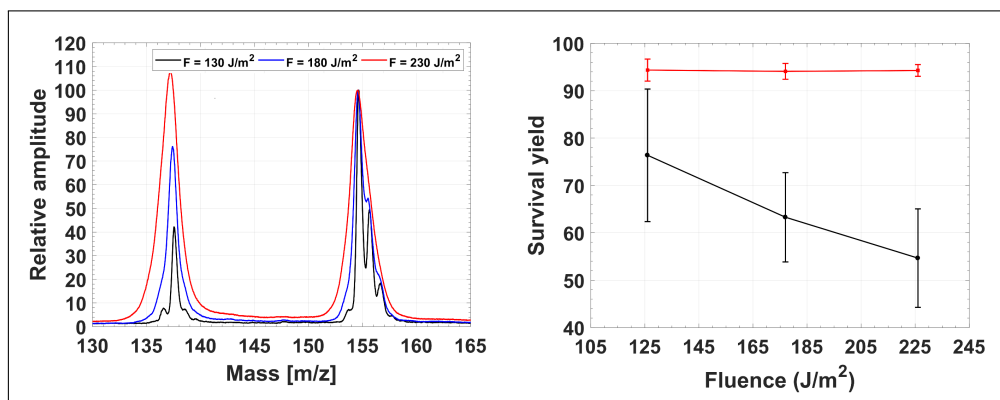
FIGURE 3.5: Mass spectra of the DHB matrix for the fluences studied, where these spectra were normalized relative to the parent peaks to calculate the survival yields. Also shown are the mean survival yields of both the DHB and BTP ions. Reproduced with permission from the ACS.[76]

When comparing the BTP survival yields with those reported for 22 ps pulses ($\sim$0.87), it becomes clear that the BTP is less sensitive to the increase in fluence. For that study, the survival yields decreased significantly when the fluence was increased to $\sim$1.3 times the BTP fragmentation threshold (even lower yields were reported for the nanosecond pulses).[66] Although it is difficult to make factual statements regarding the fragmentation mechanisms, due to the fashion in which the thresholds were defined, it is strongly believed that a continuation of an earlier reported trend was observed: a higher survival yield for reduced pulse durations. The high-pressure gradients, which result from stress-confined desorption, would explain the reduction in the amount of internal energy transferred from the DHB matrix ions to the BTP thermometer ions because there will only be a very narrow time window when these species could interact with each another. Furthermore, the limited stress-confinement from the picosecond pulses would still result in a notable amount of energy transferred due to the collisional interactions.

A quick discussion regarding the lower than previously mentioned (84 J/m^2) matrix fragmentation threshold is in order.[66] The spot size for the picosecond studies was considerably smaller (55 μm) compared to the present study (225 μm), which explains this discrepancy, because previous studies have shown that these thresholds are spot size dependent.[5, 90] It is already known that if the threshold fluence of a small spot size is used for a larger spot size, then the outcome would be extensive fragmentation and a reduction in mass resolution.[90, 91] Moreover, given that the penetration depth is about 100 nm, which is considerably less than the micron thickness of these DHB crystals, the measured signals most probably originated from the bottom surface of the crystals.[55]

Earlier studies have indicated that the DHB matrix [65] and BTP thermometer ion [66] fragmentation thresholds are comparable. But, unfortunately, a combined analysis was never performed (a similar remark was made for biomolecules).[92] Nevertheless, assuming fragmentation reactions to be unimolecular, the internal energy becomes equivalent to the concept of the effective temperature, for which it has been shown that the magnitude of the matrix fragmentation is indicative of this effective temperature.[93, 94] For these reasons, considering earlier studies and the extensive matrix fragmentation, it becomes clear that these measurements were performed under extremely hot conditions. Such reasoning further supports

the hypothesis that a minimal amount of energy was transferred from the DHB matrix to the BTP thermometer ions, even though a massive amount of material was desorbed into the gas-phase (known from the peak characteristics).

One of the most fascinating results observed in this study was the detection of a mass upper-limit, complementary to the previously observed analogues.[62, 65] Because of the difficulty in performing these measurements accurately, only a few preliminary observations will be briefly discussed. As already mentioned, an akin mass upper-limit at approximately the mass of insulin has been observed.[62, 65] Interestingly, when employing the femtosecond pulses for desorption, this mass upper-limit was reduced to approximately the mass of angiotensin I ($\sim$1300 Da). The advantage of using post-acceleration is that low extraction fields can be used within the source region,[95] which will reduce ion collisions, while also enabling the ions to have sufficient kinetic energies for near unity detection efficiencies.[79] There has been a study which suggested that for these biomolecules, the quantum detection efficiencies would decrease to $\sim$0.78, which implies that the signal of the angiotensin will be somewhat higher when considering the correction factor.[78] Both the original measurement and the detector correction is shown in Figure 3.6. Attempts were made to increase the signal intensity relative to that of the matrix, and to measure larger biomolecules, but this only resulted in a decline of the mass resolution. However, it was possible to increase the relative angiotensin intensity by using delayed extraction, which suggests that the ionisation yields could have been increased because of gas-phase reactions.[96] This result support the earlier hypothesis of Chen and Vertes: the high optical pumping rates provided by these ultrashort pulses result in a reduced temporal overlap between the matrix ions and neutral biomolecules, which limits ionisation collection efficiency.[65]
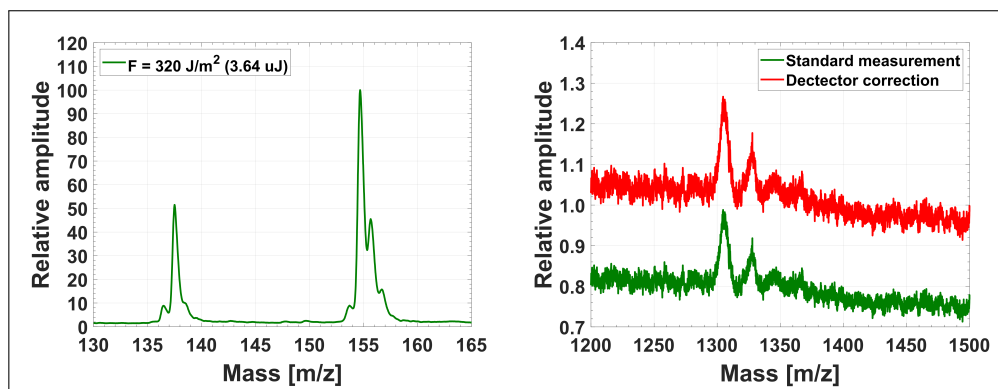
FIGURE 3.6: Angiotensin I was the largest biomolecule to be routinely measured. The intensity thereof was about two orders of magnitude less than that of the DHB matrix, even when considering a correction for the detector quantum efficiency. Reproduced with permission from the ACS.[76]

3.3   Bayesian deconvolution

Split-gradient deconvolution has been applied to the mass spectra obtained when studying ultrafast desorption, similar to the typical spectrum given in Figure 3.4. The resolution of these spectra was significantly improved when an appropriate deconvolution method was used, such as illustrated in Figure 3.7, where a second-differences prior was combined with the Lucy-Richardson algorithm. Because of

the mass improved resolution, it is possible to make a more concrete statement regarding the fragmentation process, given that it is now possible to determine the peak-to-peak ratios of additional ions. It should be mentioned that standard fitting routines could not be used for this purpose, as they are global methods and would, therefore, introduce local fitting artefacts.
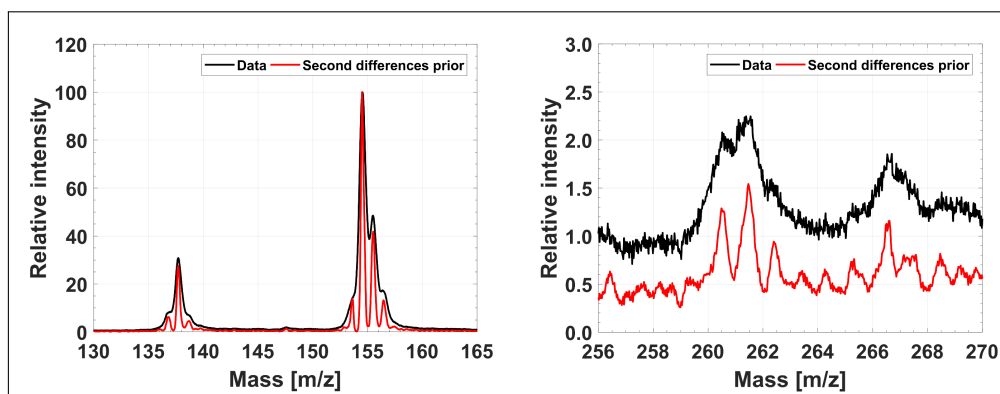
FIGURE 3.7: Comparison spectra of the DHB (m/z 154, left) and its dehydroxylated fragment (m/z 137, left), and the triphenylphosphine (m/z 262, right) ion after the deconvolution using Lucy-Richardson with the second-differences prior. Reproduced with permission from the ACS.[80]

As an example, when examining the region surrounding the DHB parent ion, the isotopic distribution thereof can be somewhat approximated. Likewise, very little can be said regarding the hydrogen loss for the DHB parent ion (m/z 153) and the dehydroxylated fragment thereof (m/z 136). However, when considering the deconvolved spectra, it is clear that all of these peaks are separated by a single atomic mass unit. The hydrogen loss could be investigated, as it is now possible to determine the ratio thereof to the parent ions (this pathway is also supported by the detection of hydrogen). Similar pathways have been reported for ultrafast dissociation studies, but could not be confirmed before deconvolution.[97, 98] In addition, it is also possible to identify the triphenylphosphine fragment utilising the isotopic signature thereof.[99] It is interesting to highlight that the increase in mass resolution (∼500 at m/z 154) is comparable in magnitude to what is often achievable by using delayed extraction.[100, 101]

The algorithm requires the following to be specified initially: the shape, prior distribution, statistics used (Poisson or Gaussian), and also the stopping criterion. These choices will depend on the dataset considered, and the validity of the given choice is determined by the quality of the recovered spectra and the convergence rates. For the discussed results a symmetric second-order polynomial peak shape was chosen, because the final results do not strongly depend on this peak shape. As previously mentioned, Poisson statistics outperforms Gaussian statistics and provide superior results, which is why only those results will be discussed.

It was found that one of the most challenging tasks was to define a universal stopping criterion. The convergence of entropy S could be also be used, however, it proved difficult to generalise since its behaviour depended on the given priors. Fortunately, within the literature, there are extensive discussions on the residuals, which is why it was decided to use the residual distribution as this convergence monitor.[72] To generalise the stopping criterion, the difference in the mean of the

residuals $\Delta\varepsilon$ was employed, in comparison to the mean of residuals ε, which was shown to likewise depend on the dataset and the choice of priors.

The convergence behaviours of the standard Lucy-Richardson algorithm ($\mathbb{B}_0$) and the second-differences prior ($\mathbb{B}_3$) are compared in Figure 3.8. It was shown that these trends agree qualitatively with those of the entropy convergence plots. Importantly, the difference in the entropy ΔS will decrease when reaching a local or global minimum. Should this happen (by monitoring a predefined threshold), then the strength of the prior was reduced by using the regularization parameter. The idea of reducing the strength of the prior is similar to the boost mechanism of Miroslav and was proved to be successful in removing the solution out of local minima.[102] In addition, this concept ensures that all of these methods converge to the same final entropy and thus allowed quantitative comparisons to be made. However, it should be emphasised that using a prior is not valuable by default. Compared to the Lucy-Richardson, only the second-difference prior offered the improved performance (152 versus 361 iterations) and quantification.
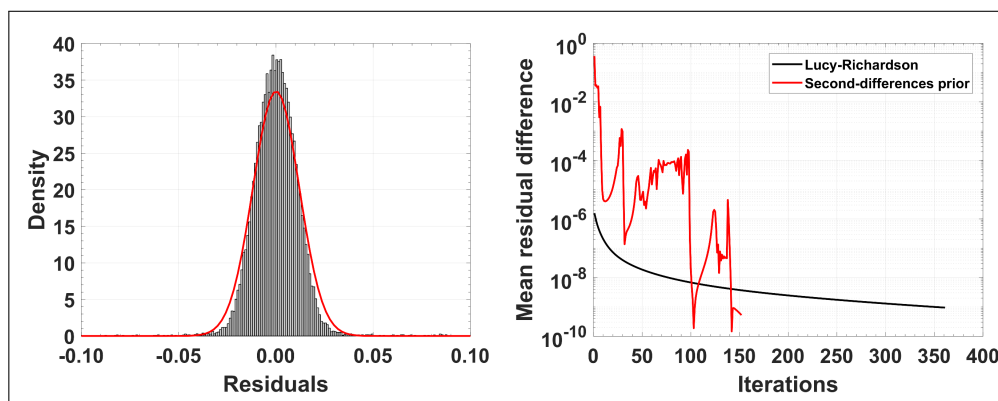
FIGURE 3.8: Residual distribution (left) for the second-differences prior ($\mathbb{B}_3$). The difference in the mean of residuals $\Delta\varepsilon$ are also compared (right) for this prior and standard Lucy-Richardson algorithm (note the convergence behaviours). Reproduced with permission from the ACS.[80]

Chapter 4

Conclusions and outlook

Within this thesis it has been demonstrated that there are numerous advantages to performing mass spectrometry measurements under the conditions of stress-confinement. Although desorption under these conditions has been theoretically described, only very few experiments have characterised the advantages thereof. Evaluation of this concept was performed at atmospheric conditions via usage of a picosecond infrared laser for studying bulk water and under vacuum conditions utilising a femtosecond ultraviolet laser with standard matrices.

The atmospheric studies indicated that the infrared picosecond laser (PIRL) produces mass spectra which qualitatively compare well to that of nebulisation techniques such as ESI, while enjoying the advantages of not requiring high voltages or gas pressures to be applied directly to the sample. Most importantly, it was illustrated that no secondary ionisation source is required, which renders this an attractive method for future mass spectrometry imaging studies because it has always been challenging to align the nebuliser with the desorption site in other techniques. Furthermore, the design of a lab-on-a-chip device enabled the localisation and individual extraction of small sample volumes.

To my knowledge, the in-vacuum experiments demonstrated for the first time that it is now possible to separate the desorption and ionisation processes with the application of ultrashort pulses. This observation was made when it was shown that the survival yields (intensity of the fragment ions relative to the parent ion) of the thermometer ions are independent of the laser pulse energies; the survival yield for the matrix decreases for the larger pulse energies without transferring any additional energy to the thermometer ions. In addition, these measurements were performed in transmission geometry, which reinforces the earlier belief that such a configuration does not pose a disadvantage over reflection (front ablation) geometries. Moreover, a Bayesian deconvolution framework was developed and characterised to improve the quantification of these fragmentation spectra. The algorithm displayed itself to be robust and capable of successfully deconvolving the time-of-flight results, with the advantage of being significantly faster than the conventional Lucy-Richardson algorithm and introducing fewer artefacts.

The most important observation made in this thesis was that both desorption and ionisation processes could be separated. Having the ability to do this, allows unprecedented control over the dynamics of the desorption process because any changes to the desorption parameters will not significantly affect the ionisation. It will be possible to take full advantage of this concept with the implementation of post-ionisation. Preliminary studies have already demonstrated the potential of post-ionisation schemes, but fragmentation was still observed, due to the transfer of internal energy. By eliminating both the transfer of energy during desorption and increasing the sensitivity, I believe that mass spectrometry measurements can genuinely be made quantitative.

Acknowledgements

I would like to start by thanking Prof. R. J. Dwayne Miller for the opportunity to form part of his research group. While being part of this group in Hamburg, I learned plenty regarding the inner workings of the greater scientific community and about what it takes to perform quality research, not just in terms of scientific originality, but also with regards to the practical applications. I should emphasise that it was a great privilege to have the academic freedom facilitated in the Miller group, and that there are very few research institutes which would allow you to pursue your own ideas independently with such blind trust.

The people with whom I spent the largest amount of time during my studies were my fellow group members. Being part of this group was a great experience, and I have so many happy, unforgettable memories. There is, however, a handful of people who need further recognition. On my day to day basis, I spent the vast majority of my time in the company of Yinfei Lu and Frederik Busse. There were times when we practically lived together in the laboratory! I am forever grateful for these memories and all of the assistance you provided me with my projects. I also need to thank our group leader, Wesley Robertson, who always ensured that we stay focused and on track. The support which Friedjof Tellkamp provided to us is not quantifiable; he has been essential to the success of this project. Similarly, the engineering support and feedback provided by Josef Gonschior and Djordje Gitaric were valuable. I am also indebted to Sascha Epp for his kind assistance in helping me finalise my thesis. I would also like to thank Sonia Utermann and Julia Quante, who were the coordinators of the Max Planck Research School IMPRS-UFAST for all of their invaluable advice and guidance. I also received a great deal of support and guidance from Michiel de Kock and Hans Eggers with regards to the Bayesian analysis project, for which I am very grateful.

I especially need to thank Prof. Dr. Arwen Pearson both for the support and guidance she has provided to me over the years. I will forever be grateful for the time and effort she invested to assist me in developing myself during my doctoral studies. She is an example of what people should aspire to, not just as a scientist, but also as a human being. The support from her group was invaluable.

I have been very fortunate to continue my career as a scientist within the group of Prof. Ian Gilmore before submitting my thesis. It is crucial for me to highlight how supporting and motivating he has been during this (hard) transition period. For me, it is a great honour to be part of his group, and I am excited about what the future holds. In a similar vein, it goes without saying that it is a tremendous inspiration for me to share an office with Dr. Martin Seah. Especially during the stressful period of simultaneously working on my thesis and finding the ropes of a national laboratory, he kept me motived and excited about the beauty of science.

Last but not least, the most important people to thank are my lovely parents, Cornelius and Marianna Pieterse. I cannot even find the words to explain to the world just how amazing they are. They are the most remarkable parents any person could have ever wished for! None of this would have been possible without their constant love and support. They always fully supported me with my choices in life, independent if I failed or succeeded. Together with my family, my friends have been just as essential to my overall happiness with life and for me to finish my doctorate. I am immensely grateful to have you all in my life. Thank you.

Bibliography

[1] McLafferty, F. W. A Century of Progress in Molecular Mass Spectrometry. *Annual Review of Analytical Chemistry* **2011**, *4*, 1–22.

[2] Burnum, K. E.; Frappier, S. L.; Caprioli, R. M. Matrix-Assisted Laser Desorption/Ionization Imaging Mass Spectrometry for the Investigation of Proteins and Peptides. *Annual Review of Analytical Chemistry* **2008**, *1*, 689–705.

[3] Winograd, N. Gas Cluster Ion Beams for Secondary Ion Mass Spectrometry. *Annual Review of Analytical Chemistry* **2018**, *11*, annurev–anchem–061516–045249.

[4] Biemann, K. Mass Spectrometry. *Annual Review of Biochemistry* **1963**, *32*, 755–780.

[5] Dreisewerd, K. The Desorption Process in MALDI. *Chemical Reviews* **2003**, *103*, 395–426.

[6] Tanaka, K.; Waki, H.; Ido, Y.; Akita, S.; Yoshida, Y.; Yoshida, T.; Matsuo, T. Protein and polymer analyses up to m/z 100 000 by laser ionization time-of-flight mass spectrometry. *Rapid Communications in Mass Spectrometry* **1988**, *2*, 151–153.

[7] Karas, M.; Hillenkamp, F. Laser Desorption Ionization of Proteins with Molecular Masses Exceeding 10 000 Daltons. *Analytical Chemistry* **1988**, *60*, 2299–2301.

[8] Yamashita, M.; Fenn, J. B. Electrospray ion source. Another variation on the free-jet theme. *The Journal of Physical Chemistry* **1984**, *88*, 4451–4459.

[9] Wilm, M.; Mann, M. Analytical Properties of the Nanoelectrospray Ion Source. *Analytical Chemistry* **1996**, *68*, 1–8.

[10] Fenn, J. B.; Mann, M.; Meng, C. K.; Wong, S. F.; Whitehouse, C. M. Electrospray ionization for mass spectrometry of large biomolecules. *Science* **1989**, *246*, 64–71.

[11] Takats, Z.; Wiseman, J. M.; Gologan, B.; Cooks, R. G. Mass spectrometry sampling under ambient conditions with desorption electrospray ionization. *Science (New York, N.Y.)* **2004**, *306*, 471–473.

[12] Lee, J.; Soper, S. A.; Murray, K. K. Microfluidics with MALDI analysis for proteomicsâĂŤA review. *Analytica Chimica Acta* **2009**, *649*, 180–190.

[13] Caprioli, R. M.; Farmer, T. B.; Gile, J. Molecular Imaging of Biological Samples: Localization of Peptides and Proteins Using MALDI-TOF MS. *Analytical Chemistry* **1997**, *69*, 4751–4760.

[14] Murray, K. K.; Russell, D. H. Liquid Sample Introduction for Matrix-Assisted Laser Desorption Ionization. *Analytical Chemistry* **1993**, *65*, 2534–2537.

[15] Li, L.; Wang, A. P. L.; Coulson, L. D. Continuous-flow matrix-assisted laser desorption ionization mass spectrometry. *Analytical Chemistry* **1993**, *65*, 493–495.

[16] Nemes, P.; Vertes, A. Laser Ablation Electrospray Ionization for Atmospheric Pressure, in Vivo, and Imaging Mass Spectrometry. *Analytical Chemistry* **2007**, *79*, 8098–8106.

[17] Sampson, J. S.; Hawkridge, A. M.; Muddiman, D. C. Generation and Detection of Multiply-Charged Peptides and Proteins by Matrix-Assisted Laser Desorption Electrospray Ionization (MALDESI) Fourier Transform Ion Cyclotron Resonance Mass Spectrometry. *Journal of the American Society for Mass Spectrometry* **2006**, *17*, 1712–1716.

[18] Rezenom, Y. H.; Dong, J.; Murray, K. K. Infrared laser-assisted desorption electrospray ionization mass spectrometry. *The Analyst* **2008**, *133*, 226–232.

[19] Trimpin, S.; Inutan, E. D.; Herath, T. N.; McEwen, C. N. Matrix-Assisted Laser Desorption/Ionization Mass Spectrometry Method for Selectively Producing Either Singly or Multiply Charged Molecular Ions. *Analytical Chemistry* **2010**, *82*, 11–15.

[20] Hiraoka, K.; Saito, S.; Katsuragawa, J.; Kudaka, I. A new liquid chromatography/mass spectrometry interface: laser spray. *Rapid Communications in Mass Spectrometry* **1998**, *12*, 1170–1174.

[21] Kudaka, I.; Kojima, T.; Saito, S.; Hiraoka, K. A comparative study of laser spray and electrospray. *Rapid Communications in Mass Spectrometry* **2000**, *14*, 1558–1562.

[22] Hiraoka, K. Laser spray: Electric field-assisted matrix-assisted laser desorption/ionization. *Journal of Mass Spectrometry* **2004**, *39*, 341–350.

[23] Laiko, V. V.; Taranenko, N. I.; Berkout, V. D.; Yakshin, M. a.; Prasad, C. R.; Lee, H. S.; Doroshenko, V. M. Desorption/ionization of biomolecules from aqueous solutions at atmospheric pressure using an infrared laser at 3 μm. *Journal of the American Society for Mass Spectrometry* **2002**, *13*, 354–361.

[24] Hiraguchi, R.; Hazama, H.; Masuda, K.; Awazu, K. Atmospheric pressure laser desorption/ionization using a 6-7 μm-band mid-infrared tunable laser and liquid water matrix. *Journal of Mass Spectrometry* **2015**, *50*, 65–70.

[25] Coon, J. J.; Harrison, W. W. Laser desorption-atmospheric pressure chemical ionization mass spectrometry for the analysis of peptides from aqueous solutions. *Analytical Chemistry* **2002**, *74*, 5600–5605.

[26] Gurdak, E.; Green, F. M.; Rakowska, P. D.; Seah, M. P.; Salter, T. L.; Gilmore, I. S. VAMAS interlaboratory study for desorption electrospray ionization mass spectrometry (DESI MS) intensity repeatability and constancy. *Analytical Chemistry* **2014**, *86*, 9603–9611.

[27] Vogel, A.; Venugopalan, V. Mechanisms of pulsed laser ablation of biological tissues. *Chemical Reviews* **2003**, *103*, 577–644.

[28] Franjic, K.; Cowan, M. L.; Kraemer, D.; Miller, R. J. D. Laser selective cutting of biological tissues by impulsive heat deposition through ultrafast vibrational excitations. *Optics Express* **2009**, *17*, 22937.

[29] Franjic, K.; Miller, R. J. D. Vibrationally excited ultrafast thermodynamic phase transitions at the water/air interface. *Physical Chemistry Chemical Physics* **2010**, *12*, 5225–5239.

[30] Zhigilei, L. V.; Garrison, B. J. Microscopic mechanisms of laser ablation of organic solids in the thermal and stress confinement irradiation regimes. *Journal of Applied Physics* **2000**, *88*, 1281–1298.

[31] Ren, L.; Robertson, W. D.; Reimer, R.; Heinze, C.; Schneider, C.; Eggert, D.; Truschow, P.; Hansen, N.-O.; Kroetz, P.; Zou, J.; Miller, R. J. D. Towards instantaneous cellular level bio diagnosis: laser extraction and imaging of biological entities with conserved integrity and activity. *Nanotechnology* **2015**, *26*, 284001.

[32] Kwiatkowski, M.; Wurlitzer, M.; Omidi, M.; Ren, L.; Kruber, S.; Nimer, R.; Robertson, W. D.; Horst, A.; Miller, R. J.; Schlüter, H. Ultrafast extraction of proteins from tissues using desorption by impulsive vibrational excitation. *Angewandte Chemie International Edition* **2015**, *54*, 285–288.

[33] Zou, J.; Wu, C.; Robertson, W. D.; Zhigilei, L. V.; Miller, R. J. D. Molecular dynamics investigation of desorption and ion separation following picosecond infrared laser (PIRL) ablation of an ionic aqueous protein solution. *The Journal of Chemical Physics* **2016**, *145*, 204202.

[34] Feng, X.; Liu, B.-F.; Li, J.; Liu, X. Advances in coupling microfluidic chips to mass spectrometry. *Mass Spectrometry Reviews* **2015**, *34*, 535–557.

[35] Gao, D.; Liu, H.; Jiang, Y.; Lin, J.-M. Recent advances in microfluidics combined with mass spectrometry: technologies and applications. *Lab on a Chip* **2013**, *13*, 3309.

[36] Urban, P. L.; Amantonico, A.; Zenobi, R. Lab-on-a-plate: Extending the functionality of MALDI-MS and LDI-MS targets. *Mass Spectrometry Reviews* **2011**, *30*, 435–478.

[37] Oedit, A.; Vulto, P.; Ramautar, R.; Lindenburg, P. W.; Hankemeier, T. Lab-on-a-Chip hyphenation with mass spectrometry: Strategies for bioanalytical applications. *Current Opinion in Biotechnology* **2015**, *31*, 79–85.

[38] Koster, S.; Verpoorte, E. A decade of microfluidic analysis coupled with electrospray mass spectrometry: An overview. *Lab on a Chip* **2007**, *7*, 1394.

[39] Lazar, I. M.; Grym, J.; Foret, F. Microfabricated devices: A new sample introduction approach to mass spectrometry. *Mass Spectrometry Reviews* **2006**, *25*, 573–594.

[40] Chambers, A. G.; Ramsey, J. M. Microfluidic Dual Emitter Electrospray Ionization Source for Accurate Mass Measurements. *Analytical Chemistry* **2012**, *84*, 1446–1451.

[41] Gibson, G. T.; Mugo, S. M.; Oleschuk, R. D. Nanoelectrospray emitters: Trends and perspective. *Mass Spectrometry Reviews* **2009**, *28*, 918–936.

[42] Nissilä, T.; Sainiemi, L.; Sikanen, T.; Kotiaho, T.; Franssila, S.; Kostiainen, R.; Ketola, R. A. Silicon micropillar array electrospray chip for drug and biomolecule analysis. *Rapid Communications in Mass Spectrometry* **2007**, *21*, 3677–3682.

[43] Mao, P.; Gomez-Sjoberg, R.; Wang, D. Multinozzle Emitter Array Chips for Small-Volume Proteomics. *Analytical Chemistry* **2013**, *85*, 816–819.

[44] Bunnage, M. E.; Chekler, E. L. P.; Jones, L. H. Target validation using chemical probes. *Nature Chemical Biology* **2013**, *9*, 195–199.

[45] Scannell, J. W.; Blanckley, A.; Boldon, H.; Warrington, B. Diagnosing the decline in pharmaceutical R&D efficiency. *Nature Reviews Drug Discovery* **2012**, *11*, 191–200.

[46] Walgren, J. L.; Thompson, D. C. Application of proteomic technologies in the drug development process. *Toxicology Letters* **2004**, *149*, 377–385.

[47] Hsieh, Y.; Chen, J.; Korfmacher, W. A. Mapping pharmaceuticals in tissues using MALDI imaging mass spectrometry. *Journal of Pharmacological and Toxicological Methods* **2007**, *55*, 193–200.

[48] Zavalin, A.; Yang, J.; Caprioli, R. Laser beam filtration for high spatial resolution MALDI imaging mass spectrometry. *Journal of the American Society for Mass Spectrometry* **2013**, *24*, 1153–1156.

[49] Zavalin, A.; Yang, J.; Haase, A.; Holle, A.; Caprioli, R. Implementation of a gaussian beam laser and aspheric optics for high spatial resolution MALDI imaging MS. *Journal of the American Society for Mass Spectrometry* **2014**, *25*, 1079–1082.

[50] Chaurand, P.; Schriver, K. E.; Caprioli, R. M. Instrument design and characterization for high resolution MALDI-MS imaging of tissue sections. *Journal of Mass Spectrometry* **2007**, *42*, 476–489.

[51] Steven, R. T.; Race, A. M.; Bunch, J. Probing the Relationship Between Detected Ion Intensity, Laser Fluence, and Beam Profile in Thin Film and Tissue in MALDI MSI. *Journal of The American Society for Mass Spectrometry* **2016**, *27*, 1419–1428.

[52] Wiegelmann, M.; Dreisewerd, K.; Soltwisch, J. Influence of the Laser Spot Size, Focal Beam Profile, and Tissue Type on the Lipid Signals Obtained by MALDI-MS Imaging in Oversampling Mode. *Journal of the American Society for Mass Spectrometry* **2016**, *27*, 1952–1964.

[53] Heise, T. W.; Yeung, E. S. Dynamics of matrix-assisted laser desorption as revealed by the associated acoustic signal. *Analytica Chimica Acta* **1995**, *299*, 377–385.

[54] Lennon, J. D.; Glish, G. L. A MALDI Probe for Mass Spectrometers. *Analytical Chemistry* **1997**, *69*, 2525–2529.

[55] Schürenberg, M.; Schulz, T.; Dreisewerd, K.; Hillenkamp, F. Matrix-assisted laser desorption/ionization in transmission geometry: Instrumental implementation and mechanistic implications. *Rapid Communications in Mass Spectrometry* **1996**, *10*, 1873–1880.

[56] Vertes, A.; Balazs, L.; Gijbels, R. Matrix-assisted laser desorption of peptides in transmission geometry. *Rapid Communications in Mass Spectrometry* **1990**, *4*, 263–266.

[57] Zavalin, A.; Yang, J.; Hayden, K.; Vestal, M.; Caprioli, R. M. Tissue protein imaging at 1 μm laser spot diameter for high spatial resolution and high imaging speed using transmission geometry MALDI TOF MS. *Analytical and Bioanalytical Chemistry* **2015**, *407*, 2337–2342.

[58] Hortal, A. R.; Hurtado, P.; Martínez-Haya, B.; Mullins, O. C. Molecular-weight distributions of coal and petroleum asphaltenes from laser desorption/ionization experiments. *Energy and Fuels* **2007**, *21*, 2863–2868.

[59] Pomerantz, A. E.; Hammond, M. R.; Morrow, A. L.; Mullins, O. C.; Zare, R. N. Two-step laser mass spectrometry of asphaltenes. *Journal of the American Chemical Society* **2008**, *130*, 7216–7217.

[60] Wu, Q.; Pomerantz, A. E.; Mullins, O. C.; Zare, R. N. Minimization of fragmentation and aggregation by laser desorption laser ionization mass spectrometry. *Journal of the American Society for Mass Spectrometry* **2013**, *24*, 1116–1122.

[61] Luo, G.; Marginean, I.; Vertes, A. Internal Energy of Ions Generated by Matrix-Assisted Laser Desorption/Ionization. *Analytical Chemistry* **2002**, *74*, 6185–6190.

[62] Demirev, P.; Westman, A.; Reimann, C. T.; Håkansson, P.; Barofsky, D.; Sundqvist, B. U. R.; Cheng, Y. D.; Seibt, W.; Siegbahn, K. Matrix-assisted laser desorption with ultra-short laser pulses. *Rapid Communications in Mass Spectrometry* **1992**, *6*, 187–191.

[63] Dreisewerd, K.; Schürenberg, M.; Karas, M.; Hillenkamp, F. Matrix-assisted laser desorption/ionization with nitrogen lasers of different pulse widths. *International Journal of Mass Spectrometry and Ion Processes* **1996**, *154*, 171–178.

[64] Papantonakis, M. R.; Kim, J.; Hess, W. P.; Haglund, R. F. What do matrix-assisted laser desorption/ionization mass spectra reveal about ionization mechanisms? *Journal of Mass Spectrometry* **2002**, *37*, 639–647.

[65] Chen, Y.; Vertes, A. Pumping Rate and Surface Morphology Dependence of Ionization Processes in Matrix-Assisted Laser Desorption Ionization. *The Journal of Physical Chemistry A* **2003**, *107*, 9754–9761.

[66] Luo, G.; Marginean, I.; Ye, L.; Vertes, A. Competing ion decomposition channels in matrix-assisted laser desorption ionization. *Journal of Physical Chemistry B* **2008**, *112*, 6952–6956.

[67] Knochenmuss, R.; Dubois, F.; Dale, M. J.; Zenobi, R. The matrix suppression effect and ionization mechanisms in matrix-assisted laser desorption/ionization. *Rapid Communications in Mass Spectrometry* **1996**, *10*, 871–877.

[68] Derwa, F.; De Pauw, E.; Natalis, P. New Basis for a Method for the Estimation of Secondary Ion Internal Energy-Distribution in Soft Ionization Techniques. *Organic Mass Spectrometry* **1991**, *26*, 117–118.

[69] Gabelica, V.; Schulz, E.; Karas, M. Internal energy build-up in matrix-assisted laser desorption/ionization. *Journal of Mass Spectrometry* **2004**, *39*, 579–593.

[70] Lu, Y.; Pieterse, C. L.; Robertson, W. D.; Miller, R. J. D. Soft Picosecond Infrared Laser Extraction of Highly Charged Proteins and Peptides from Bulk Liquid Water for Mass Spectrometry. *Analytical Chemistry* **2018**, *90*, 4422–4428.

[71] Skilling, J. In *Maximum Entropy and Bayesian Methods*; Skilling, J., Ed.; Springer Netherlands: Dordrecht, 1989.

[72] Puetter, R.; Gosnell, T.; Yahil, A. Digital Image Reconstruction: Deblurring and Denoising. *Annual Review of Astronomy and Astrophysics* **2005**, *43*, 139–194.

[73] Narayan, R.; Nityananda, R. Maximum Entropy Image Restoration in Astronomy. *Annual Review of Astronomy and Astrophysics* **1986**, *24*, 127–170.

[74] Lu, Y.; Pieterse, C. L.; Eggert, D.; Ip, C.; Busse, F.; Keskin, S.; Robertson, W. D.; Miller, R. J. D. Direct Laser Sampling of Aqueous Solutions from Lab-on-a-Chip Devices for Mass Spectrometry. *Lab on a Chip (submitted)* **2018**, 0.

[75] Jecklin, M. C.; Touboul, D.; Bovet, C.; Wortmann, A.; Zenobi, R. Which Electrospray-Based Ionization Method Best Reflects Protein-Ligand Interactions Found in Solution? A Comparison of ESI, nanoESI, and ESSI for the Determination of Dissociation Constants with Mass Spectrometry. *Journal of the American Society for Mass Spectrometry* **2008**, *19*, 332–343.

[76] Pieterse, C. L.; Busse, F.; Tellkamp, F.; Robertson, W. D.; Miller, R. J. D. Femtosecond Pumping Rate Dependence of Fragmentation Mechanisms in Matrix-Assisted Laser Desorption Ionization. *Journal of Physical Chemistry (to be submitted)* **2018**, 0.

[77] Milasinovic, S.; Cui, Y.; Gordon, R. J.; Hanley, L. Internal energy of thermometer ions formed by femtosecond laser desorption: Implications for mass spectrometric imaging. *Journal of Physical Chemistry C* **2014**, *118*, 28938–28947.

[78] Liu, R.; Li, Q.; Smith, L. M. Detection of Large Ions in Time-of-Flight Mass Spectrometry: Effects of Ion Mass and Acceleration Voltage on Microchannel Plate Detector Response. *Journal of The American Society for Mass Spectrometry* **2014**, *25*, 1374–1383.

[79] Gilmore, I. S.; Seah, M. P. Ion detection efficiency in SIMS: Dependencies on energy, mass and composition for microchannel plates used in mass spectrometry. *International Journal of Mass Spectrometry* **2000**, *202*, 217–229.

[80] Pieterse, C. L.; de Kock, M. B.; Robertson, W. D.; Eggers, H. C.; Miller, R. D. Rapid deconvolution of low-resolution time-of-flight data using Bayesian inference. *Analytical chemistry (to be submitted)* **2018**, 0.

[81] Lucy, L. B. An iterative technique for the rectification of observed distributions. *The Astronomical Journal* **1974**, *79*, 745.

[82] Richardson, W. H. Bayesian-Based Iterative Method of Image Restoration. *Journal of the Optical Society of America* **1972**, *62*, 55.

[83] Crimins, F. Numerical recipes in C++: The art of scientific computing. *Applied Biochemistry and Biotechnology* **2003**, *104*, 95–96.

[84] Lantéri, H.; Roche, M.; Aime, C. Penalized maximum likelihood image restoration with positivity constraints: Multiplicative algorithms. *Inverse Problems* **2002**, *18*, 1397–1419.

[85] Lantéri, H.; Roche, M.; Cuevas, O.; Aime, C. A general method to devise maximum-likelihood signal restoration multiplicative algorithms with non-negativity constraints. *Signal Processing* **2001**, *81*, 945–974.

[86] Gilpin, R. K.; Zhou, W. Studies of the Thermal Degradation of Acetaminophen Using a Conventional HPLC Approach and Electrospray Ionization-Mass Spectrometry. *Journal of Chromatographic Science* **2004**, *42*, 15–20.

[87] Konermann, L.; Douglas, D. J. Unfolding of proteins monitored by electrospray ionization mass spectrometry: a comparison of positive and negative ion modes. *Journal of The American Society for Mass Spectrometry* **1998**, *9*, 1248–1254.

[88] Jecklin, M. C.; Touboul, D.; Bovet, C.; Wortmann, A.; Zenobi, R. Which electrospray-based ionization method best reflects protein-ligand interactions found in solution? A comparison of ESI, nanoESI, and ESSI for the determination of dissociation constants with mass spectrometry. *Journal of The American Society for Mass Spectrometry* **2011**, *19*, 332–343.

[89] Qiao, L.; Sartor, R.; Gasilova, N.; Lu, Y.; Tobolkina, E.; Liu, B.; Girault, H. H. Electrostatic-spray ionization mass spectrometry. *Analytical Chemistry* **2012**, *84*, 7422–7430.

[90] Qiao, H.; Spicer, V.; Ens, W. The effect of laser profile, fluence, and spot size on sensitivity in orthogonal-injection matrix-assisted laser desorption/ionization time-of-flight mass spectrometry. *Rapid Communications in Mass Spectrometry* **2008**, *22*, 2779–2790.

[91] Dreisewerd, K.; Schürenberg, M.; Karas, M.; Hillenkamp, F. Influence of the laser intensity and spot size on the desorption of molecules and ions in matrix-assisted laser desorption/ionization with a uniform beam profile. *International Journal of Mass Spectrometry and Ion Processes* **1995**, *141*, 127–148.

[92] Ahn, S. H.; Park, K. M.; Bae, Y. J.; Kim, M. S. Quantitative reproducibility of mass spectra in matrix-assisted laser desorption ionization and unraveling of the mechanism for gas-phase peptide ion formation. *Journal of Mass Spectrometry* **2013**, *48*, 299–305.

[93] Knochenmuss, R. The Coupled Chemical and Physical Dynamics Model of MALDI. *Annual Review of Analytical Chemistry* **2016**, *9*, 365–385.

[94] Bae, Y. J.; Kim, M. S. A Thermal Mechanism of Ion Formation in MALDI. *Annual Review of Analytical Chemistry* **2015**, *8*, 41–60.

[95] Christian, N. P.; Colby, S. M.; Giver, L.; Houston, C. T.; Arnold, R. J.; Ellington, A. D.; Reiily, J. P. High resolution matrix-assisted laser desorption/ionization time-of-flight analysis of single-stranded DNA of 27 to 68 nucleotides in length. *Rapid Communications in Mass Spectrometry* **1995**, *9*, 1061–1066.

[96] Wang, B. H.; Dreisewerd, K.; Bahr, U.; Karas, M.; Hillenkamp, F. Gas-Phase cationization and protonation of neutrals generated by matrix-assisted laser desorption. *Journal of the American Society for Mass Spectrometry* **1993**, *4*, 393–398.

[97] Weinkauf, R.; Aicher, P.; Wesley, G.; Grotemeyer, J.; Schlag, E. W. Femtosecond versus Nanosecond Multiphoton Ionization and Dissociation of Large Molecules. *The Journal of Physical Chemistry* **1994**, *98*, 8381–8391.

[98] Smith, D. J.; Ledingham, K. W.; Kilic, H. S.; McCanny, T.; Peng, W. X.; Singhal, R. P.; Langley, A. J.; Taday, P. F.; Kosmidis, C. Ionization and dissociation of benzaldehyde using short intense laser pulses. *Journal of Physical Chemistry A* **1998**, *102*, 2519–2526.

[99] Claereboudt, J.; Claeys, M.; Geise, H.; Gijbels, R.; Vertes, A. Laser microprobe mass spectrometry of quaternary phosphonium salts: Direct versus matrix-assisted laser desorption. *Journal of the American Society for Mass Spectrometry* **1993**, *4*, 798–812.

[100] Vestal, M. L.; Juhasz, P.; Martin, S. a. Delayed Extraction Matrix-assisted Laser Desorption Time-of-flight Mass Spectrometry. *Rapid communications in mass spectrometry : RCM* **1995**, *9*, 1044–1050.

[101] Brown, R. S.; Lennon, J. J. Mass Resolution Improvement by Incorporation of Pulsed Ion Extraction in a Matrix-Assisted Laser Desorption/Ionization Linear Time-of-Flight Mass Spectrometer. *Analytical Chemistry* **1995**, *67*, 1998–2003.

[102] Morháč, M. Deconvolution methods and their applications in the analysis of -ray spectra. *Nuclear Instruments and Methods in Physics Research Section A: Accelerators, Spectrometers, Detectors and Associated Equipment* **2006**, *559*, 119–123.

Appendix A

Peer-reviewed publications

Soft Picosecond Infrared Laser Extraction of Highly Charged Proteins and Peptides from Bulk Liquid Water for Mass Spectrometry

Yinfei Lu, <u>Cornelius L. Pieterse</u>, Wesley D. Robertson, and R. J. Dwayne Miller
Analytical Chemistry, **90**(7), 4422–4428 (2018)

The paper was accepted for publication on 9 March 2018.

Direct Laser Sampling of Aqueous Solutions from Lab-on-a-Chip Devices for Mass Spectrometry

Yinfei Lu, <u>Cornelius L. Pieterse</u>, Dennis Eggert, Candice Ip, Frederik Busse, Sercan Keskin, Wesley D. Robertson, and R. J. Dwayne Miller
Under revision at Lab on a Chip.

The version presented here represents the paper as submitted to *Lab on a Chip* on 15 December 2017. The suggestions received from the reviewers are currently being incorporated and will be resubmitted soon.

Femtosecond Pumping Rate Dependence of Fragmentation Mechanisms in Matrix-Assisted Laser Desorption Ionization

<u>Cornelius L. Pieterse</u>, Frederik Busse, Friedjof Tellkamp, Wesley D. Robertson, and R. J. Dwayne Miller
Prepared to submit to the Journal of Physical Chemistry.

The version presented here represents the draft from 28 February 2018 which was being approved for submission by co-authors at the time of thesis evaluation. An updated version was submitted to the journal on 23 June 2018.

Rapid Deconvolution of Low-Resolution Time-of-Flight Data using Bayesian Inference

<u>Cornelius L. Pieterse</u>, Michiel B. de Kock, Wesley D. Robertson, Hans C. Eggers, and R. J. Dwayne Miller
Prepared to submit to Analytical Chemistry.

As the Bayesian analysis was performed on the femtosecond desorption data, it was decided first to submit that paper, since it is heavily cited in this paper. The version presented here represents the final draft from 30 April 2018. An updated version was submitted to the journal on 07 June 2018.

analytical chemistry

Article

Soft Picosecond Infrared Laser Extraction of Highly Charged Proteins and Peptides from Bulk Liquid Water for Mass Spectrometry

Yinfei Lu, Cornelius L. Pieterse, Wesley D. Robertson, and R. J. Dwayne Miller*

Max Planck Institute for the Structure and Dynamics of Matter, Luruper Chaussee 149, Hamburg 22761, Germany

S Supporting Information

ABSTRACT: We report the soft laser extraction and production of highly charged peptide and protein ions for mass spectrometry directly from bulk liquid water at atmospheric pressure and room temperature, using picosecond infrared laser ablation. Stable ion signal from singly charged small molecules, as well as highly charged biomolecular ions, from aqueous solutions at low laser pulse fluence ($\sim$0.3 J cm^{-2}) is demonstrated. Sampling via single picosecond laser pulses is shown to extract less than 27 pL of volume from the sample, producing highly charged peptide and protein ions for mass spectrometry detection. The ablation and ion generation is demonstrated to be soft in nature, producing natively folded proteins ions under sample conditions described for native mass spectrometry. The method provides laser-based sampling flexibility, precision and control with highly charged ion production directly from water at low and near neutral pH. This approach does not require an additional ionization device or high voltage applied directly to the sample.
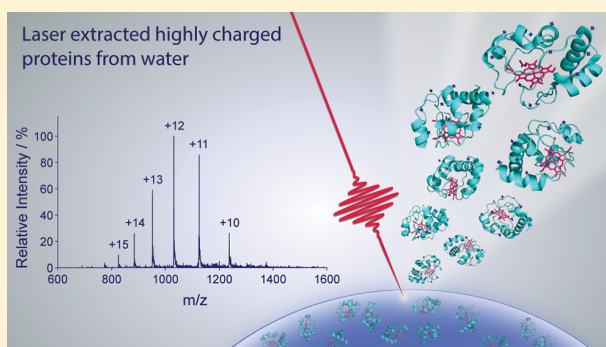
The soft precision controlled extraction of biomolecules from aqueous environments into the gas phase is a crucial step for investigating biological systems. The pioneering methods for large biomolecule gas phase ion production, which include electrospray ionization (ESI),[1] developed following the critical observation of ion production by charged droplet evaporation demonstrated by thermospray,[2] and matrix-assisted laser desorption/ionization (MALDI),[3,4] have facilitated extraordinary biological insight. ESI and subsequent ambient nebulization based methods, have been widely utilized for their ability to softly produce highly charged biomolecules, large proteins and noncovalently bonded complexes for analysis with high stability and sensitivity.[5−15] The highly charged species available has enabled the use of low mass-to-charge ratio (m/z) range mass spectrometers and facilitate fragmentation methods invaluable to proteomic identification.[16]

The control inherent to laser based techniques, such as MALDI, provides sampling flexibility and precision, which is extremely advantageous for high throughput and selective sampling, as well as for mass spectrometry (MS) imaging.[17,18] Conventional MALDI produces primarily singly charged analyte ions and is in general less soft than ESI.[19−21] The matrices employed can introduce undesirable artifacts to MS spectra and adversely affect pre-analysis sample processing for certain scenarios. Innovative solutions utilizing continuous flow liquid MALDI matrix coupled directly to vacuum for laser ionization have been developed to combine analysis with solution separation methods such as liquid chromatography.[22,23] As well, numerous techniques have been developed to enhance analyte charging by combining the laser irradiation

of matrix, tissue or aqueous solutions, with a secondary ionization device, with great success.[24−30] Atmospheric pressure (AP) MALDI systems have been utilized to ablate matrix material into the heated transfer capillary of the mass spectrometer where both highly charged peptide and protein ions were produced in the high temperature region.[31,32] The technique has been extended for the direct analysis of solution-analyte mixtures, producing highly charged species without the need for applied voltage, nebulizing gas, volatile solvents or laser irradiation termed "laserspray",[33,34] not to be confused with "laser spray" developed by Hiraoka et al. as described later. Liquid UV-MALDI at a lower laser pulse energy has been demonstrated to provide stable and sensitive (fmol) detection of highly charged ion production from both 2,5-dihydroxybenzoic acid (DHB) and cyano-4-hydroxycinnamic acid (CHCA) matrix mixtures in glycerol and trimethylamine.[35] Highly charged molecular species have also been observed from pulsed nanosecond infrared (IR) irradiation of glycerol matrixes at AP, but with limited sensitivity (50 pmol).[36] The vacuum IR ablation (0.3 to 7.5 J cm^{-2}) of standard matrix as well as water ice has been demonstrated for charged species up to 7+ for select biomolecules.[37−40]

The laser-induced production of highly charged biomolecular ions from liquid water was first demonstrated using IR heating based laser spray, which provided unique advantages over

ESI.[41−43] The method requires high laser power densities (>5 × 10^4 J cm^{−2} s^{−1}) provided by a continuous wave CO_2 laser (10.6 μm) to initiate thermally and acoustically unconfined ablation. A fast solvent flow is evaporated by the laser, which is focused within a stainless-steel nebulizer held at high voltage, to produce highly charged species similar to ESI.[41−43] The applicability of the method has been somewhat limited due to the rapid sample consumption inherent to the technique. Numerous AP-IR-MALDI (0.3 to 5 J cm^{−2}) studies utilizing pure water solutions, ice or a standard IR-matrix have demonstrated limited charging, producing singly and low charge state biomolecules similar in character to conventional MALDI.[44−48] Similar results have been observed for high-power pulsed irradiation (2.5 J cm^{−2}) using levitated water/methanol (1:1) microdroplets.[49] Additionally, sampling provided by pulsed IR irradiation, from a CO_2 laser (0.3 J cm^{−2}), of pure water-cytochrome c solutions held at a high voltage in atmosphere, resulted in spectra similar to ESI, although no other ions were observed from any other samples that were investigated, without ESI postionization.[50] Pulsed IR sampling of a continuous aqueous solution flow interface with post ionization, free of voltage applied directly to the sample, has been demonstrated for nanosecond (5.8 J cm^{−2}) and picosecond (1.9 J cm^{−2}) duration pulses. These methods both required secondary ESI ionization for highly charged ion production, though characterization of direct ionization was not the focus of the work.[27,30]

It is well established that the pulsed IR ablation of water is capable of driving a gas phase ablation plume at several times the speed of sound from the water surface.[51−53] We have shown that this entire process can be conformed to occur faster than both nucleation and cavitation shock wave formation, therefore ensuring the excess energy of the ablation process to be primarily localized in the translational energy of the excited water molecules.[52−54] These conditions are ideal for injecting nominally low vapor pressure water-soluble molecules into the gas phase with the least amount of fragmentation or thermally induced nonlinear processes for mass spectrometry applications. We have utilized picosecond infrared laser (PIRL) ablation, operating under the above-described desorption by impulsive vibrational excitation (DIVE)[52−54] conditions for the soft extraction of biological entities from tissue and water solutions analyzed offline following ablation and collection. The ablation method was shown to extract unmodified proteins and protein complexes with conserved quaternary structure, as well as functionally conserved enzymes, proteins and viruses.[55,56] The PIRL is tuned to 1-photon resonantly excite the vibrational stretching mode of water that relaxes directly to translational motions, driving water, and analyte molecules into the gas phase faster than both the thermal and acoustic relaxation times of the excited volume.[52−54] The physics of the ablation process are equally well adapted for any material removal or laser based biopsy with successful application to numerous clinical surgery scenarios[57−59] and as a cold laser tissue homogenizer to enhance proteome conservation.[60]

Here we apply pulsed picosecond infrared irradiation at low laser energies (40 μJ focused to 0.3 J cm^{−2}) for the soft, stable extraction and production of small molecule ions, as well as highly charged biological molecules, directly from bulk liquid water under atmospheric pressure. Notably, the setup is stable over long times with no secondary ionization device required. The method softly produces highly charged peptide and protein ions, which is typically characteristic for ESI, laser spray

and other nebulization based techniques, from pure liquid water over a broad pH range. The laser based method is mechanical contact free, does not require a high speed gas flow or voltage applied directly to the sample, and operates at low sample consumption rates (<27 pL per pulse) with limited energy transfer to the bulk sample. The method provides sampling flexibility for scenarios in which soft, precision online sampling is required.

■ EXPERIMENTAL METHODS

Experimental Setup. The DIVE-MS system (Figure 1) was constructed by replacing the spray chamber, nebulizer
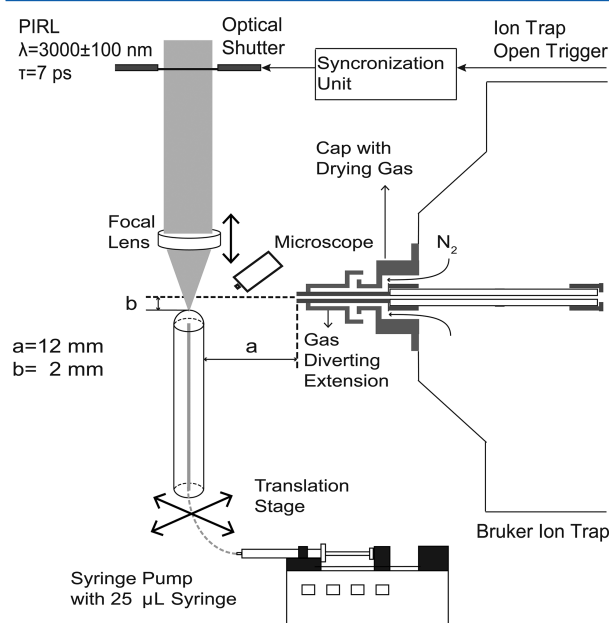
Figure 1. A schematic representation of the sample delivery, ablation, and modified ion trap MS system. Aqueous analyte solutions were delivered via capillary flow and ablated by a PIRL laser, collected and mass-analyzed by a modified ion trap mass spectrometer.

assembly, end plates, insulators and the transfer capillary mounting assembly of an ion trap mass spectrometer (Esquire 3000, Bruker) with a home designed and constructed interface for optimized access to the ablation plume. A long working distance microscope and sample delivery system was implemented to set and control the position of the ablated water/air interface to within 50 μm. Ablation pulses (either single pulse, pulse bursts or continuous 1 kHz operation) were delivered using a diode synchronized fast shutter and synchronized with ion trap collection via a home designed synchronization circuit and software. The sample delivery capillary, sample bead and ablation plume undergoing 1 kHz ablation is shown in Figure S1. A custom designed and constructed transfer capillary extension (Figure 1) was used to divert the heated nitrogen curtain gas (10 L min^{−1}), which also serves as the transfer capillary heating gas, away from the liquid sample and the ablation plume. The modification allowed full temperature and voltage control of the transfer capillary and avoided rapid sample evaporation. Noted in the text when utilized, the plume was also directly collected into the quartz transfer capillary through a standard planar spray shield end plate (Figure S2) held at high voltage. A reduced curtain gas
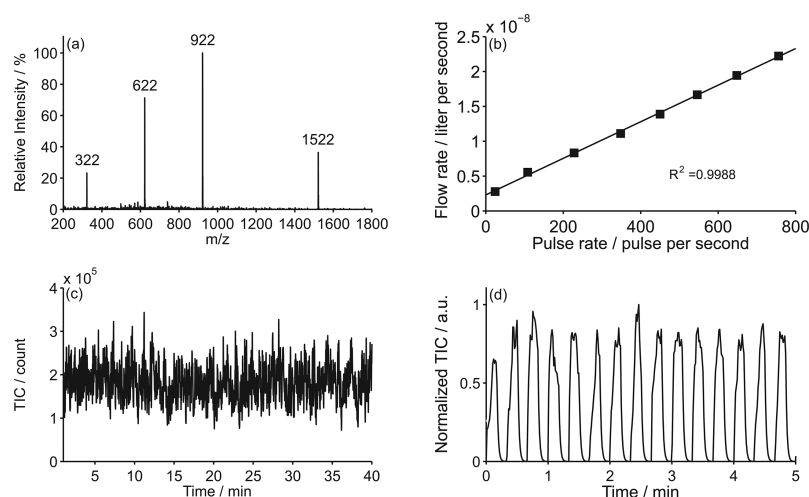
Figure 2. Characterization of PIRL-DIVE ablation of water samples. (a) DIVE-MS spectrum of $[M + H]^+$ of hexamethoxyphosphazene ($m/z = 322$), hexakis(2,2-difluoroethoxy)phosphazene ($m/z = 622$), hexakis(1H,1H,3H-tetrafluoropropoxy)phosphazene ($m/z = 922$), and hexakis(1H,1H,5H-octafluoropentoxy)phosphazene ($m/z = 1522$) from water containing trifluoroacetic acid ammonium salt (TFA) (93.1 μM) and 5% acetonitrile. The spectrum shown is the average of 5 s of data collection. (b) Sample flow rate versus pulse rate of DIVE ablation of the sample surface. The solid line represents the best fit ($R^2 = 0.9988$) of the data to a linear curve and resulted in a slope and y-intercept of $m = 26.2 \times 10^{-12}$ and $b = 2.30 \times 10^{-9}$, respectively. (c) Total ion current (TIC) versus time ($m/z = 200-2000$ range) for the same measurement as in panel a. (d) TIC versus time ($m/z = 500-1000$ range) during shuttering (20 s) of a 1 kHz ablation pulse train, confirming the DIVE ion signal dependence on laser ablation. Transfer capillary temperature was measured to be 139 °C.

flow (0.5 L min^{-1}) was used with this configuration to minimize sample evaporation and plume disruption. The actual transfer capillary temperature for all experiments was measured directly using a thermocouple. The measured value was lower than the set value when using the significantly reduced gas flow rate as well as with the collection extension. The actual measured transfer capillary temperature is noted in the text for all experiments. Nitrogen was used as the heating gas.

Sample delivery capillary tubing (precut natural PEEK, 1/16 in. outer diameter, and 0.030-in. inner diameter, TPK130, VICI) was connected to a syringe (Hamilton, 25 μL) and a syringe pump (KD Scientific) to set the sample flow rate. The exit of the PEEK sample capillary was cleaved and mounted with custom holders and mounts with the flat face of the sample capillary vertical and in front of the transfer capillary extension, or planar end plate, of the MS interface for sample ablation. The exit of the sample capillary was aligned 22 mm below the position of focal point of the laser beam. The PIRL laser was directed downward toward the sample capillary with the focal position located 12 mm away from the collection entrance and 2 mm directly below the MS ion transfer capillary axis. For each experiment, 25 μL of analyte solution was loaded into the sample syringe. A volume (<5 μL) was flushed through the PEEK tubing to produce a stable bead of aqueous sample solution (~1.9 μL), stabilized and maintained by optimizing the solution flow rate and ablation frequency. This resulted in the total amount of analyte loaded into the 25 μL syringe ranging between 250 fmol and 250 pmol, for 10 nM and 10 μM solutions, respectively. A digital long working distance microscope (Dino-lite, AD7013MTL (R4)) was used to image the sample bead. The resulting sample meniscus and laser ablation plume images provided feedback for system alignment and signal optimization. The syringe and peek sample tubing were flushed with acetone, isopropanol, and water (1 mL each), 3 cycles, between samples. This could be

accomplished in roughly 1 min. No sample contamination was observed.

DIVE-MS and ESI were performed under the optimized conditions for each method and the particular molecular species. The transfer capillary voltage of the ion trap MS was set to ±4500 V (negative and positive ion modes respectively), with a spray shield end plate offset of 500 V for both methods. Mass spectra were acquired using ESI, as the control, by mounting and optimizing the ESI nebulizer position at a right angle to the MS collection interface. Samples were delivered via a standard electrospray nebulizer (electrically grounded) with a helium nebulizer gas curtain (10 psi) and heated nitrogen curtain drying gas (10 L min^{-1}). All data were collected and analyzed using Bruker Daltonics Data Analysis software. The spectra displayed for both DIVE-MS and ESI-MS are the results of averaging 1 min of sample collection, unless when otherwise noted. The ion trap accumulation time was set to 50 ms. Collision induced dissociation measurements were performed with the precursor ion mass isolation window set to 4 mass units (m/z of the precursor ion ±2) and the fragmentation time to 40 ms. Helium was used as the collision gas and the fragmentation amplitude was varied to achieve the required degree of fragmentation. Throughout, ablation pulse bursts produced by a synchronized shutter operating at 6 Hz, containing 4 pulse bursts, and a sample flow rate of 167 nL min^{-1}, were found to be optimal and were thus employed, unless when otherwise noted.

Laser System. A PIRL, model PIRL-APLQ-3000 from Attodyne Inc., Canada, was used to deliver irradiation at the wavelength of 3000 ± 100 nm, with a pulse duration of 7 ps at a repetition rate of 1 kHz. A home-built optical system was used for beam delivery and equipped with a fast, diode synchronized high-speed external shutter for control of single and burst mode pulse selection with home designed LabVIEW software. The PIRL beam was focused onto the sample with a 25 mm calcium fluoride lens resulting in a transverse beam diameter ($1/e^2$) at

the focus of approximately 140 μm as measured by a WinCamD-FIR2−16-HRR camera. The DIVE ablation pulse energy was measured at the focal plane to be 40 μJ per pulse. The lens was adjusted to optimize ion production and ablation stability.

Sample Preparation. Stock samples and solutions of caffeine (≥99%, HPLC, MW 194.19), angiotensin I acetate salt hydrate (≥90%, HPLC, MW 1296.48), angiotensin II human (≥93%, HPLC, MW 1046.18), cytochrome *c* from equine heart (≥95%, SDS-PAGE, MW 12,384), lysozyme from chicken egg white (≥90%, single chain MW 14,300), acetic acid (≥99.99%), formic acid (LC-MS Ultra), and ammonium acetate (≥99%, HPLC), ammonium bicarbonate (≥99.5%, BioUltra), were purchased from Sigma-Aldrich Chemie GmbH (Munich, Germany). Deionized distilled water from a PURELAB Classics (>18.5 MΩ cm, ELGA) system was used. Ion trap ESI tuning mix (G2431a) was purchased from Agilent Deutschland GmbH (Waldbronn, Germany). All analytes, including peptides and proteins, were used without further purification.

All DIVE-MS solutions were prepared in pure deionized distilled water with or without acetic acid or formic acid (0.1−1%, v/v) as noted in the text. Native protein solutions were prepared on ice and in 10−50 mM ammonium acetate or ammonium bicarbonate buffer with the pH (7.0) adjusted as described previously.[10] ESI tuning mix was added to pure water at a ratio of 1:20 (v/v), resulting in a final solution containing; hexamethoxyphosphazene (71 nM, MW 321.14), hexakis (2,2-difluoroethoxy)phosphazene (357 nM, MW 621.19), hexakis (1H, 1H, 3H-tetrafluoropropoxy)phosphazene (986 nM, MW 921.19), hexakis (1H, 1H, 5H-octafluoropentoxy)phosphazene (949 nM, MW 1521.33) with trifluoroacetic acid ammonium salt (TFA) (93 μM) and 5% acetonitrile. ESI samples were prepared from the same stock solutions to the same analyte and acid concentration as the DIVE-MS samples.

■ RESULTS AND DISCUSSION

PIRL ablation was stabilized at the water/air interface by means of adjusting the sample surface via feedback from the long-working-distance microscope and by adjustments to the sample delivery and laser control system. The PIRL ablation rate for MS analysis was performed in burst mode at 6 Hz, 4 pulses per burst, unless otherwise noted. The DIVE-MS setup was characterized and optimized by using the phosphazene variants from ESI tuning mix dissolved in pure water. As shown in Figure 2a, direct ablation of the sample resulted in a spectrum composed of singly charged species, [M + H]$^+$, of hexamethoxyphosphazene (*m/z* = 322), hexakis(2,2-difluoroethoxy)phosphazene (*m/z* = 622), hexakis(1H,1H,3H-tetrafluoropropoxy)phosphazene (*m/z* = 922), and also hexakis(1H,1H,5H-octafluoropropoxy)phosphazene (*m/z* = 1522). The flow rate required to maintain the sample interface (±50 μm relative to the laser focal plane) over a range of pulse rates was measured and used to estimate the ablated volume of the liquid per laser pulse (Figure 2b). Ablation was performed at 6 Hz with the pulse number ranging from 4 to 126 pulses per burst (24−756 pulses per second). The resulting slope of the fitting curve indicated the extracted volume from the bulk water, per laser pulse, was less than 27 pL. This value corresponds to an effective DIVE extraction depth of ∼1.5 μm per pulse of the water surface, within the range predicted by fluid dynamics models.[50] Considering the analyte concentration and extraction volume, the hexamethoxyphosphazene ion, as shown in Figure 2a, is the result of the consumption of 223

amol analyte when averaging for 5 s. For the same sample, the spectrum following 1 s of signal averaging (24 ablation events) is still easily discernible (Figure S3), corresponding to 48 amol of analyte consumption. As shown in Figure 2c, the total ion current (TIC) was within 1 order of magnitude of that achieved with standard ESI (>10^5 counts). The closing of the laser shutter (20 s intervals) was implemented to segment 1 kHz pulse trains to confirm the ablation dependence of the MS signal. As shown in Figure 2d, the TIC decreased to baseline values following the shutter closing.

DIVE-MS was also applied to aqueous solutions of small molecule drugs and compared to standard ESI (Figure S4). Acetaminophen dissolved in water containing 0.5% formic acid (v/v) resulted in the characteristic protonated species, [M + H]$^+$ (*m/z* = 152), with no additional thermal or hydrolytic degradation fragment peaks, for which it is known to be susceptible.[61] Additionally, the singly charged species of acetaminophen were produced from pure water solutions (no acid added), with 10 nM solutions being successfully analyzed, corresponding to a total consumption of 39 amol of analyte (Figure S5). Caffeine dissolved in water containing 0.1% acetic acid (v/v) displayed characteristic protonated species [M + H]$^+$ (*m/z* = 195) as well, without additional fragmentation (Figure S4). Approximately an order of magnitude reduction in sample consumption was possible with DIVE-MS, as compared to standard ESI on the same modified mass spectrometer.

To evaluate the capabilities of DIVE-MS for highly charged ion production, the peptide angiotensin I (10 μM), in a water solution containing 0.1% formic acid, was analyzed (Figure 3a).
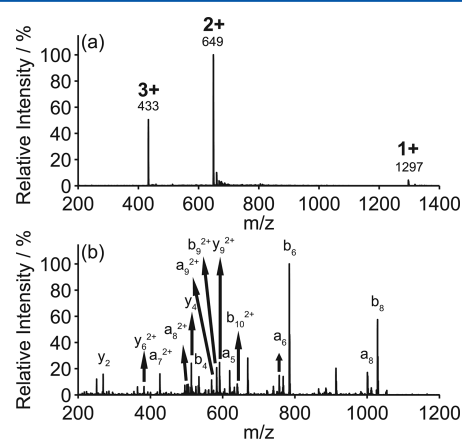
Figure 3. (a) DIVE-MS mass spectrum displaying the [M + H]$^+$, [M + 2H]$^{2+}$, and the [M + 3H]$^{3+}$ species of the peptide angiotensin I. The sample was 10 μM in water contained 0.1% formic acid (v/v). (b) DIVE-MS/MS CID spectrum of the doubly charged species, [M + 2H]$^{2+}$, of angiotensin I. Transfer capillary temperature was measured to be 199 °C.

The charged species observed following PIRL ablation of the aqueous peptide sample were similar in form to spectra generated by ESI (Figure S6a). The spectrum of angiotensin I indicated the [M + H]$^+$, [M+2H]$^{2+}$, and [M+3H]$^{3+}$ species at *m/z* = 1297, 649, and 433 respectively, with observable fractions (<10%) of adduct ions produced. The signal-to-noise obtained was comparable to that produced using standard ESI with the modified setup. For the spectrum shown, an order of magnitude decrease in the sample consumption rate was used as compared to ESI, 167 nL min^{-1} versus 3 μL min^{-1}, similar to

nanospray. The rate is adjustable and dependent on the laser sampling frequency as shown in Figure 2b. The TIC produced from the peptide solution was stable (Figure S7) and comparable in intensity to that of standard ESI, which facilitated the generation of DIVE-MS/MS spectra using fragmentation by collisionally induced dissociation (CID). The MS/MS CID spectrum of the $[M + 2H]^{2+}$ species of angiotensin I produced by DIVE-MS is shown in Figure 3b, with the corresponding ESI-MS and ESI-MS/MS spectra shown in Figure S6b. The MS/MS spectra generated by these two methods were nearly identical, demonstrating the stable production of highly charged ions for tandem mass spectrometry, as is typically utilized by standard nebulization based methods for fragmentation based proteomic identification. Successful MS analysis was as well performed from 10 nM aqueous solutions (with 0.1% formic acid) of both angiotensin I and angiotensin II with a transfer capillary temperature of 139 °C (Figure S5). The doubly charged species $[M + 2H]^{2+}$ was detected for the consumption of amounts as low as 39 amols analyte.

Charged species production and detection from single PIRL laser pulses (27 pL extraction) was implemented using angiotensin I (10 μM) in pure water (Figure S8). Modifications were made to the laser control and trap synchronization system to allow a single laser pulse to sample the solution and MS analysis performed on the single ablation plume event. The spectrum exhibited the singly, doubly and triply charge states of the peptide, with reproducible signal over long measurement times (Figure S9). The potential for single shot sampling and analysis with highly charged species production makes the technique particularly interesting for a high-throughput lab-on-a-chip coupling for proteomic investigation.

Highly charged protein ions extracted from bulk water solutions with PIRL were observed. As shown in Figure 4a, cytochrome c (10 μM) in water containing 0.1% formic acid resulted in a distribution of highly charged positive protein ions centered at 12+, consistent with the unfolded form of the protein observed in ESI studies.[62] The measurement was performed at a measured transfer capillary temperature of 74 °C using the heated collection extension. The charge state distribution of the cytochrome c ions was observed to be dependent on the sample and collection conditions, as previously reported.[63,64] A broad charge distribution centered at 8+ was observed for cytochrome c water solutions with the addition of 0.5% acetic acid (Figure S10a). The transfer capillary temperature was 36 °C and the data collected without the transfer extension. Highly negatively charged cytochrome c ions were observed from the same acidic solution (Figure S10b), without the addition of a base, in negative-ion mode operation. Similar results have been observed using standard laser spray, where IR ablation of water is performed within a nebulizer, and the ability to observe negative ions attributed to field induced species enrichment near the sample surface by the applied electric field.[42,65]

Pure water solutions containing cytochrome c (10 μM), without the addition of acid, were also investigated (Figure 4b), resulting in highly charged species production. A slight shift in the charge state distribution, from 12+ to 11+, was observed without the addition of acid, as well as an increase in the adduct abundance (Figure S11), a reflection of the population increase of the species in the near neutral pH sample. A decrease in the TIC was noted for the pure water sample though the spectra are easily discernible for the 374 fmol of analyte consumed. The
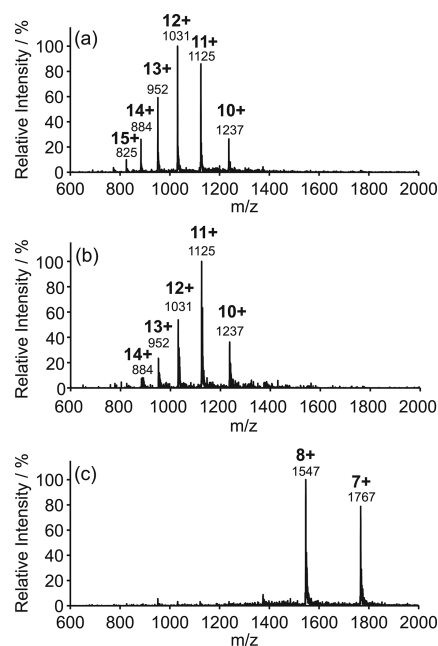
Figure 4. DIVE-MS spectrum of (10 μM) cytochrome c (a) in water containing 0.1% formic acid, (b) in acid-free pure water, and (c) in 10 mM ammonium acetate buffer. Transfer capillary temperature was measured to be 74 °C for panels a and b. For panel c, no gas diverting heated transfer extension was applied and the transfer capillary temperature was measured to be 62 °C.

increase in ion signal at low pH is likely due to the higher concentration of protons in solution available for protonation as well the increase has been proposed to contribute to charged droplets formation in ESI type processes. Pure water solutions without the addition of acid, for angiotensin I and II, and also acetaminophen, showed the same charging states (Figure S12) (transfer capillary temperature 139 °C) as compared to samples prepared at lower pH by the addition of acid. A decrease was observed in the 3+ state for angiotensin I in pure water as well as an increase in adduct formation. This is assumed to be due to the decrease concentration of protons in solution available for analyte protonation.

DIVE-MS was further applied to protein solutions prepared under sample conditions described for native MS, without the use of the additional gas diverting heated transfer extension and with a measured transfer capillary temperature of 62 °C.[9] Cytochrome c samples resulted in a spectrum (Figure 4c) composed of the +7 and +8 charge state species. The narrow distribution indicated the detected species of the protein to be in the folded native state, being softly extracted from the sample solution. The spectrum is comparable with that produced by means of standard ESI and is an indication of the soft nature of the ablation method.[62] Highly charged species were observed as well from the protein lysozyme (Figure S13). The spectrum indicated a mixture of the folded and unfolding state, likely due to the sampling conditions employed.

During DIVE ablation, water and analyte molecules within a thin layer of the liquid/air interface are driven into the gas phase at supersonic velocity, stripping analytes of bound water molecules.[51,53] Recently, molecular dynamics simulations, which characterized DIVE ablation for a protein counterion system in water, have shown that the mechanism is capable of achieving direct desolvation for gas phase ion production in

vacuum with minimal analyte damage.[66] Under the ambient conditions described here, atmospheric collision of the supersonic plume likely leads to cooling and droplet formation of the gas phase ablation plume. It is also possible that ion signal could originate from charged droplets directly ejected from the ablation site with subvaporization enthalpy,[53] similarly as produced initially in methods such as ESI and laser spray or by electrostatic charging following laser disruption of the liquid surface.[67] A transfer capillary temperature dependence revealed no change in the charge state distribution of cytochrome *c* (Figures S14 and S15) as a function of temperature but an increase in the TIC indicated some fraction of proteins were not completely desolvated as they entered the MS, similar as observed for ESI under lower than optimized desolvation conditions. This is likely due to the initial incomplete shedding of water molecules bound to the protein in the gas phase ablation plume, subsequent condensation of the gas phase water vapor/analyte in the atmosphere or incomplete evaporation of charged droplets.

It should be noted that experiments performed using the heated extension are free of curtain gas to assist in desolvation and experiments performed without the extension only utilized a minimal curtain gas flow (0.5 L min^{-1}). The ion signal was observed to be dependent on the voltage applied to the collection extension and transfer capillary, as shown for cytochrome *c* in Figure S16. Minimal MS signal was observed for voltages from 0 to −1500 V. The signal increased sharply from −1500 to −3500 V. The measurement does not however differentiate voltage dependent effects on the sample, those effecting charging or collection efficiency, from voltage dependent ion production effects that may occur inside the transfer capillary.

To investigate in the region in which charged species are produced by DIVE ablation, an electrically isolated, conductive planar mesh grid was placed between the liquid sample and the collection extension. The voltage applied to the grid was varied while the voltage of the quartz transfer capillary remained constant (−4500 V). No ion signal was observed without a voltage applied to the grid. A positive ion signal steadily increased with increased negative voltage applied to the grid, as shown in Figure S17, indicating the presence of charged species or droplets outside the MS transfer capillary. Enhanced charging by field-induced separation of ions within a bulk liquid sample has been proposed to contribute to the ionization mechanism and sensitivity observed by traditional laser spray, as well attributed to the large negative ion signals observed.[41] The large required electric field ($\sim 6 \times 10^4$ V cm^{-1}) for laser spray has been attributed to producing an ion mobility high enough to overcome the high linear velocity of the solution within the high flow sample nebulizer ($\sim$3 cm s^{-1}).[41] However, for DIVE-MS, the linear velocity of the sample flow is substantially lower (6×10^{-5} cm s^{-1}) due to the ability to operate at low sample consumption rates. Therefore, charged analytes within the sample would have sufficient velocity even at lower field values, for separation and localization near the surface. The result indicates the mechanism may contribute to enhanced ion production. Subsequent studies will further characterize the mechanism for obtaining the highly charged ion species with the noted sensitivity.

■ CONCLUSIONS

We demonstrate a soft mass spectrometry interface which couples the picosecond infrared laser sample extraction directly

to an ion trap mass spectrometer inlet without requiring a post-ionization device or high voltage applied directly to the sample solution. Ion signals from highly charged biomolecular ion species, as well singly charged small molecules, are produced by this method, which drives ablation on time scales under thermal and acoustic stress confinement for efficient coupling to translational motions and reduction of fragmentation. In addition, native protein mass spectra are obtained by employing native buffer solution. It is postulated that ionization occurs as a result of the direct desolvation of analytes from the solution or the subsequent formation of charged droplets via the cooling of the ablation plume in atmosphere. Further experiments are required to investigate the underlying ionization mechanism. In addition, it is shown that single laser pulses can be employed to extract 27 pL sample volumes. The low sample consumption, combined with the capability to produce highly charged ions, makes the method interesting for coupling to liquid chromatography or microfluidic lab-on-a-chip devices.

■ ASSOCIATED CONTENT

ⓢ Supporting Information

Additional information as noted in the text. The Supporting Information is available free of charge on the ACS Publications Web site. The Supporting Information is available free of charge on the ACS Publications website at DOI: 10.1021/acs.analchem.7b04306.

(PDF)

■ AUTHOR INFORMATION

Corresponding Author

*E-mail: dwayne.miller@mpsd.mpg.de.

ORCID ⓘ

Wesley D. Robertson: 0000-0001-9526-4217
R. J. Dwayne Miller: 0000-0003-0884-0541

Author Contributions

Y.L. and W.D.R. contributed equally. The manuscript was written through contributions of all authors. All authors have given approval to the final version of the manuscript.

Notes

The authors declare the following competing financial interest(s): R. J. Dwayne Miller is the author of a patent related to the mechanism of PIRL laser ablation.

■ REFERENCES

(1) Yamashita, M.; Fenn, J. B. *J. Phys. Chem.* **1984**, *88*, 4451−4459.
(2) Blakley, C. R.; McAdams, M. J.; Vestal, M. L. *J. Chromatogr. A* **1978**, *158*, 261−276.
(3) Karas, M.; Hillenkamp, F. *Anal. Chem.* **1988**, *60*, 2299−2301.
(4) Tanaka, K.; Waki, H.; Ido, Y.; Akita, S.; Yoshida, Y.; Yoshida, T.; Matsuo, T. *Rapid Commun. Mass Spectrom.* **1988**, *2*, 151−153.
(5) Fenn, J. B.; Mann, M.; Meng, C. K.; Wong, S. F.; Whitehouse, C. M. *Science* **1989**, *246*, 64−71.
(6) Wilm, M.; Mann, M. *Anal. Chem.* **1996**, *68*, 1−8.

(7) Wilm, M. S.; Mann, M. *Int. J. Mass Spectrom. Ion Processes* **1994**, *136*, 167−180.

(8) Hirabayashi, A.; Sakairi, M.; Koizumi, H. *Anal. Chem.* **1994**, *66*, 4557−4559.

(9) Takáts, Z.; Wiseman, J. M.; Gologan, B.; Cooks, R. G. *Anal. Chem.* **2004**, *76*, 4050−4058.

(10) Jecklin, M. C.; Touboul, D.; Bovet, C.; Wortmann, A.; Zenobi, R. *J. Am. Soc. Mass Spectrom.* **2008**, *19*, 332−343.

(11) Harris, G. A.; Galhena, A. S.; Fernández, F. M. *Anal. Chem.* **2011**, *83*, 4508−4538.

(12) Alberici, R. M.; Simas, R. C.; Sanvido, G. B.; Romão, W.; Lalli, P. M.; Benassi, M.; Cunha, I. B. S.; Eberlin, M. N. *Anal. Bioanal. Chem.* **2010**, *398*, 265−294.

(13) Takáts, Z.; Wiseman, J. M.; Gologan, B.; Cooks, R. G. *Science* **2004**, *306*, 471−473.

(14) Heron, S. R.; Wilson, R.; Shaffer, S. A.; Goodlett, D. R.; Cooper, J. M. *Anal. Chem.* **2010**, *82*, 3985−3989.

(15) Cody, R. B.; Laramée, J. A.; Durst, H. D. *Anal. Chem.* **2005**, *77*, 2297−2302.

(16) Han, X.; Aslanian, A.; Yates, J. R., III *Curr. Opin. Chem. Biol.* **2008**, *12*, 483−490.

(17) Lee, J.; Soper, S. A.; Murray, K. K. *Anal. Chim. Acta* **2009**, *649*, 180−190.

(18) Caprioli, R. M.; Farmer, T. B.; Gile, J. *Anal. Chem.* **1997**, *69*, 4751−4760.

(19) Schulz, E.; Karas, M.; Rosu, F.; Gabelica, V. *J. Am. Soc. Mass Spectrom.* **2006**, *17*, 1005−1013.

(20) Covey, T. R.; Schneider, B. B.; Javaheri, H.; LeBlanc, J. C. Y.; Ivosev, G.; Corr, J. J.; Kovarik, P. In *Electrospray and MALDI Mass Spectrometry*; Cole, R. B., Ed.; John Wiley & Sons, Inc.: Hoboken, NJ, USA, 2010; pp 441−490.

(21) Dreisewerd, K. *Chem. Rev.* **2003**, *103*, 395−426.

(22) Li, L.; Wang, A. P. L.; Coulson, L. D. *Anal. Chem.* **1993**, *65*, 493−495.

(23) Murray, K. K.; Russell, D. H. *Anal. Chem.* **1993**, *65*, 2534−2537.

(24) Sampson, J. S.; Hawkridge, A. M.; Muddiman, D. C. *J. Am. Soc. Mass Spectrom.* **2006**, *17*, 1712−1716.

(25) Nemes, P.; Vertes, A. *Anal. Chem.* **2007**, *79*, 8098−8106.

(26) Rezenom, Y. H.; Dong, J.; Murray, K. K. *Analyst* **2008**, *133*, 226−232.

(27) Huang, F.; Murray, K. K. *Rapid Commun. Mass Spectrom.* **2010**, *24*, 2799−2804.

(28) Robichaud, G.; Barry, J. A.; Muddiman, D. C. *J. Am. Soc. Mass Spectrom.* **2014**, *25*, 319−328.

(29) Flanigan, P.; Levis, R. *Annu. Rev. Anal. Chem.* **2014**, *7*, 229−256.

(30) Zou, J.; Talbot, F.; Tata, A.; Ermini, L.; Franjic, K.; Ventura, M.; Zheng, J.; Ginsberg, H.; Post, M.; Ifa, D. R.; Jaffray, D.; Miller, R. J. D.; Zarrine-Afsar, A. *Anal. Chem.* **2015**, *87*, 12071−12079.

(31) Trimpin, S.; Inutan, E. D.; Herath, T. N.; McEwen, C. N. *Mol. Cell. Proteomics* **2010**, *9*, 362−367.

(32) Trimpin, S.; Inutan, E. D.; Herath, T. N.; McEwen, C. N. *Anal. Chem.* **2010**, *82*, 11−15.

(33) Pagnotti, V. S.; Inutan, E. D.; Marshall, D. D.; McEwen, C. N.; Trimpin, S. *Anal. Chem.* **2011**, *83*, 7591−7594.

(34) Trimpin, S.; Wang, B.; Inutan, E. D.; Li, J.; Lietz, C. B.; Harron, A.; Pagnotti, V. S.; Sardelis, D.; McEwen, C. N. *J. Am. Soc. Mass Spectrom.* **2012**, *23*, 1644−1660.

(35) Cramer, R.; Pirkl, A.; Hillenkamp, F.; Dreisewerd, K. *Angew. Chem., Int. Ed.* **2013**, *52*, 2364−2367.

(36) König, S.; Kollas, O.; Dreisewerd, K. *Anal. Chem.* **2007**, *79*, 5484−5488.

(37) Overberg, A.; Karas, M.; Bahr, U.; Kaufmann, R.; Hillenkamp, F. *Rapid Commun. Mass Spectrom.* **1990**, *4*, 293−296.

(38) Berkenkamp, S.; Karas, M.; Hillenkamp, F. *Proc. Natl. Acad. Sci. U. S. A.* **1996**, *93*, 7003−7007.

(39) Pirkl, A.; Soltwisch, J.; Draude, F.; Dreisewerd, K. *Anal. Chem.* **2012**, *84*, 5669−5676.

(40) Witt, L.; Pirkl, A.; Draude, F.; Peter-Katalinić, J.; Dreisewerd, K.; Mormann, M. *Anal. Chem.* **2014**, *86*, 6439−6446.

(41) Hiraoka, K.; Saito, S.; Katsuragawa, J.; Kudaka, I. *Rapid Commun. Mass Spectrom.* **1998**, *12*, 1170−1174.

(42) Kudaka, I.; Kojima, T.; Saito, S.; Hiraoka, K. *Rapid Commun. Mass Spectrom.* **2000**, *14*, 1558−1562.

(43) Hiraoka, K. *J. Mass Spectrom.* **2004**, *39*, 341−350.

(44) Laiko, V. V.; Taranenko, N. I.; Berkout, V. D.; Yakshin, M. A.; Prasad, C. R.; Lee, H. S.; Doroshenko, V. M. *J. Am. Soc. Mass Spectrom.* **2002**, *13*, 354−361.

(45) Von Seggern, C. E.; Moyer, S. C.; Cotter, R. J. *Anal. Chem.* **2003**, *75*, 3212−3218.

(46) Hiraguchi, R.; Hazama, H.; Masuda, K.; Awazu, K. *J. Mass Spectrom.* **2015**, *50*, 65−70.

(47) Coon, J. J.; Harrison, W. W. *Anal. Chem.* **2002**, *74*, 5600−5605.

(48) Von Seggern, C. E.; Gardner, B. D.; Cotter, R. J. *Anal. Chem.* **2004**, *76*, 5887−5893.

(49) Warschat, C.; Stindt, A.; Panne, U.; Riedel, J. *Anal. Chem.* **2015**, *87*, 8323−8327.

(50) Sampson, J. S.; Muddiman, D. C. *Rapid Commun. Mass Spectrom.* **2009**, *23*, 1989−1992.

(51) Vogel, A.; Venugopalan, V. *Chem. Rev.* **2003**, *103*, 577−644.

(52) Franjic, K.; Cowan, M. L.; Kraemer, D.; Miller, R. J. D. *Opt. Express* **2009**, *17*, 22937−22959.

(53) Franjic, K.; Miller, R. J. D. *Phys. Chem. Chem. Phys.* **2010**, *12*, 5225−5239.

(54) Siwick, B. J.; Dwyer, J. R.; Jordan, R. E.; Miller, R. J. D. *Science* **2003**, *302*, 1382−1385.

(55) Kwiatkowski, M.; Wurlitzer, M.; Omidi, M.; Ren, L.; Kruber, S.; Nimer, R.; Robertson, W. D.; Horst, A.; Miller, R.; Schlüter, H. *Angew. Chem., Int. Ed.* **2015**, *54*, 285−288.

(56) Ren, L.; Robertson, W. D.; Reimer, R.; Heinze, C.; Schneider, C.; Eggert, D.; Truschow, P.; Hansen, N.-O.; Kroetz, P.; Zou, J.; Miller, R. J. D. *Nanotechnology* **2015**, *26*, 284001.

(57) Amini-Nik, S.; Kraemer, D.; Cowan, M. L.; Gunaratne, K.; Nadesan, P.; Alman, B. A.; Miller, R. J. D. *PLoS One* **2010**, *5*, e13053.

(58) Böttcher, A.; Kucher, S.; Knecht, R.; Jowett, N.; Krötz, P.; Reimer, R.; Schumacher, U.; Anders, S.; Münscher, A.; Dalchow, C.; Miller, R. J. D. *Eur. Arch. Otorhinolaryngol.* **2015**, *272*, 941−948.

(59) Jowett, N.; Wöllmer, W.; Reimer, R.; Zustin, J.; Schumacher, U.; Wiseman, P. W.; Mlynarek, A. M.; Böttcher, A.; Dalchow, C. V.; Lörincz, B. B.; Knecht, R.; Miller, R. J. D. *Otolaryngol.–Head Neck Surg.* **2014**, *150*, 385−393.

(60) Kwiatkowski, M.; Wurlitzer, M.; Krutilin, A.; Kiani, P.; Nimer, R.; Omidi, M.; Mannaa, A.; Bussmann, T.; Bartkowiak, K.; Kruber, S.; Uschold, S.; Steffen, P.; Lübberstedt, J.; Küpker, N.; Petersen, H.; Knecht, R.; Hansen, N. O.; Zarrine-Afsar, A.; Robertson, W. D.; Miller, R. J. D.; Schlüter, H. *J. Proteomics* **2016**, *134*, 193−202.

(61) Gilpin, R. K.; Zhou, W. *J. Chromatogr. Sci.* **2004**, *42*, 15−20.

(62) Konermann, L.; Douglas, D. J. *J. Am. Soc. Mass Spectrom.* **1998**, *9*, 1248−1254.

(63) Shi, X.; Takamizawa, A.; Nishimura, Y.; Hiraoka, K.; Akashi, S. *Rapid Commun. Mass Spectrom.* **2008**, *22*, 1430−1436.

(64) Šamalikova, M.; Matečko, I.; Müller, N.; Grandori, R. *Anal. Bioanal. Chem.* **2004**, *378*, 1112−1123.

(65) Hiraoka, K.; Asakawa, Y.; Yamamoto, Y.; Nakamura, M.; Ueda, K. *Rapid Commun. Mass Spectrom.* **2001**, *15*, 2020−2026.

(66) Zou, J.; Wu, C.; Robertson, W. D.; Zhigilei, L. V.; Miller, R. J. D. *J. Chem. Phys.* **2016**, *145*, 204202.

(67) Qiao, L.; Sartor, R.; Gasilova, N.; Lu, Y.; Tobolkina, E.; Liu, B.; Girault, H. H. *Anal. Chem.* **2012**, *84*, 7422−7430.

Direct Laser Sampling of Aqueous Solutions from Lab-on-a-Chip Devices for Mass Spectrometry

Lab on a Chip

Article

Direct Laser Sampling of Aqueous Solutions from Lab-on-a-Chip Devices for Mass Spectrometry

Y. Lu[a,ł], C. L. Pieterse[a], D. Eggert[c], Candice Ip[a,b], F. Busse[a], S. Keskin[a,d], W. D. Robertson[a,ł] and R. J. D. Miller*[a,e]

Coupling of microfluidic lab-on-a-chip (LOC) devices to mass spectrometry (MS) is experimentally challenging and in some cases limiting to device applicability. Here, we demonstrate a matrix-free, mechanical contact-free, picosecond infrared laser (PIRL) based sampling method for coupling miniaturized devices directly to mass spectrometry. We develop an optically clear, nanofabricated aqueous solution sorting array and characterize its application for localization of thin (~ 2 micron) water films containing picoliter volumes of aqueous analyte solutions. The coordinated registration, solution localization, precision laser sampling and MS analysis of these volumes is demonstrated within their evaporation time under atmospheric conditions (~ 300 ms). The PIRL laser is transmitted through the device for sampling and direct ion production, providing increased flexibility and ion collection efficiency. Notably, the technique is capable of producing molecular ions and multilply charged peptides directly from water, making it particularly suited for proteomics applications. The high sensitivity, laser-based sampling does not require the use of chemical matrices which in some cases can limit and overwhelm intended LOC device processing.

Introduction

Lab-on-a-chip (LOC) technologies have provided innovative solutions widely utilized in life science research, drug discovery and biodiagnostics. These sample localization, sorting and microfluidic flow devices provide numerous advantages for instrument miniaturization, facilitating improved sensitivity and high throughput analysis with low sample consumption or cross contamination.[1, 2] Mass spectrometry (MS), in combination with soft, gas phase ion production methods, has been extremely successful and heavily relied upon for coupling these devices for analysis of small molecules, drugs and biomolecules including peptides and proteins for proteomic applications.

Matrix-assisted laser desorption/ionization (MALDI)[3, 4] and electrospray ionization (ESI)[5, 6] were the first demonstrated and still the most heavily relied upon methods for the soft or more correctly intact production of labile biomolecular gas phase ions, such as proteins and peptides. Significant effort has thus been invested in the efficient coupling of these methods to LOC devices.[1, 2, 7-12] MALDI, as a laser-based technique, offers high flexibility and sampling precision and has been successfully utilized for numerous offline and online interfaces for MS coupling of LOC devices.[11-13] Chip-based sample localization devices have been developed to overcome the sample deposition heterogeneity inherent to MALDI and to provide quantitative post-processing analysis for dried matrix samples.[12, 14-16] The technique is highly applicable to the high throughput analysis of deposited dried samples and recent advances have been made to integrate dynamic sample processing microfluidics and MALDI-MS into the same platform such as, for example, direct coupling to liquid chromatography separation.[17] Most limiting for MALDI/LOC coupling, however, is the mandatory chemical matrix that requires an additional offline deposition and drying step, which can result in spectral artifacts and complicate or overwhelm the intended LOC process. In addition, the low charge states typically produced can further limit the proteomic analysis.

The multiply charged ions produced by means of ESI type nebulization-based methods allow use of low mass-to-charge ratio (m/z) range systems and facilitate fragmentation-based methods that have provided the foundation for proteomic analysis.[18-20] However, even though such advantages have led these methods to be heavily utilized in LOC/MS coupling, these methods can reduce sampling flexibility in comparison to the

a. Max Planck Institute for the Structure and Dynamics of Matter, Hamburg 27761, Germany.
* Email: dwayne.miller@mpsd.mpg.de
b. University of British Columbia, 2329 West Mall, Vancouver, BC V6T 1Z4, Canada
c. Heinrich Pette Institute, Leibniz Institute for Experimental Virology, Martinistraße 52, 20251 Hamburg, Germany.
d. Current Address: Leibniz Institute for New Materials, D-66123 Saarbrücken, Germany
e. Departments of Chemistry and Physics, University of Toronto, 80 St George Street, Toronto M5S 1H6, Ontario, Canada
ł These authors contributed equally

laser-based methods, as they typically require a high voltage or pressure applied to the sample, and in some cases necessitate the use of volatile solvents and/or accompanying gas flows.[1, 2, 7, 8] The design and fabrication of ESI coupled LOC systems are also extremely challenging with the added complexity and limitations occurring in effectively coupling these devices to standard nebulizers without leakages or dead volumes.

Significant advances have been achieved with integrated nebulizers, fabricated directly into LOC devices,[1, 2, 7, 8, 21-24] with even time-resolved protein-ligand binding dynamics monitored with a single such microfluidic platform.[25] These nebulizers must, however, overcome the challenges of both varying the device processing flow rate and pressure, as these parameters can destabilize the electrospraying process, which in turn alters the ionization efficiency and will therefore adversely constrain quantitative measurements.[25] To facilitate a high-throughput analysis, dual[24] and multi-emitter systems of high accuracy and sensitivity have also been developed.[26] Offline post-processing arrays of micro-fabricated nebulizer tips are commonly utilized together with pipette based systems, providing sample delivery and pressure for nano-ESI arrays.[21] In addition, as an alternative to the tip based nebulizers, surface acoustic wave nebulization (SAWN) devices have demonstrated great promise for LOC/MS coupling, although they further require fabrication into a LOC device at each desired sampling position.[27-29] In general, these nebulization methods have not been able to provide the sampling flexibility available by laser based methods.

Recently, we have described the application of a picosecond infrared laser (PIRL) operating under desorption by impulsive vibrational excitation (DIVE) conditions to extract intact and functional peptides, proteins and protein oligomers from solutions and tissue.[30, 31] Under these conditions the excitation volume is thermally and acoustically confined such that minimal energy is transferred to the surrounding solution and device structure. Notably, the ultrafast DIVE extraction method has been demonstrated to produce both singly as well as highly charged peptide and protein ions directly from the surface of bulk aqueous solutions.[32] The highly charged protein and peptide ion distributions observed are similar to those generated by nebulization-based methods and can be beneficial for proteomic applications by providing access to high mass ranges with enhanced m/z values. In addition, the method facilitates an analyte detection limit of a few attomoles for aqueous solutions. The setup described does not require an additional voltage, heat or pressure applied to the sample simplifying the design and operation and provides additional laser based sampling flexibility.

Here, we develop an optically transparent, self-localizing, sample-sorting chip device for aqueous solutions. The chip consists of nanofabricated wells utilized to create local instabilities in a water bead contact line in order to both promote adhesion and liquid capture, as previously described for bulk silica.[14] Although a quantitative analysis is not

demonstrated here, the device represents a proof of concept for further developments toward quantitative sampling of aqueous volumes for MS. We present a setup which utilizes a novel image processing based fiducial registration software to coordinate the localization of aqueous thin cylindrical films, which are subsequently ablated following transmission of the laser through the nanofabricated device. The subsequent ablation plume is then atmospherically coupled directly to an ion trap mass spectrometer. The sampling is mechanically contact-free and demonstrated to softly and efficiently extract analyte ions from the localized aqueous solution on the device surface before the evaporation of individual wells occurs (< 300 ms). Notably, the presented laser sampling method can produce both singly and multiply charged biomolecular ions, as we have shown previously for bulk aqueous solutions, for analysis with high sensitivity, requiring no additional post-ionization device.

Experimental

Fabrication of optically transparent arrays

Double-side polished fused silica wafers with 500 μm thickness were used for fabrication with 300 nm of nitride deposited on one side by plasma-enhanced chemical vapour deposition (PECVD). A mask was designed and used to transfer the array of well features onto the nitride side of the wafer using standard UV-lithography to produce picoliter wells. The well features were etched until reaching the glass surface by reactive ion etching with SF_6 and O_2 plasmas. The wafer was diced into chips (15 mm x 15 mm) by means of using a diamond blade.

Prior to experiments, the chips were cleaned by sonicating sequentially with acetone, isopropanol and deionized water to remove the photoresist residues and finally dried with compressed Helium. The fabrication resulted in an optically transparent picoliter well array constructed into the thin silica nitride layer, producing an array of 100 micron diameter, 300 nm depth wells. The infrared transmission at 3 microns was measured to be approximately 80% for the unfocused beam through the array.

Picoliter well characterization by confocal laser scanning microscopy

The final structures were characterized by light microscopy and the depth of the features was measured using a profilometer. In order to image individual wells loaded and filled, the array was cooled to 4°C and filled with an aqueous solution containing 0.02% (w/v) FITC-Dextran (Sigma-Aldrich Chemie GmbH, Hamburg, Germany). The array of nanowells was placed in a sealed humidified chamber constructed from a glass bottom culture dish (P35G-1.5-10-C, MatTek Corporation, Ashland, MA, USA). The cooling and humidified environment prevented the evaporation of the localized aqueous solution contained within the wells for tens of minutes, facilitating

confocal imaging. The three-dimensional (3D) images were acquired using a confocal laser scanning microscope (C2+, Nikon GmbH, Düsseldorf, Germany) equipped with a 20x objective (CFI Plan Apo Lambda 20X/0.75, Nikon GmbH). A 488 nm diode-pumped solid-state laser (Melles Griot GmbH, Bensheim, Germany) was used for excitation of the FITC-Dextran. A beam splitter (405/488/543/640, Nikon GmbH) was combined with a bandpass emission filter (515/30 Nikon GmbH) to separate the excitation light from the emission light. In order to correct for spherical aberrations, fluorescently labelled latex beads (0.1 and 1.0 μm Carboxylate-Modified FluoSpheres, yellow-green fluorescent (505/515), Thermo Fisher Scientific Inc., Waltham, MA, USA) were imaged under the same conditions as a reference. The water volumes in 25 wells were measured using the Bitplane Imaris software (v. 8.2.1, Bitplane AG, Zurich, Switzerland) to calculate the average volume.

Array imaging, wetting and ablation synchronization

An automated well registration, loading and sampling system was designed and constructed utilizing a customized low profile chip mount to allow the direct imaging of the chip surface for laser ablation synchronization.[33] High-precision mechanical slip-stick piezo translation stages (SLC-2445, SmarAct, Oldenburg, Germany), with a closed loop positioning sensor (±1 nm precision), were used for chip translation. A home designed image processing based fiducial auto-alignment software was developed to register all of the wells and control chip scanning, wetting and synchronize laser ablation.[33] This was achieved using images obtained via a long working distance (95 mm) microscope (QI-OPTIQ, Waltham, USA). The high refractive index of Si_3N_4, compared to bare fused silica, provided contrast for the empty wells due to the difference in reflectivity. Wells loaded with aqueous solution appeared darker in the image (see Figure S1). A diode synchronized, high-speed shutter was utilized to allow synchronization of the laser ablation with chip scanning, well loading and positioning. A wait delay-time between the loading and positioning of the well and opening of the laser shutter was implemented (50 ms). The loading was achieved via a pulled and tapered glass capillary tip mounted on a 3D translation stage, which was brought close to the chip surface to drag a hanging drop over the array. Sample was loaded in to each well by registration, scanning the aqueous sample bead onto the well array and allowing the localized sample to dry within each well. Laser sampling and MS analysis were then performed following rehydration of the well using a deionized water bead. For the peptide, and limit of detection measurements, the loaded wells were sampled directly following sample localization and without rehydration. The sampling was always performed before evaporation of the well. For the experiments involving peptide solutions, aqueous solutions were laser sampled and analysed directly following loading and before evaporation. Laser pulse bursts containing 100 pulses were focused through the transparent chip onto the localized solution in transmission geometry, with no secondary ionization or nebulization device. A representative image of scanning, loading and ablation of water from the individual wells under atmospheric conditions is shown in Figure 1, with a sampled and emptied well (lower contrast) indicated by an arrow.

Mass spectrometry analysis

The analysis was carried out with a modified ion trap mass spectrometer (Esquire3000, Bruker, Germany). As shown in Figure 1, a custom designed ion collection interface was used to minimize disruption of the ablation plume in order to optimize the collection efficiency. A reduced curtain gas flow (0.5 L min^{-1}) was used to minimize sample evaporation and plume disruption. The actual transfer capillary temperature for all experiments was measured directly using a thermocouple to be 70 °C, significantly lower than the set value due to the use of the reduced gas flow rate. The transfer capillary voltage of the ion trap MS was set to -4500 kV, with a spray shield endplate offset of 500 V. All data were collected and analyzed using Bruker Daltonics Data Analysis software. The ion trap accumulation time was set to 10 ms unless otherwise noted.

Laser system

The samples were irradiated by a picosecond infrared laser (PIRL-APLQ-3000, Attodyne Inc., Toronto, Canada) producing pulses with a duration of 10 ps at λ=3000 ±100 nm and a repetition rate of 1 kHz. The beam delivery system and a fast external shutter were implemented for control of single and burst mode pulse selection using a fast photodiode (PDA20H-EC, Thorlabs GmbH, Munich, Germany) for synchronization. The beam was focused onto the sample using a 25 mm anti-reflectance coated CaF_2 lens resulting in a transverse beam diameter at the focus of approximately 140 μm, as measured with a WinCamD-FIR2-16-HRR camera. The pulse energy was measured at the sample plane to be on average 40 μJ per pulse. The position of the focusing lens was adjusted to optimize ion production.

Chemicals and sample preparation

Ion trap ESI tuning mix (G2431a) was purchased from Agilent Deutschland GmbH (Waldbronn, Germany) and added to deionized water at a ratio of 1:4 (v/v) for standard experiments. The resulting solution contained a concentration of 1.5 μM for hexakis(2,2-difluoroethoxy) phosphazene (HexPE), together with trifluoroacetic acid ammonium salt (TFA) (400 μM) and 20% acetonitrile. Additional samples were further diluted from this stock, for the limit of detection measurements resulting in a HexPE concentration of 30 nM in a water solution containing 2% acetonitrile. A bead of 200 nL was loaded onto the chip for sampling for all experiments. Several additional phosphazene variants were contained in the mixture but not investigated in this study. Stock samples of angiotensin I human (≥ 93%, HPLC) were purchased from Sigma-Aldrich Chemie Gmbh (Munich, Germany) and the deionized distilled water was from a PURELAB Classic (>18.5 MΩ·cm, ELGA). All analytes, including small molecules and peptides, were used without further purification.
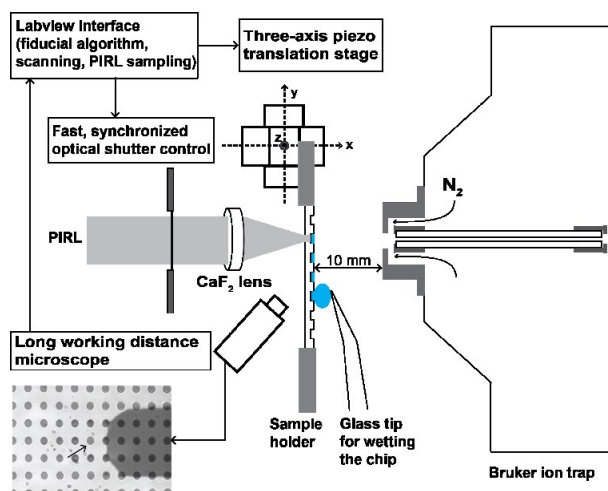
Figure 1. A schematic representation of the PIRL-DIVE coupled MS system. A micro array chip was mounted on a three-axis piezo translation stage and aligned axial to the center of the ion trap inlet. The wetted well was ablated by PIRL irradiation after propagating through the chip array. A long working distance microscope image of a loaded well array undergoing ablation is shown (lower left panel) in which a sampled well is noted by the arrow.

Results and discussion

Characterization of the picoliter array

The volume of the localized solution within the individually loaded microwells undergoes rapid evaporation (<300 ms) under standard atmospheric humidity and temperature conditions. For characterization by confocal laser scanning microscopy, the array was cooled and placed in a sealed humidified chamber. A representative 3D profile of an individual loaded well filled with an aqueous solution is shown in Figure 2. The localized volume demonstrated a positive meniscus, as predicted for the fabricated aspect ratio of D/d = 333.[14] The central thickness of the localized aqueous disk was measured to be 2.1 μm, with the height of the liquid at the edges of the well of 0.35 μm. The total localized volume was measured to be on average 9.5 pL. The sampling time of the wells is sufficiently fast in the PIRL scanning mode of the chip that we can use this as the working volume.
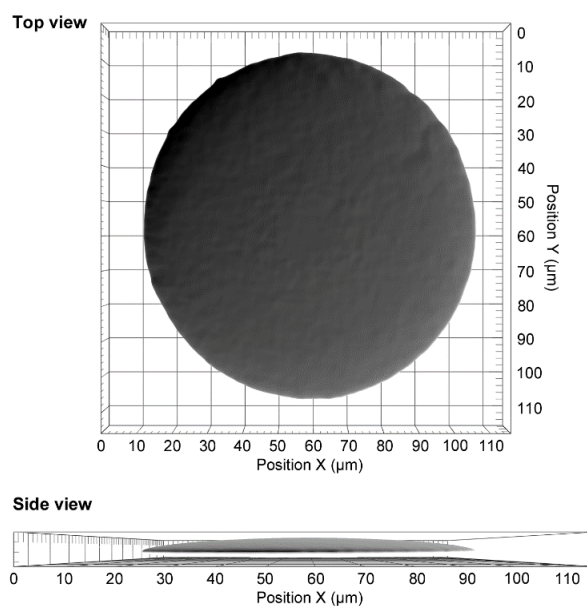
Figure 2. Liquid profile produced by confocal microscopy of an individual microwell. The total localized volume was measured to be 9.5 pL.

Atmospheric mass spectrometry coupling

Sample well registration, loading, scanning, and laser sampling of the picoliter array was optimized using the small molecule compound HexPE in the dried sample configuration. A bead (200 nL) of HexPE diluted in water (300 femtomoles of analyte) was loaded onto the array resulting in the dried analyte localized within the individual wells. This resulted in approximately 460 attomole of analyte being loaded into individual wells for the selected area, after which a pure water bead was used to scan and rehydrate each well. A pulse train of 100 shots was propagated through the chip to ablate the localized aqueous volume within the well before evaporation. The ablation plume was directly collected and analysed by the MS. The total ion current (TIC) shown in Figure 3 (a) indicates that ion signal was generated for each row of wells. The ion signal decreased to zero counts during the return of the chip to the start position for loading.

The time-averaged mass spectrum shown in Figure 3 (b), displayed the singly charged, protonated species typical of the compound. The system loaded and sampled the array at a rate of approximately 10 Hz, limited by the maximum scan speed of the piezo stages and the distance between adjacent wells. The variation in intensity of the TIC of each row is primarily due to a timing mismatch of ion trap collection and plume ablation, as a dead time exists and no synchronization was implemented. Further variations could occur from both alignment and walk-off effects associated with chip scanning, since the high numerical aperture focusing utilized here is inherently sensitive to the alignment (± 50 μm). These effects can be

Please do not adjust margins
Lab on a Chip
Page 8 of 11
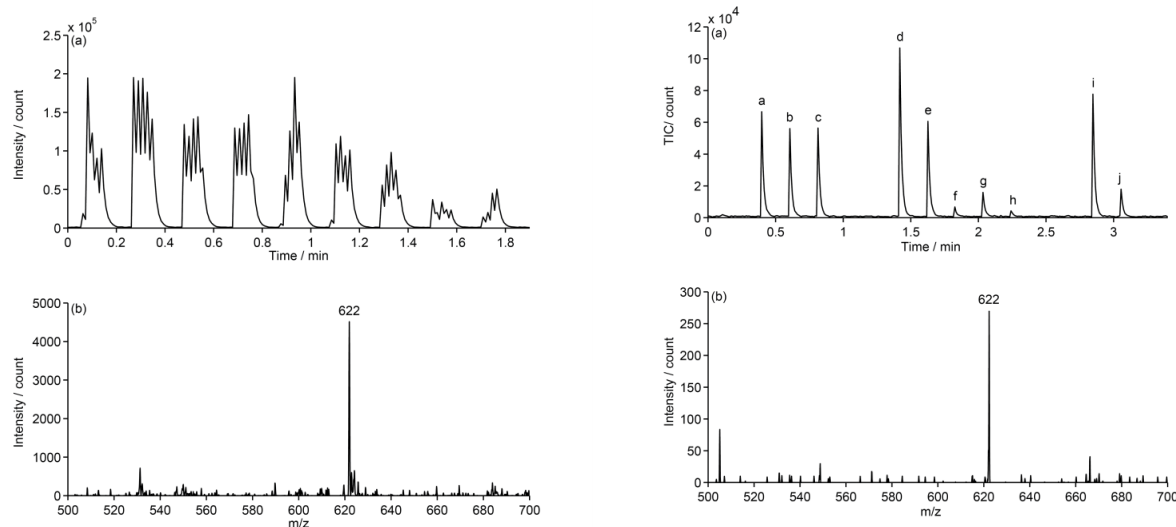
Figure 3. (a) Total ion current (TIC) of HexPE for the mass range of frame (b), illustrating signal from each row of the array. Due to the array scan path, every second row contributes to TIC response. (b) Average mass spectrum for the TIC of frame (a), clearly showing the protonated species of HexPE.

overcome by using lower NA focusing or implementing more precision alignment methods.

In order to detect and identify molecules localized in single isolated wells of the array, modifications to the sample registration and laser synchronization software were made to restrict sampling to a single well per scanned and loaded row, leaving the remaining wells undisturbed. Figure 4 (a) shows the TIC following sampling of a single well from each row of the array, which resulted in ion signal for the majority of sites. The spectrum obtained from every single well was resolved, as shown in Figure 4 (b) for site (h) displaying the HexPE compound. Comparable spectra were produced from each individual well site in the TIC, as shown in Figure 5. The absence of ion signal in some positions was noted as well as intensity variations from the single wells. Microwell (d), which showed the highest TIC, exhibited the highest intensity with minimal background. The wells (a), (b), (c), (e) and (j), which shared roughly the same TIC signal level, resulted in a similar mass spectra signal intensity with negligible background noise. The magnitude of the ion intensity following sampling of wells (f), (g) and (h) was relatively smaller, though the spectra of the compound were still discernible with sufficient signal to noise. These variations in signal intensity are attributed to those described previously, as no trap collection synchronization or high precision alignment was implemented.

Figure 4. (a) Total ion current of an aqueous solution of HexPE scanned and loaded onto the array with only a single well sampled from each row. (b) Average mass spectrum of peak (h) shown in (a), illustrating even for the smallest signal amplitude.

The lowest amount of analyte successfully measured using the setup described for PIRL-DIVE sampling directly from the LOC surface was 6 femtomoles. The spectrum, shown in Figure S2(a), is the result of a 200 nL bead (30 nM of analyte dissolved in pure water, 2% acetonitrile) of the sample loaded onto the array and analysed directly following localization, but before drying, producing the typical TIC, such as shown in Figure S2(b), with the ion current increasing for alternating rows. As only every odd row contributed to TIC, the total sample contributing to the TIC and spectrum was about one half.

The application of PIRL-DIVE sampling of aqueous solutions of biomolecules directly from the array was performed using the peptides angiotensin II. Multiply charged ion distributions were observed from the chip surface similar in form to those produced in PIRL-DIVE-MS experiments where ions are extracted directly from bulk water. As shown in Figure 6, angiotensin II (1 µM) samples resulted in both the singly and doubly charge states, $[M+H]^+$, $[M+2H]^{2+}$ (m/z = 1046 and 524), respectively, with good signal to noise directly from the pL water volume of the chip wells. No fragmentation or chemical modification was observed. The spectrum shown is the result of the consumption of 200 femtomoles of analyte.
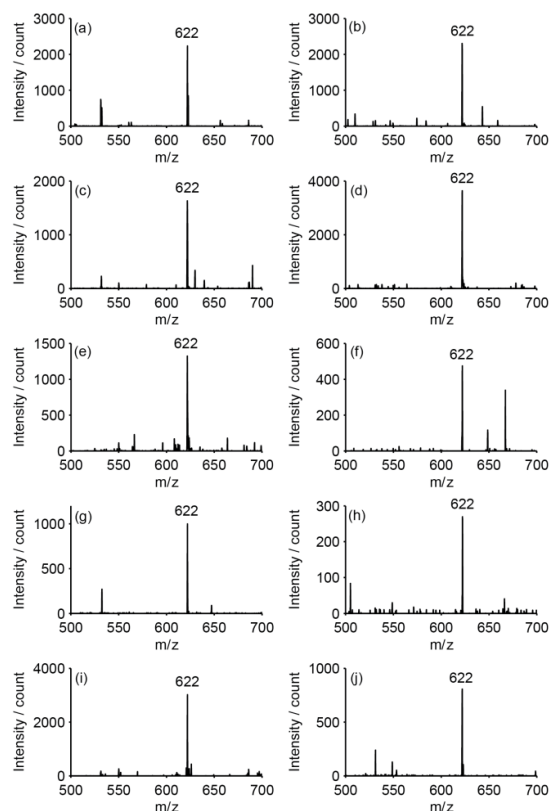
Figure 5. The PIRL-DIVE mass spectrum averaged from peaks in Figure 4 (a), showing the protonated species of HexPE. (a)-(j) correspond to the TIC labelled with the same letter in Figure 4 (a).
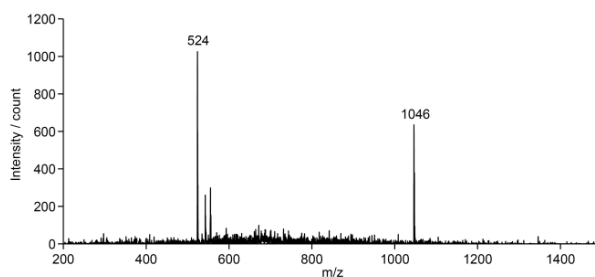
Figure 6. TIC and corresponding spectrum from 1 μM angiotensin II with 0.05% acetic acid: both the singly and doubly charged states of the peptide are observed. The sample consumption for the spectrum is 200 fmol.

Conclusions

We demonstrate the localization of ultra-thin aqueous sample solutions using an optically transparent LOC device in combination with direct sampling via PIRL-DIVE laser ablation for MS analysis. The sampling features of the sampling method overcome several of the experimental limitations associated with coupling LOC to MS utilizing standard techniques and the laser based control could potentially be advantageous as a high precision, highly flexible sampling technique. The application of PIRL-DIVE to the aqueous solution-sorting device for MS resulted in precision sampling for high sensitivity analyte detection, without the typically required chemical matrix or the requirement for secondary ionization. The high speed for both sample preparation and throughput is an important feature of this approach.

The multiply charged peptide molecular ion species produced using PIRL-DIVE sampling of the device, which are typical of fixed nebulization devices, makes the technique a potential solution for analysis from proteomic LOC devices requiring fast and flexible sampling at high speed with laser precision and control. Direct PIRL-DIVE sampling further provides the ability to significantly reduce the sampling volume by reducing the focal spot size and sampling depth.[34] As well, PIRL-DIVE sampling can easily be applied for the extraction of molecular ions from the front surface of most LOC devices, as well as extending the applicability of devices fabricated in fused silica or other optically (3 μm) transparent material by leaving the front surface open for optimized ion collection or other experimental investigations. The method's ability to couple directly to water further opens up possibilities for general microfluidic applications utilizing water as a medium for transport overcoming the requirement for solvents and additives that disrupt device function.

The precision and ultrafast nature of PIRL-DIVE makes it applicable to numerous experimental scenarios including extraction of molecules and complexes for MS analysis following ultrafast mixing. The developed device and sampling method in itself represents a proof of concept system for quantitative MS sampling of water similar in concept to arrays developed for quantitative analysis for post processing of dried MALDI samples.[15] Toward this goal, further efforts will be focused to develop sample sorting and microfluidic systems to optimize this method.

Acknowledgements

References

1. X. Feng, B.-F. Liu, J. Li and X. Liu, *Mass Spectrom. Rev.*, 2015, 34, 535-557.
2. D. Gao, H. Liu, Y. Jiang and J.-M. Lin, *LChip*, 2013, 13, 3309-3322.
3. K. Tanaka, *Angew. Chem. Int. Ed.*, 2003, 42, 3860-3870.
4. M. Karas and F. Hillenkamp, *Anal. Chem.*, 1988, 60, 2299-2301.
5. M. Yamashita and J. B. Fenn, *J. Phys. Chem.*, 1984, 88, 4451-4459.
6. J. B. Fenn, M. Mann, C. K. Meng, S. F. Wong and C. M. Whitehouse, *Science*, 1989, 246, 64-71.
7. I. M. Lazar, J. Grym and F. Foret, *Mass Spectrometry Reviews*, 2006, 25, 573-594.
8. S. Koster and E. Verpoorte, *Lab on a Chip*, 2007, 7, 1394-1412.
9. Y. Temiz, R. D. Lovchik, G. V. Kaigala and E. Delamarche, *Microelectron. Eng.*, 2015, 132, 156-175.
10. P. S. Dittrich and A. Manz, *Nat. Rev. Drug Discov.*, 2006, 5, 210-218.
11. J. Lee, S. A. Soper and K. K. Murray, *Anal. Chim. Acta*, 2009, 649, 180-190.
12. P. L. Urban, A. Amantonico and R. Zenobi, *Mass Spectrometry Reviews*, 2011, 30, 435-478.
13. A. Oedit, P. Vulto, R. Ramautar, P. W. Lindenburg and T. Hankemeier, *Current Opinion in Biotechnology*, 2015, 31, 79-85.
14. A. Zarrine-Afsar, C. Müller, F. O. Talbot and R. J. D. Miller, *Anal. Chem.*, 2011, 83, 767-773.
15. M. Pabst, S. R. Fagerer, R. Köhling, S. K. Küster, R. Steinhoff, M. Badertscher, F. Wahl, P. S. Dittrich, K. Jefimovs and R. Zenobi, *Anal. Chem.*, 2013, 85, 9771-9776.
16. E. Miele, M. Malerba, M. Dipalo, E. Rondanina, A. Toma and F. D. Angelis, *Adv. Mater.*, 2014, 26, 4179-4183.
17. I. M. Lazar and J. L. Kabulski, *Lab on a Chip*, 2013, 13, 2055-2065.
18. R. M. Alberici, R. C. Simas, G. B. Sanvido, W. Romão, P. M. Lalli, M. Benassi, I. B. S. Cunha and M. N. Eberlin, *Anal. Bioanal. Chem.*, 2010, 398, 265-294.
19. G. A. Harris, A. S. Galhena and F. M. Fernández, *Anal. Chem.*, 2011, 83, 4508-4538.
20. X. Han, A. Aslanian and J. R. Yates Iii, *Curr. Opin. Chem. Biol.*, 2008, 12, 483-490.
21. S. Zhang and C. K. Van Pelt, *Expert Review of Proteomics*, 2004, 1, 449-468.
22. G. T. T. Gibson, S. M. Mugo and R. D. Oleschuk, *Mass Spectrom. Rev.*, 2009, 28, 918-936.
23. T. Nissilä, L. Sainiemi, T. Sikanen, T. Kotiaho, S. Franssila, R. Kostiainen and R. A. Ketola, *Rapid Communications in Mass Spectrometry*, 2007, 21, 3677-3682.
24. A. G. Chambers and J. M. Ramsey, *Analytical Chemistry*, 2012, 84, 1446-1451.
25. Y. Cong, S. Katipamula, C. D. Trader, D. J. Orton, T. Geng, E. S. Baker and R. T. Kelly, *LChip*, 2016, DOI: 10.1039/C6LC00183A.
26. P. Mao, R. Gomez-Sjoberg and D. Wang, *Analytical chemistry*, 2013, 85, 816-819.
27. A. Mar, F. James and Y. Y. Leslie, *Nanotechnology*, 2008, 19, 455103.
28. H. Sedgwick, F. Caron, P. B. Monaghan, W. Kolch and J. M. Cooper, *Journal of The Royal Society Interface*, 2008, 5, S123-S130.
29. K. Tveen-Jensen, F. Gesellchen, R. Wilson, C. M. Spickett, J. M. Cooper and A. R. Pitt, *Sci. Rep.*, 2015, 5, 9736.
30. M. Kwiatkowski, M. Wurlitzer, M. Omidi, L. Ren, S. Kruber, R. Nimer, W. D. Robertson, A. Horst, R. Miller and H. Schlüter, *Angew. Chem. Int. Ed.*, 2015, 54, 285-288.
31. L. Ren, W. D. Robertson, R. Reimer, C. Heinze, C. Schneider, D. Eggert, P. Truschow, N.-O. Hansen, P. Kroetz, J. Zou and R. J. D. Miller, *Nanotechnology*, 2015, 26, 284001.
32. Y. Lu, C. L. Pieterse, W. D. Robertson and R. J. Miller, *Anal. Chem.*, 2017, submitted.
33. W. D. Robertson, L. R. Porto, C. J. X. Ip, M. K. T. Nantel, F. Tellkamp, Y. Lu and R. J. Dwayne Miller, *Review of Scientific Instruments*, 2015, 86, 086105.
34. K. Franjic and R. J. D. Miller, *PCCP*, 2010, 12, 5225-5239.

Supporting Information

Direct Laser Sampling of Aqueous Solutions from Lab-on-a-Chip Devices for Mass Spectrometry

Y. Lu[a,ŧ], C. L. Pieterse[a], D. Eggert[c], Candice Ip[a,b], F. Busse[a], S. Keskin[a,d], W. D. Robertson[a,ŧ] and R. J. D. Miller[*a,e]
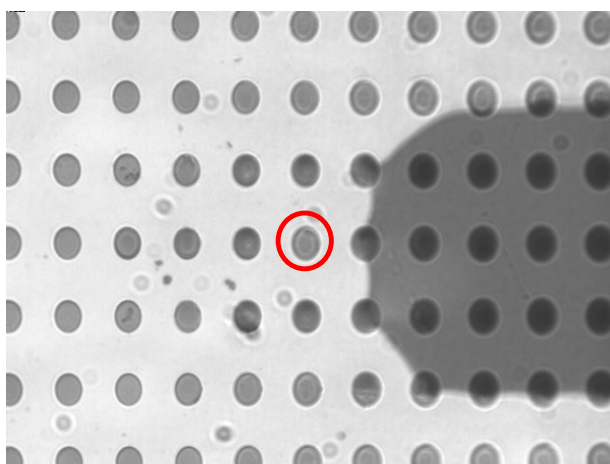
Figure S1. Image of wells wetted by sample bead during chip scanning. The ablated and emptied well is marked with red circle and is lighter in contrast to the surrounding filled wells.
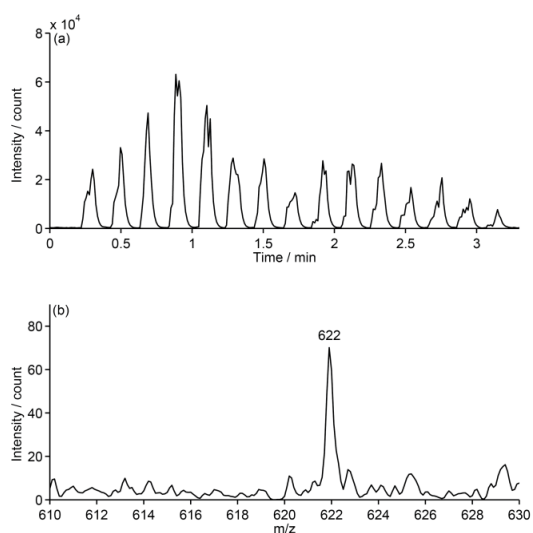
Figure S2. (a) Total ion current of a 30 femtomoles aqueous solution of HexPE (b) Average mass spectrum from TIC in Figure S2 (a), corresponding to the sample being loaded and sampled directly from the aqueous self-sorting array.

Femtosecond Pumping Rate Dependence of Fragmentation Mechanisms in Matrix-Assisted Laser Desorption Ionization

Cornelius L. Pieterse,[†] Frederik Busse,[†] Friedjof Tellkamp,[†] Wesley D. Robertson,[†] and R. J. Dwayne Miller[*,†,‡]

[†]*Max Planck Institute for the Structure and Dynamics of Matter, Luruper Chaussee 149, 22761 Hamburg, Germany*

[‡]*Departments of Chemistry and Physics, University of Toronto, 80 St. George Street, Toronto, Ontario, M5S 3H6, Canada.*

E-mail: dwayne.miller@mpsd.mpg.de

Abstract

The benzyltriphenylphosphonium (BTP) thermometer ion is utilized to characterize the fragmentation mechanisms of matrix-assisted laser desorption/ionization (MALDI) for ultraviolet femtosecond laser pulses. We demonstrate that the survival yield of the BTP approaches unity under these conditions, which suggests that a minimal amount of fragmentation is occurring. It is also shown that the survival yield of BTP is insensitive to the laser fluence. However, the magnitude of the fragmentation for the matrix increased notably for the same fluence range. These results indicate that the amount of internal energy transferred from the matrix ions to the BTP thermometer ions is minimal because the femtosecond pulses applied here occur within the stress confinement regime. This observation is in agreement with recent molecular dynamics simulations which predict that it should be possible to the separate desorption and ionization processes in the regime of stress confined ablation. Our preliminary results indicate that angiotensin is the largest biomolecule which could be routinely measured with these pulses, supporting the assumption that ionization is hindered by a reduced temporal overlap of matrix and analyte ions.

Graphical TOC Entry

Introduction

Shortly after the initial reports by Karas and Hillenkamp on the analysis of large biomolecules using matrix-assisted laser desorption/ionization (MALDI),[1] the influence of the laser pulse duration on the desorption/ionization mechanism was discussed.[2] This study demonstrated that ultrashort (femtosecond) pulses could be applied similarly as to nanosecond pulses, with the only recognized disadvantage being that there exists an accessible mass upper limit. In this study, Demirev *et al.* compared the mass spectra generated by using either a nitrogen ($\lambda = 337$ nm, $\tau = 3$ ns) or a dye laser ($\lambda = 248$ nm, $\tau = 560$ fs) interfaced to a linear time-of-flight mass spectrometer. This was the first study to clearly indicate that the MALDI process is primarily dependent on the laser pulse fluence and not the irradiance. It was further observed that the intensity of insulin ions ($\sim$5000 Da), relative to the ferulic acid matrix ions, was significantly smaller for the femtosecond versus nanosecond pulses.[2] Following this study, there have only been a small number of studies investigating ultrashort pulses for the purpose of desorbing and ionizing biomolecules in MALDI.[3–6] In support of this observation, when comparing the photoionised neutrals and directly desorbed ions for two nitrogen lasers (550 ps versus 3 ns), Karas *et al.* reported that the only difference between the mass spectra produced by these lasers was a small difference in the fluence thresholds.[3] Papantonakis *et al.* performed a comprehensive study in order to help illuminate the ionization mechanisms by comparing the mass spectra produced by a nitrogen ($\lambda = 337$ nm, $\tau = 3$ ns), a Nd:YAG ($\lambda = 266$ nm, $\tau = 2$ ns) and also a Ti:Sapphire ($\lambda = 266$ nm, $\tau = 120$ fs) laser.[4] In agreement with the earlier reports, their mass spectra appeared nearly identical for all of the different systems investigated. However, it should be mentioned that their analytes were diluted to relatively low matrix-to-analyte ratios (100:1 for angiotensin II and β-cyclodextrin and 10:1 for erythromycin), which is in contrast with other investigations where this ratio is generally at least an order of magnitude larger.[2–7] It is well-established that for a matrix-to-analyte ratio smaller than ~ 100, the matrix peaks are quite often suppressed relative to the analyte peaks, so it is difficult to compare these results with those of other studies.[7,8] Nevertheless, for the majority of their reported mass spectra, the analyte-to-matrix peak ratio was smaller for the femtosecond versus nanosecond pulses.[4]

The first quantitative comparison between ultrashort picosecond ($\lambda = 355$ nm, $\tau = 22$ ps) and nanosecond ($\lambda = 337$ nm, $\tau = 4$ ns) pulses were performed by Chen and Vertes through studying various biomolecules prepared in the matrixes 2,5-dihydroxybenzoic acid (DHB),[9] sinapinic acid (SA), and also α-cyano-4-hydroxycinnamic acid (CHCA) pellets.[5] Their results corroborated all of the previous observations for ultrashort pulses, while also reporting that all of the investigated matrices are significantly more likely to fragment when irradiated with the longer pulses. Most importantly, analogous to the observation for femtosecond pulses,[2] it was reported that insulin was the upper mass-limit for picosecond pulses. The explanation by Chen and Vertes was that considering the high optical pumping rates achievable with the picosecond pulses, the temporal overlap between these neutral biomolecules and the matrix ions in the desorption plume is too small to result in sufficient ionization.[5] Furthermore, since

the internal energy of a molecular ion determines the potential fragmentation pathways, this is a compelling method to characterize the softness of the given desorption method.[10] For this reason, the collisional transfer of energy from the matrix to the analyte was investigated by using the thermometer ion benzyltriphenylphosphonium (BTP) in a subsequent study.[6] The simple structure and known fragmentation channels of the benzylpyridinium species render them attractive candidates to monitor the transfer of energy during the desorption process because they are already present in the solid phase as preformed ions.[11–13] Comparing these nanosecond and picosecond lasers, it was reported that the picosecond pulses resulted in a lower net transfer of energy.[6] This observation was interpreted to be the result of picosecond desorption occurring under stress confinement conditions, whereas the nanosecond desorption process was only thermally confined.[14] Molecular dynamics simulations suggested that when operating under stress confinement conditions, the desorption and ionization processes should be separable, which would allow a unique control over the measurement conditions.[15] This has recently raised interest for the resonant excitation and ablation of aqueous solutions and tissues using picosecond infrared lasers to facilitate extremely soft material extraction under stress confinement conditions.[15–17] The usage of this method demonstrated that it is possible to extract proteins and enzymes while conserving their quaternary structures.[18,19]

All of the mentioned studies used the almost exclusively implemented reflection geometry. The usage of a transmission geometry has been reported during the early days of MALDI,[20–23] but has never attracted a large amount of interest within the MALDI community. However, the highest imaging spatial resolution has been reported recently by using such a geometry, which indicates that there is clearly a need for revisiting the application thereof, since there are far less geometrical restrictions with regards to the focusing optics.[24,25] The qualitatively similar results obtained when comparing the transmission to the reflection geometry for the imaging of cells is indicative that the sample thickness is not a point at issue.[25] Nevertheless, a quantitative study to determine whether the transmission geometry is inferior to its reflection counter-part would be highly beneficial to future instrumentation developments. Vertes *et al.* were the first to realize a transmission geometry on a modified LAMMA 500-type system.[20] Several peptides were analysed by applying the solutions to transmission electron-microscope grids without the presence of a metallic substrate. One of the main conclusions was that since high-quality spectra were obtained, the participation of a metal substrate in the desorption process is, therefore, less likely.[20] Heise and Yeing studied the desorption process dynamics by employing a quartz microbalance, and although no mass spectra were generated, it was shown that the desorption thresholds are higher for the transmission geometry.[22]

Schürenberg *et al.* were the first and only to perform a comparison between the reflection geometry and the transmission geometry for both peptides and proteins, where they noticed distinct differences for the plume dynamics.[21] Similar to earlier studies by these authors,[26] both geometries were investigated using a fibre-coupled nitrogen laser with a relatively large ($\sim$200 μm) spot size. Although both DHB and CHCA generated good quality, qualitatively similar mass spectra, CHCA resulted in less reproducible results, unless special sample prepa-

4

ration methods were employed. Similar to the earlier studies,[22] the threshold fluences tended to be larger for the transmission geometry. A noteworthy result from this study was that the mean ion velocities for the transmission geometry were significantly lower than those of the reflection geometry. The discrepancy was attributed to a spatial confinement within a thick sample layer and the resulting turnaround time it takes for the molecules to be accelerated towards the ion extraction optics. Nevertheless, it was shown the measured spectra are still in quantitative agreement for both geometries, especially with regards to the mass resolution and analyte fragmentation.[21] We found it surprising initially that no additional studies were performed until only rather recently since the transmission geometry appears to offer several advantages over the standard reflection geometry.

In this work, we report on the transfer of internal energy which occurs during ultraviolet, femtosecond desorption by probing the fragmentation mechanism of BTP thermometer ions. It was decided to perform these measurements in a transmission geometry since the internal energy transferred during the desorption process has not been studied before for this system. The survival yield of the BTP is shown to approach unity for the pulse energies studied, which is in agreement with molecular dynamics simulations which anticipated that the desorption and ionization processes would become separable under stress confinement conditions. We, therefore, demonstrated that a transmission geometry with femtosecond lasers could be used in a similar fashion as to the standard reflection geometry with nanosecond lasers.

Experimental

Experiments were carried out on a home-built linear time-of-flight mass spectrometer, which is schematically illustrated in Figure 1. The samples were desorbed using the third harmonic ($\lambda = 343$ nm, $\tau = 190$ fs) output of a regeneratively amplified Yb:KGW oscillator (Pharos SP 1.5mJ, Light Conversion, Vilnius, Lithuania) with an output pulse-to-pulse stability better than 0.5% rms over 24 hours. The measurements were performed in a transmission geometry by focusing the near-Gaussian beam to a spot diameter of 225 ± 7 μm (per $1/\text{e}^2$ definition) at the sample surface using a $L = 750$ mm lens (LA4716-UV-ML, Thorlabs GmbH, Munich, Germany) located outside the vacuum chamber. The spot size was regularly determined with high-precision knife-edge measurements. The pulse energy could be set between 2 and 10 μJ, as measured before experiments using a calibrated photodiode (S120VC, Thorlabs GmbH), resulting in peak fluences of between ~100 and 500 J/m^2 at the sample surface. The sample holder was mounted on three nanometer-precision stages (SLC series, SmarAct, Oldenburg, Germany) which enabled an area of approximately 1×1 cm^2 to be scanned relative to the laser focal position. The sample was imaged from the backside using a long working distance microscope (Optem Fusion, Qioptiq Photonics GmbH, Göttingen, Germany).
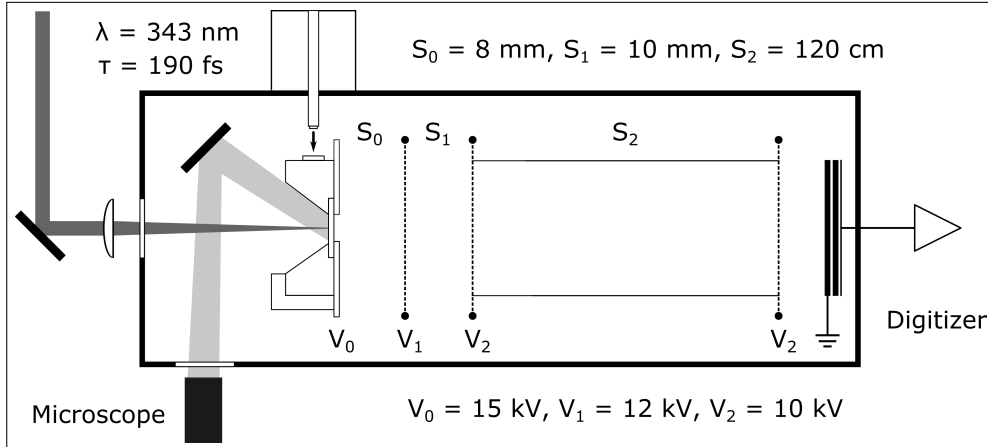
Figure 1: Experiments were performed in a transmission geometry on a linear time-of-flight mass spectrometer, in which the laser beam strikes the backside of the substrate co-linearly with the ion extraction axis. Refer to text for further details (figure is not drawn to scale).

Following desorption, positive ions were accelerated to a nominal kinetic energy of 5 keV in a static, two-stage extraction region, supplemented with an 10 keV post-acceleration stage, resulting in a total energy of 15 keV upon reaching the detector.[27] In order to achieve these conditions, the sample and the extraction grid was maintained at 15 and 12 kV respectively, while the flight tube was maintained at 10 kV to facilitate post-acceleration. Distances were set to $S_0 = 8$ mm between the sample surface and the extraction grids, and to $S_1 = 10$ mm between the extraction grid and the field-free drift region, which had a length of $S_2 = 120$ cm. Stabilized, high-precision, digital power supplies were used for all of these experiments (EHS series, Iseg Spezielelektronik GmbH, Radeberg, Germany). Only positive ions were measured using a dual-stage chevron microchannel plate detector (F9890, Hamamatsu, Bridgewater, USA) with a built-in signal decoupling circuit, which was recorded by using an 8-bit digitizer (DC211, Acquiris, Plan-les-Ouates, Switzerland). The signal acquisition was triggered by a fast photodetector (DET10A/M, Thorlabs) located to measure stray light. Synchronization was coordinated by using a computer controlled delay generator (DG645, Stanford Research Systems, Sunnyvale, USA). The pressure inside the analyser chamber was in general better than 2.0×10^{-7} mbar at the beginning of the measurements immediately after sample loading, improving to a pressure of better than 8.0×10^{-8} mbar at the end of the measurement.

Double side polished fused silica wafers of ∼1 mm thickness were employed as the sample substrate, which is transparent in the wavelength range studied. The surface of a single side was roughened with 600 grit sandpaper, facilitating small crystal formation and therefore improving sample homogeneity. Substrates were cleaned according to established MALDI protocols, stored in ethanol, and finally air dried with a nitrogen gas stream before usage.[28] The analytes, benzyltriphenylphosphonium chloride (99 %) and angiotensin I acetate salt hydrate (90 %), were purchased from Sigma-Aldrich Chemie GmbH (Munich, Germany). The matrix DHB was purchased from Bruker Daltonik GmbH (Bremen, Germany). Analyte

6

solutions (0.1 mg/ml) were prepared in deionized water (PURELAB Classics, ELGA) with 0.1% trifluoroacetic acid (TFA). The matrix solution (10 mg/ml) was prepared in a standard 1:2 (v/v) mixture of acetonitrile and deionized water with 0.1% TFA.[29] All chemicals were used without further purification.

Matrix and analyte solutions were mixed 1:2 to yield a molar matrix-to-analyte ratio of ∼3000.[5,10] Droplets containing 3.0 μl of this mixture were spotted on the roughened substrate and rapidly vacuum dried to produce more uniform crystals,[10,30] since this protocol is known to result in improved quantification and reproducibility.[31,32] In addition, for all of the results presented here, the samples were prepared in a single spotting and drying cycle to ensure that the crystallization conditions were identical, and only those samples showing similar dried droplet sizes were selected. The results obtained with the matrix CHCA was of an inferior quality compared to the DHB and the repeatability was challenging (other workers have also made this observation, especially for the transmission geometry).[21,31] For these reasons, it was decided to focus on DHB in this study exclusively. The laser spot size, fluence, sample preparation protocol, and the magnitude of the extraction and post-acceleration fields was implemented in accordance with the conditions previously employed for the transmission geometry to facilitate a quantitative and reproducible comparison.[21,26]

The lowest fluence reported here (126 J/m^2) was about 1.5 times greater than the DHB matrix fragmentation threshold and was selected because BTP did not significantly fragment for the studied fluence range. Usage of the matrix fragmentation threshold was motivated by observing that the fragmentation thresholds of the DHB matrix[5] and BTP thermometer[6] ions were comparable for picosecond pulse durations.[5,6] The complete area associated with a given sample was scanned for laser fluence values within a range between 1.5 and 2.7 times the fragmentation threshold. Only those single shot spectra for which the largest peak was above a defined threshold were averaged while each spectrum was calibrated using the DHB matrix and BTP theremometer parent ion peaks. This strategy resulted in about 500 spectra being averaged per sample, with the resulting spectrum, therefore, being more representative of the given sample, in contrast to measuring a large number of spectra at a single position. Following the same methodology as previous studies,[6,10] the survival yields α were calculated as $\alpha = \sum I_M / (\sum I_M + \sum I_F)$, where $\sum I_M$ and $\sum I_F$ are the integrated abundances of the quasi-molecular parent and fragment ions respectively.[13] For DHB only the dehydroxylated fragment was considered, while for BTP both the benzyl and triphenylphosphine fragments were. The resulting yield distributions were used to determine the mean survival yields.

Results and discussion

Following the same methodology as previous studies, which compared the effects of different pumping rates on the MALDI mechanism,[5,6] the survival yields for both the DHB matrix[5] and the BTP thermometer[6] ions were measured for various fluences. A typical mass spectrum obtained when studying such a fragmentation mechanism is shown in Figure 2, from which the DHB matrix (m/z 154) and the BTP thermometer (m/z 353) parent ion peaks are visible. It is immediately clear that the BTP only slightly fragmented since the peaks associated with both the benzyl (m/z 91, fragment F1) and triphenylphosphine radicals (m/z 262, fragment F2) are hardly visible. However, the dehydroxylated DHB ion (m/z 137) is pronounced.
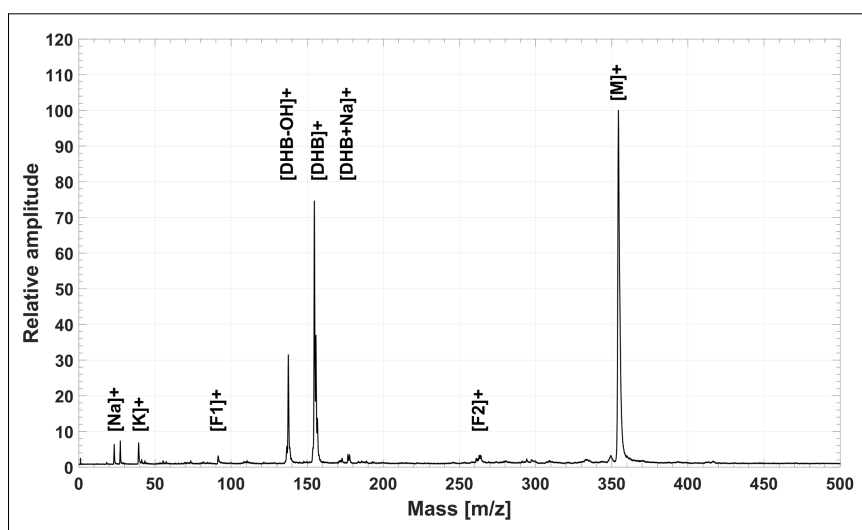
Figure 2: Mass spectrum for the low fluence (126 J/m^2) measurement showing the molecular BTP thermometer ion (M, m/z 353) and the DHB matrix ion (m/z 154), as well as both the BTP thermometer ion fragments. Refer to the text for additional details.

Figure 3 shows the peaks of interest normalized to the DHB and BTP parent ion peaks for different fluences. Unfortunately, similar crystallization conditions could only be achieved for a limited number of samples within one batch, limiting the number of fluence datapoints. Nevertheless, the reproducibility between samples within the same batch was high, such as shown in Figure S1 for several measurements performed under similar conditions. The mean survival yields for DHB and BTP, as averaged over the complete sample area, are shown in Figure 4. Within experimental uncertainty, the BTP survival yield (~0.95) was independent of the fluence for the energies studied (1.5 to 2.7 times the matrix fragmentation threshold). The shot-to-shot and position dependent signal fluctuations are characterized by the survival yield histogram shown in Figure 4. This histogram shows the survival yield of the BTP ions for the lowest fluence measurement, which exhibits the same characteristic features as noted from previous studies.[10] Since this distribution is skewed, the maximum survival yield is in reality much higher than the given mean. These results indicate that the DHB fragmentation

threshold is lower than that of BTP and that even under conditions where large portions of the DHB fragment, the BTP still remains intact. Nevertheless, these survival yields are still suitable to monitor the energy content of these ions and the associated transfer thereof.
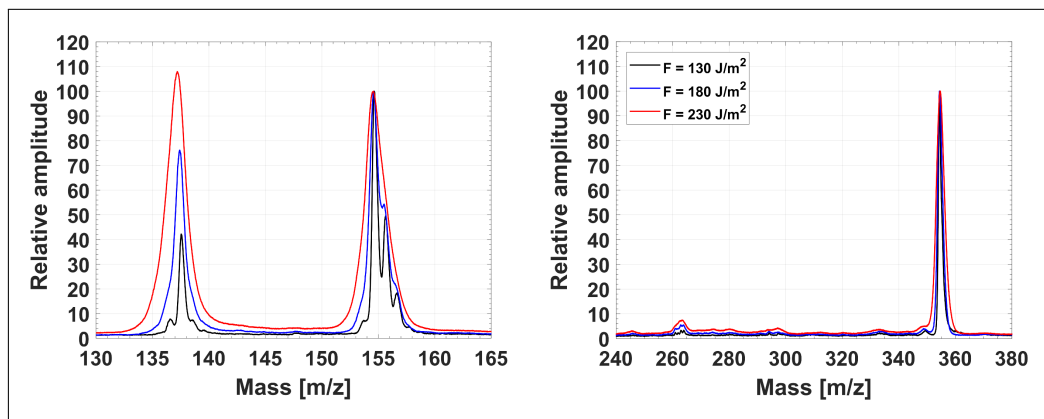
Figure 3: Mass spectra of the DHB matrix and BTP thermometer ions for fluences studied. The spectra was normalized relative to the parent peaks to calculate the survival yields.

In comparison, the previous study with 22 ps pulses reported a lower BTP survival yield (∼0.87) which was notably more sensitive to the fluence.[6] While the results presented there contained a large uncertainty, they showed a distinct decrease in BTP survival yield (∼0.67) when increasing the fluence to 1.3 times the BTP fragmentation threshold. Moreover, even lower survival yields were observed for nanosecond pulses.[6] Even though care must be taken when comparing different threshold definitions, we believe we observed a continuation of the trends reported for the comparison of nanosecond and picosecond pulse durations: a higher survival yield for the shorter pulse durations.[6] A reduced transfer of internal energy from the matrix to the analyte molecules can be explained by high-pressure gradients which result from stress confined desorption; the energy deposition step is completed well before any noticeable movement of sample material can occur,[14] which results in the very short time window during which both species can interact. While the picosecond pulses only resulted in a partial stress confinement,[6] the femtosecond pulses utilized here lead to fully stress confined desorption and transferred even less internal energy to the thermometer ions. Although spectral variations in the absorption coefficient could potentially yield an alternative explanation of the observed trend, recent results indicate the differences in wavelength between the different lasers would not explain the different survival yields.[33,34]

It should be noted that a lower matrix fragmentation threshold (84 J/m^2) was observed than for previous studies. However, since the present spot size (225 μm) is considerably larger than for the picosecond studies (55 μm), the different fragmentation thresholds should not be unexpected: earlier studies have shown that the thresholds are a function of the spot size.[35,36] It is established that by using the threshold fluence of the small spot size for a larger spot size would result in both extensive fragmentation and loss of mass resolution.[26,36] The detection

threshold of DHB for the spot size of this study is also in accord with previous studies.[26,33] For a better comparison, we will only compare the relative increase of the pulse energy above the fragmentation threshold, since that will determine the magnitude of fragmentation.
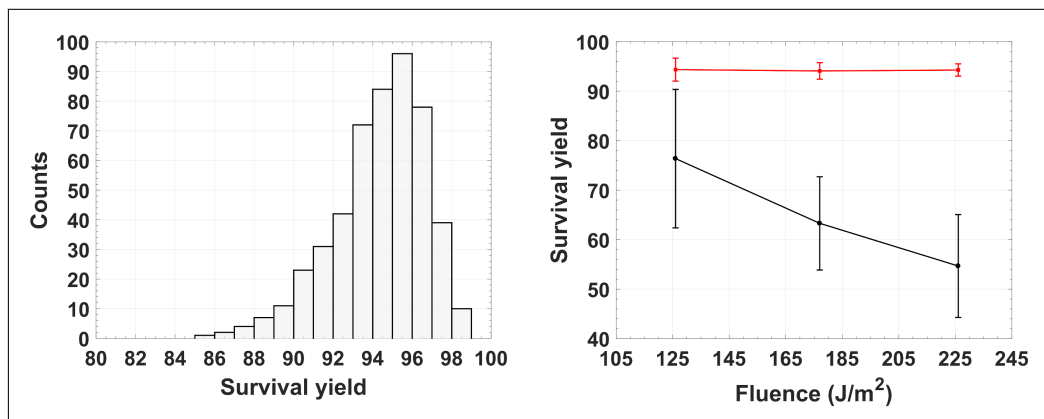
Figure 4: Survival yield distribution of the BTP ions for the low fluence measurement. Also shown are the mean survival yields of the BTP and DHB ions for the fluence range studied.

It is important to highlight that fragmentation of the DHB matrix increased significantly for the maximum pulse energies studied. Earlier pumping rate studies did not consider a very broad fluence range for the ultrashort pulses, which impedes detailed comparisons from being performed. Most importantly, the previous studies only reported either on the DHB matrix[5] or the BTP thermometer[6] ions, but a combined analysis was unfortunately not performed. However, these studies did indicate that the fragmentation thresholds of the DHB and BTP ions were comparable for the picosecond pulse durations. A similar observation has also been made when studying liable biomolecules using nanosecond pulses.[37] Assuming unimolecular reactions, the internal energy becomes equivalent to the concept of an effective temperature. It is established that the effective temperature within the desorption plume can be deduced from the extent of matrix fragmentation.[38,39] Therefore, considering earlier studies, combined with both the peak broadening and excessive matrix fragmentation observed for high fluence values, it is clear that these measurements were performed under particularly hot conditions. The next step would be to investigate these dynamics using delayed extraction since it has been shown that the survival yield tends to be notably higher under such conditions.[11,12]

These observations thus provide additional support for the hypothesis that the amount of internal energy transferred from the DHB matrix ions to the BTP thermometer ions were minimal, even though a significant amount of material has been ejected into the gas-phase. Molecular dynamics simulations describing the desorption of a model peptide by a picosecond infrared laser anticipated a similar observation: when operating under the conditions of stress confinement, the desorption and ionization processes should be separable, therefore allowing the desorption process to be optimized by adjusting the pulse fluence, followed by optimizing the ion separation process using an appropriate electric field.[15]

In order to understand the fragmentation mechanism inherent to the desorption process, it is required to experimentally isolate this process while also mitigating other fragmentation mechanisms. Another common fragmentation mechanism is meta-stable decay, which occurs along the drift tube as a consequence of the collisional energy acquired by ions from multiple collisions with neutral molecules within the desorption plume.[40–43] The prevailing approach is to reduce the transfer of collisional energy by implementing delayed extraction.[41] As a result of this approach, it is thus possible to probe certain temporal characteristics associated with the desorption process.[12] However, due to an added level of complexity, experiments are often rather performed under continuous conditions. Fortunately, by usage of post-acceleration,[43] it was possible to employ low extraction fields within the source region, which reduces these ion collisions, but still ensured that the ions have sufficient kinetic energies to result in unity detection efficiencies.[44] The main disadvantage of this approach is that the time window for metastable decay to occur is increased,[40] but since measurements were performed under low residual gas pressures, the probability of this occurring was significantly reduced.[41] Another advantage of the post-acceleration scheme is that the fragments formed within the drift tube will also be accelerated to sufficient kinetic energies for detection.[43] Even though it was not within the scope of the present study, a preliminary analysis shows that the magnitude of the metastable fragmentation occurring is minimal. Given that static extraction conditions were used, it was unexpected that only such a small amount of meta-stable decay occurred.[45] To rule out the low extraction field conditions, measurements were performed under considerably higher extraction fields, but there was no significant difference in the results.

The aspect which intrigued the authors most was the observation that there exists a mass upper-limit when using ultrashort laser pulses for desorption.[2,5] Due to the high-complexity of these measurements, we will only report our preliminary results here, since an investigation of performing desorption of peptides and proteins with ultrashort pulses are to be discussed elsewhere. As already mentioned, Demirev *et al.* reported that for the femtosecond pulses a significantly larger yield of matrix ions were produced.[2] These results were corroborated by a subsequent investigation by Chen and Vertes for picosecond pulses.[5] Our preliminary results supplement both of these observations: angiotensin I (∼1300 Da) was the largest biomolecule which could be routinely measured, even though the intensity thereof was about two orders of magnitude less than that of the DHB matrix (see Figure S2 for the comparison). It should be mentioned that increasing the fluence resulted in a deterioration of mass resolution, but the ratio of analyte-to-matrix ions did not increase. The relative intensity of the peptide ion did, however, increase when using delayed extraction, which suggests that the ionization yield was probably increased due to more time being available for gas-phase reactions to occur.[43] This observation is in agreement with the hypothesis that due to very high optical pumping rates achievable with ultrashort pulses, the temporal overlap between the neutral biomolecules and the matrix ions in the plume is too small to result in sufficient ionization.[5] Such a mechanism would explain why Chen and Vertes managed to routinely measure insulin ions for picosecond pulses, in comparison to our experiments where we were limited to angiotensin.[46]

Conclusions

We have demonstrated that the survival yield of the BTP thermometer ion approach unity upon desorption with ultraviolet femtosecond pulses. It is shown that, within experimental uncertainty, the fragmentation as a direct consequence of the desorption process is relatively insensitive to the laser pulse energies in the region close to the detection threshold. However, the magnitude of matrix fragmentation into dehydroxylated ions increased significantly over the same pulse energy range. Therefore, combined with the peak broadening observed for the higher pulse energies, it is evident that the measurements were performed under unusually hot conditions, which supports the hypothesis that the internal energy transferred from the matrix to the thermometer ions were minimal, even though ample material was ejected into the gas-phase. This observation is in agreement with recent molecular dynamics simulations since those results anticipated that it should be possible to separate desorption and ionization processes using stress confinement conditions.

We, therefore, observed an extension of the earlier trends identified comparing nanosecond to picosecond pulse durations, which reported the higher survival yield for the shorter pulses. The femtosecond pulses applied here fall within the stress confinement regime, which explains why these pulses would transfer less internal energy to the thermometer ions than picosecond pulses, which will only lead to partial stress confinement. Preliminary results indicated that angiotensin was the largest biomolecule which could be routinely measured. It should be noted that the intensity of this peptide was approximately two orders of magnitude less than that of the matrix. This result supports an earlier hypothesis that the ionization yield is low due the temporal overlap between the neutral biomolecules and the matrix ions being too small to result in the sufficient ionization.

Supporting Information Available
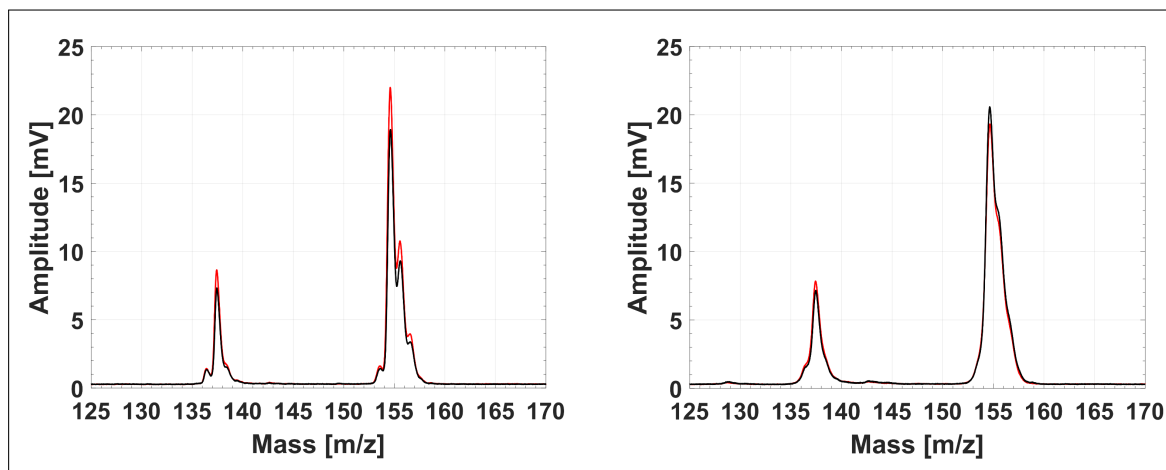
Figure S1: Repeatability is high within a given batch of samples, such as shown here for two measurements performed under identical conditions for two different batches.
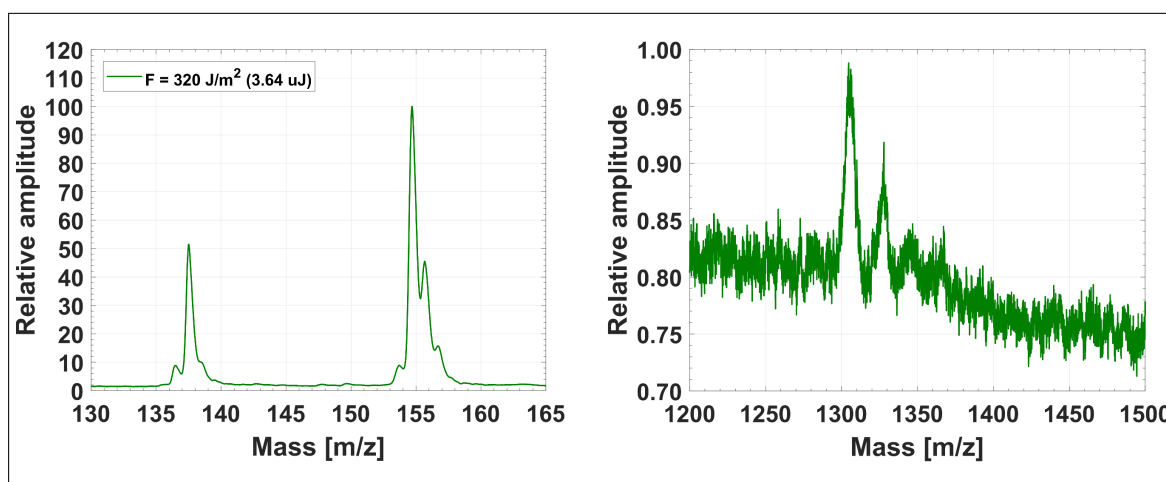
Figure S2: Angiotensin was the largest biomolecule to be routinely measured. Note that the peak intensity thereof was about two orders of magnitude less than that of the DHB matrix.

References

(1) Karas, M.; Hillenkamp, F. Laser Desorption Ionization of Proteins with Molecular Masses Exceeding 10 000 Daltons. *Analytical Chemistry* **1988**, *60*, 2299–2301.

(2) Demirev, P.; Westman, A.; Reimann, C. T.; Håkansson, P.; Barofsky, D.; Sundqvist, B. U. R.; Cheng, Y. D.; Seibt, W.; Siegbahn, K. Matrix-assisted laser desorption with ultra-short laser pulses. *Rapid Communications in Mass Spectrometry* **1992**, *6*, 187–191.

(3) Dreisewerd, K.; Schürenberg, M.; Karas, M.; Hillenkamp, F. Matrix-assisted laser desorption/ionization with nitrogen lasers of different pulse widths. *International Journal of Mass Spectrometry and Ion Processes* **1996**, *154*, 171–178.

(4) Papantonakis, M. R.; Kim, J.; Hess, W. P.; Haglund, R. F. What do matrix-assisted laser desorption/ionization mass spectra reveal about ionization mechanisms? *Journal of Mass Spectrometry* **2002**, *37*, 639–647.

(5) Chen, Y.; Vertes, A. Pumping rate and surface morphology dependence of ionization processes in matrix-assisted laser desorption ionization. *Journal of Physical Chemistry A* **2003**, *107*, 9754–9761.

(6) Luo, G.; Marginean, I.; Ye, L.; Vertes, A. Competing ion decomposition channels in matrix-assisted laser desorption ionization. *Journal of Physical Chemistry B* **2008**, *112*, 6952–6956.

(7) Knochenmuss, R.; Dubois, F.; Dale, M. J.; Zenobi, R. The matrix suppression effect and ionization mechanisms in matrix-assisted laser desorption/ionization. *Rapid Communications in Mass Spectrometry* **1996**, *10*, 871–877.

(8) Knochenmuss, R. The Coupled Chemical and Physical Dynamics Model of MALDI. *Annual Review of Analytical Chemistry* **2016**, *9*, 365–385.

(9) Strupat, K.; Karas, M.; Hillenkamp, F. 2,5-Dihydroxybenzoic acid: a new matrix for laser desorptionâĂŤionization mass spectrometry. *International Journal of Mass Spectrometry and Ion Processes* **1991**, *111*, 89–102.

(10) Luo, G.; Marginean, I.; Vertes, A. Internal energy of ions generated by matrix-assisted laser desorption/ionization. *Analytical Chemistry* **2002**, *74*, 6185–6190.

(11) Yoon, S. H.; Moon, J. H.; Kim, M. S. A Comparative study of in- and post-source decays of peptide and preformed ions in matrix-assisted laser desorption ionization time-of-flight mass spectrometry: Effective temperature and matrix effect. *Journal of the American Society for Mass Spectrometry* **2010**, *21*, 1876–1883.

(12) Gabelica, V.; Schulz, E.; Karas, M. Internal energy build-up in matrix-assisted laser desorption/ionization. *Journal of Mass Spectrometry* **2004**, *39*, 579–593.

(13) Milasinovic, S.; Cui, Y.; Gordon, R. J.; Hanley, L. Internal energy of thermometer ions formed by femtosecond laser desorption: Implications for mass spectrometric imaging. *Journal of Physical Chemistry C* **2014**, *118*, 28938–28947.

(14) Zhigilei, L. V.; Garrison, B. J. Microscopic mechanisms of laser ablation of organic solids in the thermal and stress confinement irradiation regimes. *Journal of Applied Physics* **2000**, *88*, 1281–1298.

(15) Zou, J.; Wu, C.; Robertson, W. D.; Zhigilei, L. V.; Miller, R. J. D. Molecular dynamics investigation of desorption and ion separation following picosecond infrared laser (PIRL) ablation of an ionic aqueous protein solution. *The Journal of Chemical Physics* **2016**, *145*, 204202.

(16) Vogel, A.; Venugopalan, V. Mechanisms of Pulsed Laser Ablation of Biological Tissues. *Chemical Reviews* **2003**, *103*, 577–644.

(17) Franjic, K.; Miller, R. J. D. Vibrationally excited ultrafast thermodynamic phase transitions at the water/air interface. *Physical Chemistry Chemical Physics* **2010**, *12*, 5225–5239.

(18) Ren, L.; Robertson, W. D.; Reimer, R.; Heinze, C.; Schneider, C.; Eggert, D.; Truschow, P.; Hansen, N.-O.; Kroetz, P.; Zou, J. et al. Towards instantaneous cellular level bio diagnosis: laser extraction and imaging of biological entities with conserved integrity and activity. *Nanotechnology* **2015**, *26*, 284001.

(19) Kwiatkowski, M.; Wurlitzer, M.; Omidi, M.; Ren, L.; Kruber, S.; Nimer, R.; Robertson, W. D.; Horst, A.; Miller, R. J.; Schlüter, H. Ultrafast extraction of proteins from tissues using desorption by impulsive vibrational excitation. *Angewandte Chemie International Edition* **2015**, *54*, 285–288.

(20) Vertes, A.; Balazs, L.; Gijbels, R. Matrix-assisted laser desorption of peptides in transmission geometry. *Rapid Communications in Mass Spectrometry* **1990**, *4*, 263–266.

(21) Schürenberg, M.; Schulz, T.; Dreisewerd, K.; Hillenkamp, F. Matrix-assisted laser desorption/ionization in transmission geometry: Instrumental implementation and mechanistic implications. *Rapid Communications in Mass Spectrometry* **1996**, *10*, 1873–1880.

(22) Heise, T. W.; Yeung, E. S. Dynamics of matrix-assisted laser desorption as revealed by the associated acoustic signal. *Analytica Chimica Acta* **1995**, *299*, 377–385.

(23) Lennon, J. D.; Glish, G. L. A MALDI probe for mass spectrometers. *Analytical chemistry* **1997**, *69*, 2525–9.

(24) Zavalin, A.; Yang, J.; Hayden, K.; Vestal, M.; Caprioli, R. M. Tissue protein imaging at 1 μm laser spot diameter for high spatial resolution and high imaging speed using transmission geometry MALDI TOF MS. *Analytical and Bioanalytical Chemistry* **2015**, *407*, 2337–2342.

(25) Zavalin, A.; Todd, E. M.; Rawhouser, P. D.; Yang, J.; Norris, J. L.; Caprioli, R. M. Direct imaging of single cells and tissue at sub-cellular spatial resolution using transmission geometry MALDI MS. *Journal of Mass Spectrometry* **2012**, *47*, 1473–1481.

(26) Dreisewerd, K.; Schürenberg, M.; Karas, M.; Hillenkamp, F. Influence of the laser intensity and spot size on the desorption of molecules and ions in matrix-assisted laser desorption/ionization with a uniform beam profile. *International Journal of Mass Spectrometry and Ion Processes* **1995**, *141*, 127–148.

(27) Wiley, W. C.; McLaren, I. H. Time-of-flight mass spectrometer with improved resolution. *Review of Scientific Instruments* **1955**, *26*, 1150–1157.

(28) Shen, Z.; Thomas, J. J.; Averbuj, C.; Broo, K. M.; Engelhard, M.; Crowell, J. E.; Finn, M. G.; Siuzdak, G. Porous silicon as a versatile platform for laser desorption/ionization mass spectrometry. *Analytical Chemistry* **2001**, *73*, 612–619.

(29) Vorm, O.; Roepstorff, P.; Mann, M. Improved Resolution and Very High Sensitivity in MALDI TOF of Matrix Surfaces Made by Fast Evaporation. *Analytical Chemistry* **1994**, *66*, 3281–3287.

(30) Cohen, S. L.; Chait, B. T. Influence of matrix solution conditions on the MALDI-MS analysis of peptides and proteins. *Analytical Chemistry* **1996**, *68*, 31–37.

(31) Nicola, A. J.; Gusev, A. I.; Proctor, A.; Jackson, E. K.; Hercules, D. M. Application of the fast-evaporation sample preparation method for improving quantification of angiotensin II by matrix-assisted laser desorption/ionization. *Rapid Communications in Mass Spectrometry* **1995**, *9*, 1164–1171.

(32) Gusev, A. I.; Wilkinson, W. R.; Proctor, A.; Hercules, D. M. Improvement of Signal Reproducibility and Matrix/Comatrix Effects in MALDI Analysis. *Analytical Chemistry* **1995**, *67*, 1034–1041.

(33) Robinson, K. N.; Steven, R. T.; Bunch, J. Matrix Optical Absorption in UV-MALDI MS. *Journal of The American Society for Mass Spectrometry* **2018**, *29*, 501–511.

(34) Soltwisch, J.; Jaskolla, T. W.; Hillenkamp, F.; Karas, M.; Dreisewerd, K. Ion yields in UV-MALDI mass spectrometry as a function of excitation laser wavelength and optical and physico-chemical properties of classical and halogen-substituted MALDI matrixes. *Analytical Chemistry* **2012**, *84*, 6567–6576.

(35) Dreisewerd, K. The Desorption Process in MALDI. *Chemical Reviews* **2003**, *103*, 395–426.

(36) Qiao, H.; Spicer, V.; Ens, W. The effect of laser profile, fluence, and spot size on sensitivity in orthogonal-injection matrix-assisted laser desorption/ionization time-of-flight mass spectrometry. *Rapid Communications in Mass Spectrometry* **2008**, *22*, 2779–2790.

(37) Ahn, S. H.; Park, K. M.; Bae, Y. J.; Kim, M. S. Quantitative reproducibility of mass spectra in matrix-assisted laser desorption ionization and unraveling of the mechanism for gas-phase peptide ion formation. *Journal of Mass Spectrometry* **2013**, *48*, 299–305.

(38) Knochenmuss, R. MALDI ionization mechanisms: The coupled photophysical and chemical dynamics model correctly predicts 'temperature'-selected spectra. *Journal of Mass Spectrometry* **2013**, *48*, 998–1004.

(39) Bae, Y. J.; Kim, M. S. A Thermal Mechanism of Ion Formation in MALDI. *Annual Review of Analytical Chemistry* **2015**, *8*, 41–60.

(40) Wu, K. J.; Shaler, T. A.; Becker, C. H. Time-of-Flight Mass Spectrometry of Underivatized Single-Stranded DNA Oligomers by Matrix-Assisted Laser Desorption. *Analytical Chemistry* **1994**, *66*, 1637–1645.

(41) Kaufmann, R.; Chaurand, P.; Kirsch, D.; Spengler, B.; Karas, M. Post-source decay and delayed extraction in matrix-assisted laser desorption/ionization-reflectron time-of-flight mass spectrometry. Are there trade-offs? *Rapid Communications in Mass Spectrometry* **1996**, *10*, 1199–1208.

(42) Karas, M.; Bahr, U.; Strupat, K.; Hillenkamp, F.; Tsarbopoulos, A.; Pramanik, B. N. Matrix Dependence of Metastable Fragmentation of Glycoproteins in MALDI TOF Mass Spectrometry. *Analytical Chemistry* **1995**, *67*, 675–679.

(43) Christian, N. P.; Colby, S. M.; Giver, L.; Houston, C. T.; Arnold, R. J.; Ellington, A. D.; Reiily, J. P. High resolution matrix-assisted laser desorption/ionization time-of-flight analysis of single-stranded DNA of 27 to 68 nucleotides in length. *Rapid Communications in Mass Spectrometry* **1995**, *9*, 1061–1066.

(44) Gilmore, I. S.; Seah, M. P. Ion detection efficiency in SIMS: Dependencies on energy, mass and composition for microchannel plates used in mass spectrometry. *International Journal of Mass Spectrometry* **2000**, *202*, 217–229.

(45) Spengler, B.; Kirsch, D.; Kaufmann, R.; Cotter, R. J. Metastable decay of peptides and proteins in matrix-assisted laser-desorption mass spectrometry. *Rapid Communications in Mass Spectrometry* **1991**, *5*, 198–202.

(46) Wang, B. H.; Dreisewerd, K.; Bahr, U.; Karas, M.; Hillenkamp, F. Gas-Phase cationization and protonation of neutrals generated by matrix-assisted laser desorption. *Journal of the American Society for Mass Spectrometry* **1993**, *4*, 393–398.

Rapid Deconvolution of Low-Resolution Time-of-Flight Data using Bayesian Inference

Cornelius L. Pieterse,[†] Michiel B. de Kock,[‡] Wesley D. Robertson,[†]

Hans C. Eggers,[‡,§] and R.J. Dwayne Miller*[,†,¶]

[†]*Max Planck Institute for the Structure and Dynamics of Matter, Luruper Chaussee 149, 22761 Hamburg, Germany*

[‡]*Department of Physics, Stellenbosch University, P/Bag X1, Matieland 7602, South Africa*

[¶]*Departments of Chemistry and Physics, University of Toronto, 80 St. George Street, Toronto, Ontario, M5S 3H6, Canada.*

[§]*National Institute for Theoretical Physics, P/Bag X1, 7602 Matieland, South Africa*

E-mail: dwayne.miller@mpsd.mpg.de

1

Abstract

The deconvolution of low-resolution time-of-flight data has numerous advantages including the ability to extract additional information from the experimental data. We augment the well-known Lucy-Richardson deconvolution algorithm by various Bayesian prior distributions and show that a prior of second-differences of the signal outperforms the standard Lucy-Richardson algorithm by accelerating the rate of convergence by a factor of two and preserving the peak amplitude ratios of a larger fraction of the total peaks. A stopping criterion and boosting mechanism is implemented to ensure that these methods converge to the same final entropy and that local minima are avoided. Improvement by a factor of two in mass resolution of the signal allowed more accurate quantification of the spectra. The general method is demonstrated in this paper by the deconvolution of fragmentation pathway peaks of the benzyltriphenylphosphonium thermometer ion following femtosecond ultraviolet laser desorption.

Introduction

Mass spectrometry (MS) is practiced in various settings, including commercial applications such as quality control[1] and pharmacokinetics,[2] as well as basic scientific investigations such as proteomics[3] and biological pathway analysis.[4] While operation of mass spectrometers can be regarded as a routine and high-throughput task, the correct interpretation of the spectra requires a chemistry background and often ample experience. Recent interest in the detection of biomarkers[5] further underlines the significance of accurate and thorough interpretation of mass spectrometric data. It has been demonstrated that it is possible to distinguish between healthy and unhealthy domains of mammalia tissue sections when comparing their respective mass spectrometric data.[6–8] This opens up the possibility of compiling a mass spectrometric database of biomarkers associated with recognized diseases for the identification of unhealthy tissue.[8–10] The ability to distinguish between these domains should permit the accurate identification of critical boundaries using mass spectrometric imaging techniques.

When investigating an extensive mass range, the large amounts of acquired data present an inescapable dilemma: one must either deal with very large raw data sets or else compress the raw data by averaging. While compression is a simple and adequate solution for many applications, there are cases where it destroys valuable information. A typical example would be pulsed laser beam analyses within which it might be of interest to study the mass spectra as a function of depth or shot number.[11–14]

While it has always lurked in the background, the data compression dilemma has not been acute in mass spectrometry so far, largely because investigations and results were either qualitative in nature or couched in simple terms such as one-dimensional time-independent data. As more complex measurements such as mass spectrometry imaging become feasible, the negative effects of the trade-off between much larger data sets and information loss are increasingly being felt. Each additional variable or differential quantity results in a significant increase in the number of possible outcomes, resulting in low signal-to-noise ratios.

It is of course also possible to obtain good results by brute force long acquisition times, but this may have unintended consequences. As an example, more accurate measurements could be obtained by the use of the minimum focal spot size of the laser beam to maximize resolution in mapping the boundary between two domains. The resulting longer acquisition time, however, is self-defeating because signal intensity drops in time due to the decreasing number of ions available for sampling.[15,16] It is common knowledge that the concentration of biomarkers of interest is usually orders of magnitude lower than than that of background, closely related mass species in the surrounding tissue, which frequently includes species which contribute to ion suppression and, therefore, hinder detection of these biomarkers.[3,17]

In a similar vein, mass spectrometry signals originating from a variety of ion sources are generally not constant in time. These time variabilities introduce correlations and thereby obscures the genuine average mass spectrum. For example, the intensity chromatographs of liquid samples irradiated by laser pulses under atmospheric conditions are highly transient. The fluctuating liquid interface is translated within the focal plane of the laser beam, which produces the undesired outcome of fluctuations in the signal intensity measured by the mass spectrometer.[18] These fluctuations introduce the above-mentioned time correlation artifacts, so that time averaging is inappropriate, at least until the appropriate time correlation scales have been determined. Time-dependent mass spectroscopy has turned out to be much more challenging than originally expected.

Faced with such complications, one may opt for shorter runs with less data. Shorter acquisition times, however, make it harder to distinguish signal from noise and to disentangle peaks. There is no escape from the dilemma. There is, however, a way to obtain quantitative answers even when the data is sparse and/or multivariate or complex. Encountering the same issues, other fields such as particle physics and cosmology have increasingly applied the methods of Bayesian inference with success.[19–21] It hence seems natural to us to apply similar methods to mass spectroscopy images.

In this paper, we examine the application of Bayesian methods to time-of-flight mass spectrometry data. Our two main objectives are to test the use of Bayesian deconvolution to improve mass resolution of peaks and to evaluate the robustness of this framework. The improved resolution of a deconvolved signal permits more quantitative statements regarding the fragmentation pathway of a well-known thermometer ion upon femtosecond ultraviolet desorption. Once the proposed deconvolution methods have been stress-tested in this simple environment, they may be extended to assist in decoupling of shot-to-shot phenomena.

As a valuable candidate measurement to examine the potential applicability and value of developing such a Bayesian framework, we selected a fragmentation pathway study, which characterizes the internal energy transfer occurring between the matrix and the analyte ions during the laser desorption. Although matrix-assisted laser desorption/ionization (MALDI) is routinely used,[22] the underlying ionization mechanisms are not well understood and are therefore still recurrently investigated.[23–25] Since the internal energy of an ion determines the potential fragmentation pathways, it is a powerful technique to characterize the softness of a given ionization mechanism.[26–28] However, due to the specific nature of these measurements, it is not experimentally desirable to increase the mass resolution by means of implementing delayed ion extraction or an ion reflectron, since either of these interventions could eliminate valuable quantitative information from the mass spectra.[29,30] We, therefore, used as a case study the linear mass spectra produced by internal energy transferred during the desorption process to the benzyltriphenylphosphonium (BTP) thermometer ion.

The relevant experiments were performed on an in-house designed linear time-of-flight mass spectrometer with a mass resolution of approximately 200 in the mass range of interest. As this system has been discussed before,[31] we sketch the relevant information only briefly. The third harmonic ($\lambda = 343$ nm, $\tau = 190$ fs) output pulses from a regeneratively amplified Yb:KGW oscillator (Pharos SP1.5, Light Conversion, Vilnius, Lithuania) was used for sample irradiation. Desorption was performed in a transmission geometry, after which the positive ions were accelerated to a nominal kinetic energy of 5 keV in a static, two-stage extraction region, supplemented by a 10 keV post-acceleration stage reaching the detector. Positive ions were detected with a dual-stage chevron microchannel plate detector (F9890, Hamamatsu, Bridgewater, USA). These ion signals were recorded by an 8-bit digitizer (DC211, Acquiris, Plan-les-Ouates, Switzerland) operating at an 1 ns sampling rate. For all the data presented, 100 single-shot spectra were averaged before performing the deconvolution. The final results were normalized relative to the 2,5-dihydroxybenzoic acid (DHB)[32] matrix parent ion.

Theory

In this section, we derive and discuss several Bayesian deconvolution methods for extracting the underlying signal from low-resolution time-of-flight data. Our approach is based on the well-established Lucy-Richardson deconvolution algorithm[33,34] which we supplemented with Bayesian prior distributions.

We show that a Gaussian prior based on the second-differences of the signal outperforms the standard Lucy-Richardson algorithm in terms of preserving the peak amplitude ratios for a larger fraction of the total number of peaks. To enable comparisons, a stopping criterion is introduced which monitors the mean distribution of residuals, which in combination with a boosting mechanism, ensures that the algorithm does not wind up in a local minimum and that all of the methods reach the same result.

Linear deconvolution

From a statistics viewpoint, one-dimensional mass spectrometric data is represented as a set of discrete counts n_b, one for each m/z interval, channel or *bin b* where the joint intervals of bins $b = 1, 2, \ldots, B$ cover the entire m/z interval. Barring other pertinent information, the individual events counted in any bin during the acquisition time are considered *exchangeable*;[35] suggesting that the total bin counts n_b follow a Poisson distribution

$$p(n_b \mid \lambda_b) = e^{-\lambda_b} \lambda_b^{n_b} / n_b! \qquad n_b = 0, 1, 2, \ldots, \infty \qquad b = 1, 2, \ldots, B, \tag{1}$$

where for each bin the parameter $\lambda_b > 0$, which is proportional to the acquisition time period, represents the true *signal* or expected value of counts in that bin. The vector $\boldsymbol{n} = \{n_b\}_{b=1}^B$, therefore, represents the time-averaged data of the experiment. Assuming that counts n_b are mutually independent, the joint probability of all counts given the parameters $\boldsymbol{\lambda} = \{\lambda_b\}_{b=1}^B$, also termed the *likelihood*, is given by

$$p(\boldsymbol{n} \mid \boldsymbol{\lambda}) = \prod_{b=1}^B p(n_b \mid \lambda_b). \tag{2}$$

By assumption, the data $\boldsymbol{n}$ is the sum of counts originating from underlying, but spectrally broadened, narrow peaks: each n_b is the *convolution* of these narrow peak counts. The task at hand is to reverse that convolution and to separate low-resolution data into high-resolution peaks using *deconvolution*, using where possible other pertinent information such as isotopic signatures or detector response. The goal is to find a set of parameters $\boldsymbol{s}^* = \{s_b^*\}_{b=1}^B$ which represent the best guesses of the amplitudes of a possible narrow unsmudged peak for each bin b, interpreting any small s_b^* as background noise rather than a true peak. Research on deconvolution with Poisson likelihoods started during the mid-eighties after seminal papers by Shepp and Vardi[36] and by Geman and Geman[37]; a recent review of the literature appears in Bertero et al.[38] and reviews focussed on astronomy, Puetter et al.[21] and Starck et al.[39] Books dedicated to the subject are Hansen et al.[40], Jansson[41] and Young et al.[42]

Convolution and deconvolution are modelled as linear processes. Let s_c be the true peak amplitude in bin c and let $\mathbb{A}$ be the $B \times B$ square matrix whose components $\mathbb{A}_{bc}$ constitute the peak broadening contribution which s_c makes to data in nearby bins b. The matrix $\mathbb{A}$ is usually termed the point spread function (PSF). Then the Poisson parameter in bin b is, in component and vector-matrix notation respectively,

$$\lambda_b = \sum_c \mathbb{A}_{bc} \boldsymbol{s}_c \qquad \text{or} \qquad \boldsymbol{\lambda} = \mathbb{A}\boldsymbol{s}. \tag{3}$$

Provided that the PSF depends only on the separation between the bins b and c, the matrix

$\mathbb{A}$ becomes a *Toeplitz matrix* whose components depend only on the difference between the row and column indices, $\mathbb{A}_{bc} = F_{b-c}$ where F is some non-negative function, which we can write somewhat ambiguously as $\mathbb{A}_{b-c}$. The Poisson parameters can then be written as the convolution equation

$$\lambda_b = \sum_c F_{b-c}\, \boldsymbol{s}_c. \tag{4}$$

If in addition, the point spread function has finite support (i.e. the number of neighbouring bins c contributing to λ_b is finite), then the Toeplitz matrix $\mathbb{A}$ has a block-diagonal form. Under these assumptions and limitations, the likelihood Eq. (2) can be rewritten as

$$p(\boldsymbol{n}\,|\,\mathbb{A}, \boldsymbol{s}) = \prod_b p(n_b\,|\,(\mathbb{A}\boldsymbol{s})_b) = \prod_b e^{-(\mathbb{A}\boldsymbol{s})_b}\,(\mathbb{A}\boldsymbol{s})_b^{n_b}\,/n_b!\,. \tag{5}$$

Applying Stirling's approximation $\log n! \simeq n \log n - n$ to all counts n_b, the negative logarithm of the likelihood reduces to a variant of the Kullback-Leibler divergence,

$$L[\boldsymbol{s}] = -\log p(\boldsymbol{n}\,|\,\mathbb{A}, \boldsymbol{s}) \simeq \mathbf{1}^\mathsf{T}\,(\mathbb{A}\boldsymbol{s} - \boldsymbol{n}) + \boldsymbol{n}^\mathsf{T} \log \frac{\boldsymbol{n}}{(\mathbb{A}\boldsymbol{s})}, \tag{6}$$

where $\mathbf{1}^\mathsf{T}$ is a row vector of ones and for a notational simplicity we write $\boldsymbol{n}^\mathsf{T} \log \boldsymbol{n}/(\mathbb{A}\boldsymbol{s}) \equiv \sum_b n_b \log[n_b/(\mathbb{A}\boldsymbol{s})_b]$, i.e. the division and the logarithm are taken pointwise. This variant of the Kullback-Leibler divergence is called the I-divergence[43] which is the consistent measure for images and data which are non-negative. By enforcing the normalization of the matrix $\mathbf{1}^\mathsf{T}\mathbb{A} = \mathbf{1}^\mathsf{T}$, as appropriate for convolutions, this expression simplifies to

$$L[\boldsymbol{s}] = I[\boldsymbol{n}\,|\,\mathbb{A}\boldsymbol{s}] = \mathbf{1}^\mathsf{T}\,(\boldsymbol{s} - \boldsymbol{n}) + \boldsymbol{n}^\mathsf{T} \log \frac{\boldsymbol{n}}{\mathbb{A}\boldsymbol{s}}. \tag{7}$$

The I-divergence, or also called relative entropy, $I[\boldsymbol{n}\,|\,\mathbb{A}\boldsymbol{s}]$, replaces the metric distance that appears in the usual least-squares method and can be considered as the data fidelity term. It is convex, non-negative and coercive on the non-negative orthant (the higher-dimensional generalization of the octant), implying that a minimum exists which is global and unique. The gradient and Hessian of the I-divergence are given by

$$\nabla I[\boldsymbol{n}\,|\,\mathbb{A}\boldsymbol{s}] = \mathbb{A}^\mathsf{T}\left(\mathbf{1} - \frac{\boldsymbol{n}}{\mathbb{A}\boldsymbol{s}}\right), \qquad \nabla^2 I[\boldsymbol{n}\,|\,\mathbb{A}\boldsymbol{s}] = \mathbb{A}^\mathsf{T}\mathrm{diag}\left(\frac{\boldsymbol{n}}{(\mathbb{A}\boldsymbol{s})^2}\right)\mathbb{A}. \tag{8}$$

Lucy-Richardson and Poisson algorithms

To solve the system of equations (8), the minimizer $\boldsymbol{s}^*$ of the I-divergence must be determined. The linear terms in the divergence imply that the solution must obey the constraint

$$\sum_b s_b^* = \sum_b n_b. \tag{9}$$

Moreover, the logarithm necessarily requires that $s_b^* > 0$ for all b. As the convolution is a linear operation, perfect reconstruction of the data would, in general, require both negative and positive parameter values, and this positivity condition, therefore, complicates matters considerably. In effect, it forces minimizers of the I-divergence to be sparse, i.e. the solution $\boldsymbol{s}^*$ must lie near to the boundary of the non-negative orthant. This is called the *checkerboard effect*[44] or *night-sky reconstruction*.[45] If the underlying signal contains extended objects (i.e. the object spans more than one bin), this will conflict with the sparsity precondition and the algorithm should be stopped as soon as an appropriate solution is found. The algorithm is therefore semi-convergent. The main problem is that the likelihood does not contain all the relevant information on what constitutes an image, and running it longer will only generate less plausible configurations.

Up to this point, the algorithm has followed the generally assumed superiority of Lucy-Richardson closely. To integrate it into a Bayesian framework, an appropriate prior for $\boldsymbol{s}$ must be specified. Instead of maximizing just the likelihood, the task becomes a maximization of the joint probability, which is the product of likelihood times source prior $p(\boldsymbol{n}, \boldsymbol{s}) = p(\boldsymbol{n} \,|\, \mathbb{A}, \boldsymbol{s})\, p(\boldsymbol{s})$, or equivalently minimization of the sum of the negative log likelihood and log prior $P[\boldsymbol{s}] = -\log p(\boldsymbol{s})$,

$$J[\boldsymbol{s}] = L[\boldsymbol{s}] + \beta P[\boldsymbol{s}], \tag{10}$$

where we have introduced a regularization parameter β which mediates the strength of the likelihood relative to the prior. Conventionally, the regularization parameter is placed with the prior instead of the likelihood.[46] To solve the system iteratively, we apply the gradient descent method in a general form,

$$\boldsymbol{s}_{j+1}^* = \boldsymbol{s}_j^* - \alpha f[\boldsymbol{s}_j^*] \nabla J[\boldsymbol{s}_j^*], \tag{11}$$

where α is a relaxation factor, $f[\boldsymbol{s}_j^*]$ is the Lagrange function that ensures the constraint and $\nabla J[\boldsymbol{s}_j^*]$ is the gradient. If α is chosen appropriately and $f[\boldsymbol{s}_j^*]$ is a positive function within the domain of $\boldsymbol{s}^*$, each iteration will lower the I-divergence, and the process will converge. To enforce the positivity constraint, we set $f[\boldsymbol{s}^*] = \boldsymbol{s}^*$ such that a system that starts from a

positive solution will stay positive. It corresponds to performing the transform $\boldsymbol{s} = \exp[\boldsymbol{t}]$, seeking a minimum in $\boldsymbol{t}$ and then transforming back to $\boldsymbol{s}$. Inserting Eq. (8) gives

$$\boldsymbol{s}_{j+1}^* = \boldsymbol{s}_j^* - \alpha \boldsymbol{s}_j^* \left\{ \boldsymbol{1} - \mathbb{A}^\top \left(\frac{\boldsymbol{n}}{\mathbb{A}\boldsymbol{s}_j^*} \right) + \beta \nabla P[\boldsymbol{s}_j^*] \right\}. \tag{12}$$

Setting $\alpha = 1$ and without a prior, we have the multiplicative form of the algorithm, which is the standard Lucy-Richardson algorithm,

$$\boldsymbol{s}_{j+1}^* = \boldsymbol{s}_j^* \mathbb{A}^\top \left(\frac{\boldsymbol{n}}{\mathbb{A}\boldsymbol{s}_j^*} \right). \tag{13}$$

This multiplicative form explicitly enforces the positivity constraint and therefore reduces the computational requirements of the algorithm significantly. Our own numerical investigation has indicated this form has significant advantages over its competitors. The Lucy-Richardson algorithm was introduced independently by Lucy[33] and Richardson.[34] It was rederived by Sheppi and Verdi[36] as an example of th eExpectation-Maximization(EM) algorithm,[47] which is itself a specific case of the Majorization-Minization approach.[48] To include the prior, we need to split the gradient into positive and negative parts,

$$\nabla P[\boldsymbol{s}^*] = \boldsymbol{u}^* - \boldsymbol{v}^*, \tag{14}$$

where $\boldsymbol{u}^* \geq 0$ and $\boldsymbol{v}^* \geq 0$ for all b. Rewriting the derivative equation as

$$\boldsymbol{s}^* \left(1 + \beta \boldsymbol{u}^* \right) = \boldsymbol{s}^* \mathbb{A}^\top \left(\frac{\boldsymbol{n}}{\mathbb{A}\boldsymbol{s}^*} \right) + \beta \boldsymbol{v}^* \tag{15}$$

which can then be solved iteratively with

$$\boldsymbol{s}_{j+1}^* = \boldsymbol{s}_j^* \left\{ \mathbb{A}^\top \left(\frac{\boldsymbol{n}}{\mathbb{A}\boldsymbol{s}^*} \right) + \beta \boldsymbol{v}_j^* \right\} / \left(1 + \beta \boldsymbol{u}_j^* \right). \tag{16}$$

This algorithm is called the split-gradient method (SGM).[49,50] The SGM in the multiplicative form is not always convergent due to the influence of the prior. When this occurs, we need to reduce the regularization parameter β to change the behaviour of the algorithm to be closer to that of the Lucy-Richardson algorithm which we already know is semi-convergent.[36] To summarize, the following issues need to be addressed:

1. A stopping criterion is required for the semi-convergence of the algorithm.

2. A useful prior distribution corresponding to the type of solutions we prefer is required.

3. The regularization parameter β must be adjusted so that the SGM is convergent.

Priors for the SGM

A computational simple prior distribution to consider is a Gaussian distribution[46] with the choice of an appropriate Toeplitz matrix $\mathbb{B}_j$ and a scale parameter Λ,

$$p(\boldsymbol{s} \mid \Lambda, \mathbb{B}_j) = \left(\frac{\Lambda}{2\pi}\right)^{B/2} e^{-\Lambda \boldsymbol{s}^{\mathsf{T}} \mathbb{B}_j^{\mathsf{T}} \mathbb{B}_j \boldsymbol{s}/2}. \tag{17}$$

The possible matrices $\mathbb{B}_j$, $j = 0, 1, 2, 3, 4$ reflect the underlying generic information as follows. We may have generic knowledge that the prior distribution depends either on the signal itself, or we may know that it depends on a discrete difference between signals, or even on higher-order differences. The choice of $\mathbb{B}_0 = 0$ then reflects the desire to have no prior at all, while dependence on the signal itself would motivate usage of $\mathbb{B}_1 = \mathbb{I}$, or if a constant function is preferred, the first differences of the signal

$$\mathbb{B}_2 = \begin{bmatrix} -1 & 1 & 0 & 0 & 0 & 0 & \dots & 0 \\ 0 & -1 & 1 & 0 & 0 & 0 & \dots & 0 \\ \vdots & & & \ddots & & & & \vdots \\ 0 & \dots & 0 & 0 & 0 & -1 & 1 & 0 \\ 0 & \dots & 0 & 0 & 0 & 0 & -1 & 1 \end{bmatrix}. \tag{18}$$

Choices to use higher-order signal differences are reflected in the corresponding second-order difference matrix

$$\mathbb{B}_3 = \begin{bmatrix} -1 & 2 & -1 & 0 & 0 & 0 & \dots & 0 \\ 0 & -1 & 2 & -1 & 0 & 0 & \dots & 0 \\ \vdots & & & \ddots & & & & \vdots \\ 0 & \dots & 0 & 0 & -1 & 2 & -1 & 0 \\ 0 & \dots & 0 & 0 & 0 & -1 & 2 & -1 \end{bmatrix}, \tag{19}$$

or alternatively, even a third-order difference,

$$\mathbb{B}_4 = \begin{bmatrix} 1 & -4 & 6 & -4 & 1 & 0 & \dots & 0 \\ 0 & 1 & -4 & 6 & 4 & 1 & \dots & 0 \\ \vdots & & & \ddots & & & & \vdots \\ 0 & \dots & 1 & -4 & 6 & -4 & 1 & 0 \\ 0 & \dots & 0 & 1 & -4 & 6 & -4 & 1 \end{bmatrix}. \tag{20}$$

As indicated previously, all these matrices are Toeplitz Matrices, which conveniently represent the convolution operation. As the scale parameter Λ appears only in the prior, it need not be a variable but can be replaced by its expectation value,

$$\Lambda^* = \frac{B}{1 + s^* \mathbb{B}_j^\intercal \mathbb{B}_j \boldsymbol{s}^*}, \tag{21}$$

where B is the total number of bins or elements. Λ^* can be computed on each iteration and normalizes the prior contribution. The stopping criterion, monitoring the mean distribution of residuals, and regularization parameter β are to be discussed below. The residuals are defined as the difference between the reconstructed data using our minimizers $\mathbb{A}\boldsymbol{s}^*$ and the raw time-of-flight experimental data.

Gaussian SGM

In order to investigate the effect of the underlying error distributions, we also implemented an alternative approach by simply replacing the Poisson likelihood with a Gaussian distribution. Following the same steps as in the Poisson case, we obtain an iteration prescription

$$\boldsymbol{s}_{j+1}^* = \boldsymbol{s}_j^* \left\{ \left(\frac{\mathbb{A}^\intercal \boldsymbol{n}}{\mathbb{A}^\intercal \mathbb{A} \boldsymbol{s}^*} \right) + \beta \boldsymbol{v}_j^* \right\} / \left(1 + \beta \boldsymbol{u}_j^* \right). \tag{22}$$

Without the prior, this algorithm is called the Image Space Reconstruction Algorithm (ISRA) or Muller Algorithm, which was originally proposed by Lanteri *et al.*[51] and later analyzed by De Pierro[52] and Daube-Witherspoon and Muehllehner.[53]

Results and discussion

Experimental test case

We have applied split-gradient deconvolution methods to laser desorption mass spectrometry time-of-flight data; the experimental setup has been described in Ref. 31. A representative example of the data obtained when investigating a BTP fragmentation pathway is shown in Figure 1; both the parent peaks of the BTP thermometer (m/z 353) and DHB matrix ions (m/z 154) are pronounced. The BTP fragmentation signature is known to primarily consist of the benzyl (m/z 91) and triphenylphosphine (m/z 262) ions.[27] However, since femtosecond pulses are used, the fragmentation is reduced such that these peaks are barely visible.[31] The soft nature of desorption with ultrashort pulses has been discussed elsewhere.[27,28,31]
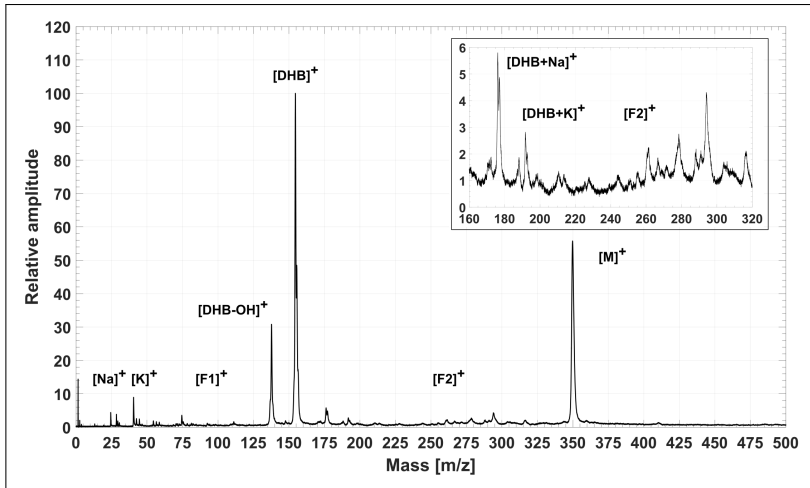
Figure 1: Mass spectrum after averaging $N = 100$ single-shot spectra. While the parent peaks of the BTP thermometer (m/z 353) and the DHB matrix (m/z 154) ions stand out clearly, the benzyl (m/z 91) and triphenylphosphine (m/z 262) ions are barely visible.

The mass resolution is significantly improved using an appropriate deconvolution method, as shown in Figure 2 for the standard Lucy-Richardson algorithm and a modification thereof by applying the second-difference prior. The deconvolved signal facilitated a more quantitative conclusion regarding the fragmentation pathway as it resulted in an improved resolution and, therefore, enabled peak-to-peak ratios to be defined. Of the five priors investigated ($\mathbb{B}_0$ to $\mathbb{B}_4$), only the standard Lucy-Richardson algorithm ($\mathbb{B}_0$) and the second-differences prior ($\mathbb{B}_3$) are discussed in this section since these two methods produced the best results. Both these methods deconvolved the data into the underlying signals while the peak amplitude ratios are evidently preserved. However, the second-differences prior performed better than Lucy-Richardson in deconvolving the underlying peak structures such as dehydroxylated DHB. This superior performance was observed for the majority of peaks, especially for those

11

having relatively small amplitudes such as triphenylphosphine. For both these methods, the recovered spectra (not shown here) overlapped the data well, which signifies an appropriate deconvolution since the deconvolved signal is capable of recovering the data.

The Lucy-Richardson algorithm is semi-convergent after an initial deconvolution period, which suggests that further iterations will not substantially improve the likelihood while continuing to increase the sparsity of the solution. By adding the prior, the initial deconvolution is guided closer to an appropriate solution which accelerates the convergence and therefore also decreases the number of iterations that can introduce sparsity, thus preserving the peak amplitudes ratios. As an illustrative example, we show in Figure S1 (see supporting information) two histograms comparing the respective preservation of the peak amplitude ratios, defined as the relative difference between the signal and data. Although these distributions have similar centroids, the distribution of the prior method is skewed towards the lower-end, thereby indicating the better relative peak amplitude preservation. Subsequent studies will investigate whether the isotopic distributions are equally well preserved.
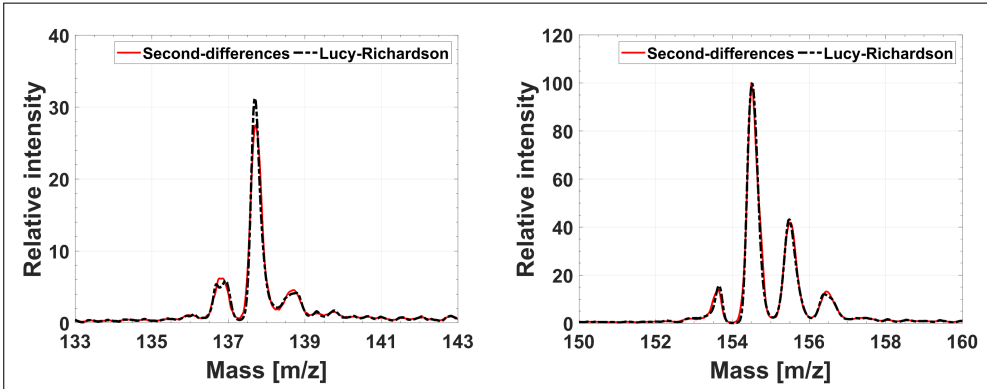
Figure 2: Comparison spectra of DHB (m/z 154, right) and its dehydroxylated fragment (m/z 137, left) after deconvolution was performed using the standard Lucy-Richardson algorithm ($\mathbb{B}_0$) and also the Lucy-Richardson algorithm with the second-differences prior ($\mathbb{B}_3$).

Our immediate goal is to enhance confidence in our methods for accurately quantifying ion fragmentation. However, given the low mass resolution ($\sim$200), it was difficult to succeed in doing this before deconvolution. For example, examining the region following the DHB parent ion, the isotopic distribution thereof can be approximated. Nevertheless, it is hard to make a realistic statement regarding the hydrogen loss peaks (m/z 136 and 153) other than inferring their likely existence. Likewise, very few conclusions can be drawn about the dehydroxylated fragment other than to determine its peak intensity ratio relative to the parent. At a minimum, the deconvolution appears to be successful in that each of the peaks in Figure 2 are separated by single atomic mass units. The hydrogen loss is also supported by the hydrogen peak visible in Figure 1, which suggests that an in-source mechanism is responsible for this fragmentation pathway.[54–56] While similar pathways have been reported in previous studies when using ultrashort pulses, they could not be corroborated for these

measurements before deconvolution was performed. The benzyl fragment is still not visible, which could indicate this pathway is suppressed, while it is at this time possible to identify the triphenylphosphine fragment using its mass signature.[57,58] When comparing the deconvolved signal to the data, Figure 3 illustrates that the deconvolution facilitated an enhanced peak identification process due to the increase in the mass resolution ($\sim$500 at m/z 154). It is important to recognize that this improvement is comparable in magnitude to that offered by using delayed ion extraction.[29,30]
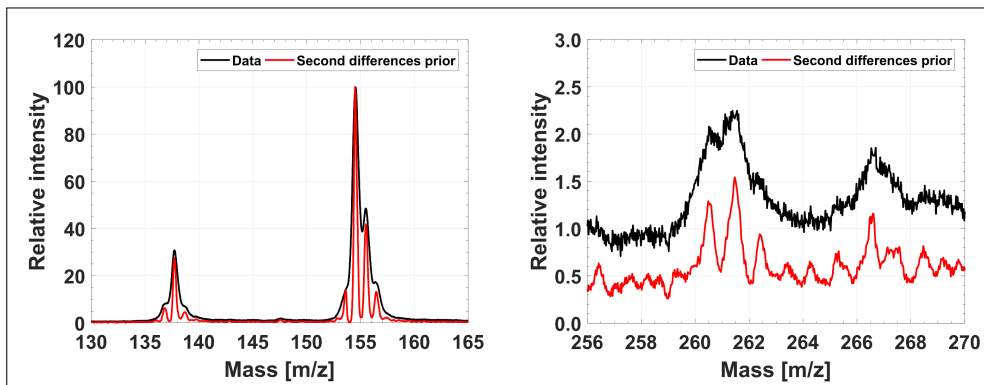
Figure 3: Comparison spectra of the DHB (m/z 154, left) and its dehydroxylated fragment (m/z 137, left), as well the triphenylphosphine (m/z 262, right) ion after deconvolution was performed using the Lucy-Richardson algorithm with the second-differences prior.

Numerical challenges

We will briefly discuss our algorithm, its usage and arising challenges. It requires the user to make choices regarding the peak shape, the prior distribution, the type of statistics applied, either Poisson (Lucy-Richardson) or Gaussian (ISRA), and a stopping criterion. The choices primarily depend on the data being considered. The effectiveness of these options is judged by the speed of convergence and the quality of the recovered spectra. Here we discuss the implementation of the algorithm and address these choices as they arise. The pseudocode for the algorithm and its variables are discussed in the supporting information.

The primary input into the algorithm consists of the initial values for the signal in the `Signal` vector and the data in the `Data` vector, which are equal in length. Other inputs are two smaller vectors `Prior` and `Peak` which both represent convolution kernels, i.e. representations of the Toeplitz matrices $\mathbb{A}$ and $\mathbb{B}$, which will be convolved with the `Signal` vector. `Signal` is iteratively updated until the convergence criteria are satisfied, while `Data`, `Peak` and `Prior` remain unchanged. The update depends on the convolution of the current `Signal` with the `Peak` and `Prior` vectors. `Peak` was chosen as a symmetric second-order polynomial since the results do not strongly depend on the peak shape, given that it is unimodal.

While the convergence of the entropy S could be used as a stopping criterion, this proved difficult to generalize since its behaviour depends strongly on the given prior. Fortunately, the distribution of the residuals is discussed in the deconvolution literature, which asserts that, for a meaningful reconstruction, the residuals should follow a Gaussian distribution centred around zero.[21] As an example, the distribution of residuals is shown in Figure 4(a) for the second-differences prior. Since this distribution satisfies the above-mentioned requirements, we decided to survey its behaviour to monitor the state of the deconvolution process. Our stopping criterion requires that the *difference in the mean of the residuals* $\Delta\varepsilon$ must fall below a predefined tolerance $\varepsilon_{\mathrm{TOL}}$ for a predefined number of iterations $\mathrm{N_{MAX}}$. In addition, a constant-sign criterion is implemented due to the oscillation of the *mean of the residuals* ε around zero (not shown here). Importantly, since the magnitude of the *mean of the residuals* ε depends on the dataset and prior, it cannot be used as a universal stopping criterion; rather, the change $\Delta\varepsilon$ should be used. The number of additional iterations to perform once the *change in the mean of the residuals* has fallen below the threshold (and the oscillations levelled off) was empirically determined to be $\mathrm{N_{MAX}} = 10$. The respective convergence behaviour of the standard Lucy-Richardson algorithm ($\mathbb{B}_0$) and the second-differences prior ($\mathbb{B}_3$) are compared in Figure 4(b). We confirmed that these trends agree qualitatively with the behaviour of the entropy convergence plots.
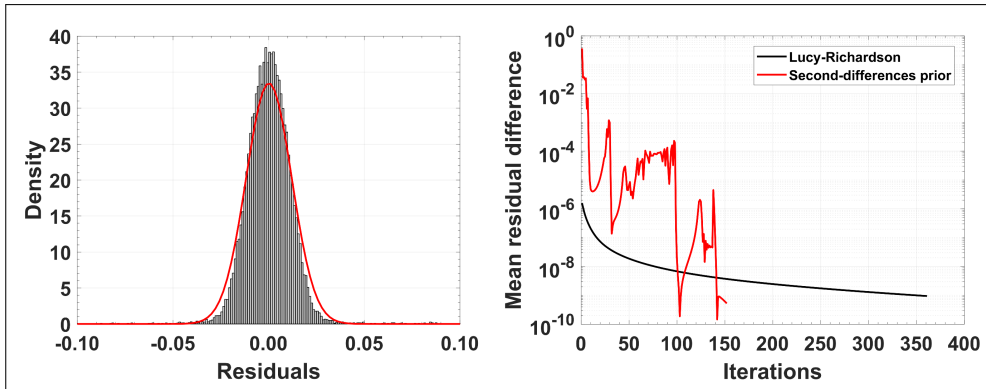
Figure 4: Residual distribution (left) for the second-differences prior discussed in Figure 2. The *difference in the mean of residuals* $\Delta\varepsilon$ are also shown (right) for this prior and standard Lucy-Richardson. The prior reaches the same level of difference $\Delta\varepsilon$ as Lucy-Richardson, but in fewer iterations, which therefore preserves the quality of the reconstruction.

The differences in entropies $\Delta\mathrm{S}$ will decrease upon approaching local and global minima. Should this difference be below a defined tolerance $\Delta\mathrm{S_{TOL}}$, the strength of the prior is reduced by using scaling the regularization parameter β with the amount β_Δ smaller than unity. The attenuation of the prior is akin to the boost mechanism introduced by Miroslav to dislodge the solution out of a local minimum.[59] Figure 5(b) indicates that the prior guides the algorithm during the initial phase of the deconvolution since the influence of β is rather significant, but it is increasingly suppressed by the boosting mechanism. Further, note that without such a

boosting mechanism, the Tikhonov regularization prior ($\mathbb{B}_1$) would have been permanently stranded within a local minimum,[60] as indicated by the stepping behaviour of the entropy in Figure 5(a). Most importantly, this mechanism ensures that all the methods converge to the same final entropy, thereby permitting quantitative comparison of results as a function of different priors for the given dataset, providing additional reassurance that the selected stopping criterion is indeed appropriate.
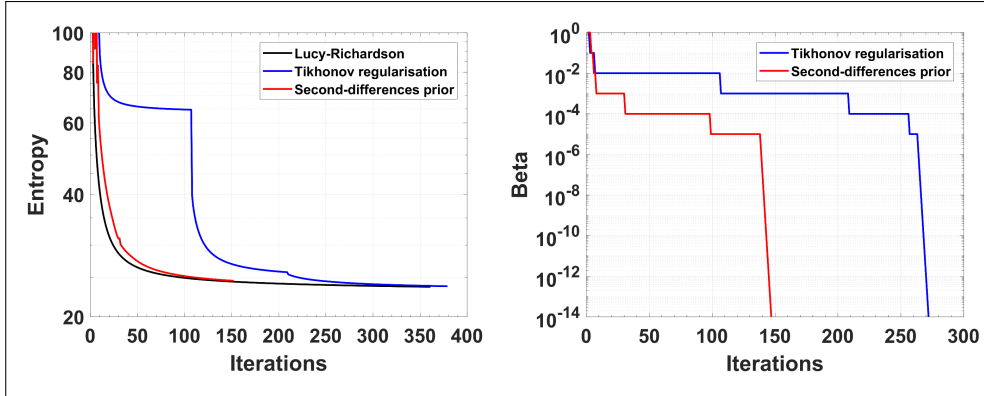
Figure 5: Convergence of the entropy (left) for the standard Lucy-Richardson algorithm and the second-differences and Tikhonov regularization priors. While during the initial iterations the influence of the prior (right) is large, it is rapidly suppressed by the boost mechanism.

We emphasize, however, that inclusion of a prior is not beneficial by default. Relative to the standard Lucy-Richardson algorithm, only the second-differences prior improved the rate of convergence (152 versus 361 iterations). The Tikhonov regularization prior produced the highest quality spectra in avoiding overfitting (spurious small peaks) and correctly identifying most of the physically meaningful peaks, but at the expense of the slightly longer convergence time than the Lucy-Richardson algorithm (379 versus 361 iterations). Both the first ($\mathbb{B}_2$) and third-differences ($\mathbb{B}_4$) priors resulted in ill-defined peak shapes, which is not unexpected since these priors discourage sharp features (dependence on signal differences) in the solution.

Although ion counting was performed, it was not known which error distribution would be the most suitable for this data since the mass average is considered in this analysis. For that reason, both Poisson and Gaussian error statistics were tested by using the Lucy-Richardson and the ISRA algorithms respectively. As noted by others, and as also shown in Figure S2, the Lucy-Richardson algorithm converges significantly faster (361 versus 1988 iterations) while providing the superior deconvolution results (the ISRA algorithm is more susceptible to introducing artifact peaks). Currently, it is not known whether this is due to the stopping criterion, although the residual distributions appear to be qualitatively similar, or whether this conclusion applies universally to these algorithms. Even though the results of not using priors are shown, these characteristics were observed for all of the priors investigated. In addition, preliminary results indicate that this observation also applies to single-shot spectra

and will be further investigated in subsequent studies.

Conclusions

We have demonstrated the advantages of deconvolving low-resolution mass spectrometry data by using the well-established Lucy-Richardson algorithm both with and without priors. Various priors were applied so as to extract a more meaningful signal from the experimental data. For the data investigated in this analysis, it was shown that the Gaussian prior based on the second-differences of the signal outperforms the standard Lucy-Richardson algorithm as evidenced by an accelerated convergence and preservation of a larger fraction of the peak amplitudes ratios. A stopping criterion which monitors the mean distribution of residuals was included to facilitate these comparisons. This in combination with a boosting mechanism, ensures that the algorithm does not wind up in a local minimum and that all of the methods reach the same result. The Image Space Reconstruction (ISRA) algorithm was also studied, as it was not known initially whether Gaussian statistics might be more appropriate for the experimental test data. However, as noted previously, Lucy-Richardson converges faster and is less prone to overfitting. For all of the investigated methods, the improved resolution of the deconvolved signal allowed a more precise statement to be made regarding the fragmentation of the benzyltriphenylphosphonium thermometer ion upon femtosecond desorption. Further studies will extend the framework introduced in this work to assist in the interpretation and decoupling of MALDI shot-to-shot phenomena.

Acknowledgements

Supporting Information Available

The algorithm requires the arrays $Signal, Peak, Prior$ and $Data$, representing respectively the initial signal, the peak and prior point spread functions (PSF), and the raw data. With reference to algorithm 1, the $\star$ operator returns the convolution of two arrays, `mean()` returns the mean of the input array, `sum()` the total of an array, `flip()` reverses the elements of an array, and the plus $(+)$ and minus $(-)$ subscripts returns an array containing only positive or negative elements.

Algorithm 1 Split-gradient method

1:   $N \leftarrow 0; \beta \leftarrow 1.0; \beta_\Delta \leftarrow 0.9; \varepsilon_{tol} \leftarrow 10^{-9}; N_{max} \leftarrow 100; \Delta S_{tol} \leftarrow 0.01$
2:   $(OldEntropy, Recon) = \text{GETENTROPY}(Data, Signal, Peak)$
3:   $\varepsilon_{old} = \text{MEAN}(Data - Recon)$
4:   **while** $N < N_{max}$ **do**
5:      $Conv \leftarrow Signal \star Peak$
6:      $Penalty \leftarrow Signal \star Prior$
7:      $\Lambda \leftarrow \text{MEAN}(1 + Penalty^2)$
8:      $Deriv \leftarrow (Data/Conv) \star \text{FLIP}(Peak)$
9:      $Penalty \leftarrow Penalty \star \text{FLIP}(Prior)$
10:     $Penalty_+ \leftarrow (Penalty/\Lambda)_+$
11:     $Penalty_- \leftarrow (Penalty/\Lambda)_-$
12:     $Signal \leftarrow Signal \times (Deriv - \beta \times Penalty_-)/(1 + \beta \times Penalty_+)$
13:     $(NewEntropy, Recon) \leftarrow \text{GETENTROPY}(Data, Signal, Peak)$
14:     $\Delta S \leftarrow NewEntropy - OldEntropy$
15:     $OldEntropy \leftarrow NewEntropy$
16:     $\varepsilon_{new} \leftarrow \text{MEAN}(Recon - Data)$
17:     **if** $\Delta S < \Delta S_{\text{TOL}}$ **then**
18:        $\beta = \beta \times \beta_\Delta$
19:     **end if**
20:     **if** $(\varepsilon_{old} \times \varepsilon_{new} < 0) \parallel ((\varepsilon_{old} - \varepsilon_{new}) > \varepsilon_{\text{TOL}})$ **then**
21:        $N \leftarrow 0$
22:     **else**
23:        $N \leftarrow N + 1$
24:     **end if**
25:     $\varepsilon_{old} = \varepsilon_{new}$
26: **end while**
27: **function** $\text{GETENTROPY}(Data, Signal, Peak)$
28:     $Recon \leftarrow Signal \star Peak$
29:     $Entropy \leftarrow data \times \log(data/recon)$
30:     $Out \leftarrow \text{SUM}(entropy + signal - data)$
31:     **return** $(Out, Recon)$
32: **end function**
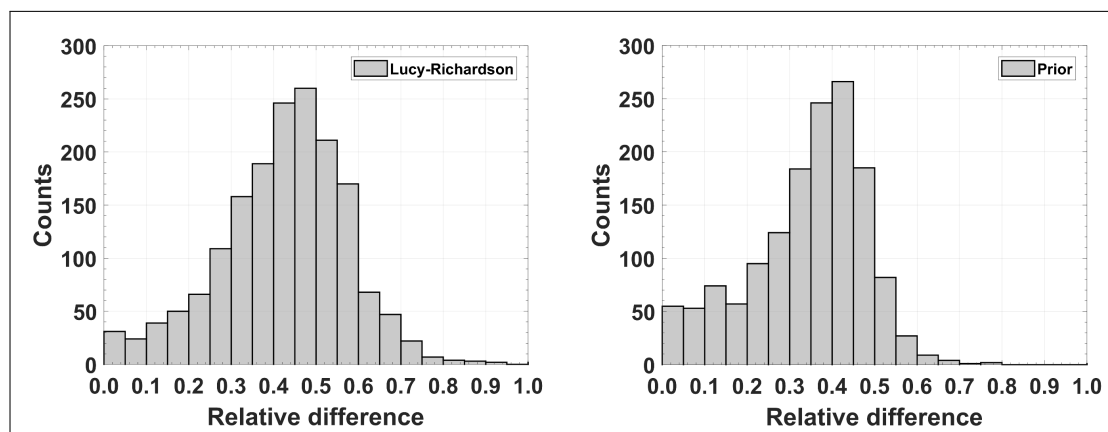
Figure S1: Histograms of the relative differences between the signal and data, with data being the reference, for the Lucy-Richardson (left) and second-differences prior (right) algorithms. Although these distributions have similar centroids, the prior distribution is skewed towards the lower-end, which indicates a better amplitude preservation.
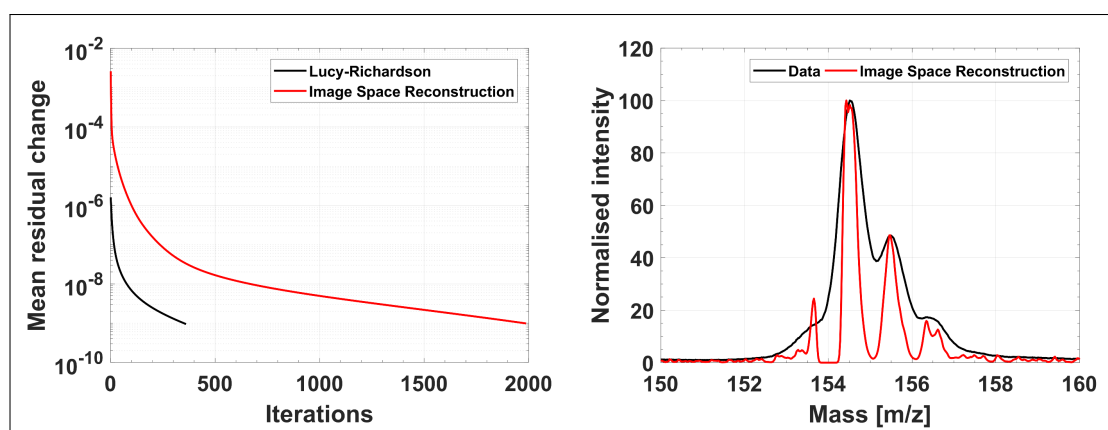
Figure S2: Change in the mean of the residuals (left) for the standard Lucy-Richardson and Image Space Reconstruction algorithms. Also shown are the comparison spectra of the DHB ion (m/z 154, right), clearly showing the introduced artifacts.

References

(1) Liang, Y.-Z.; Xie, P.; Chan, K. Quality control of herbal medicines. *Journal of Chromatography B* **2004**, *812*, 53–70.

(2) Wiseman, J. M.; Ifa, D. R.; Zhu, Y.; Kissinger, C. B.; Manicke, N. E.; Kissinger, P. T.; Cooks, R. G. Desorption electrospray ionization mass spectrometry: Imaging drugs and metabolites in tissues. *Proceedings of the National Academy of Sciences* **2008**, *105*, 18120–18125.

(3) Ong, S.-E.; Mann, M. Mass spectrometry–based proteomics turns quantitative. *Nature chemical biology* **2005**, *1*, 252–262.

(4) Cravatt, B. F.; Simon, G. M.; Yates Iii, J. R. The biological impact of mass-spectrometry-based proteomics. *Nature* **2007**, *450*, 991–1000.

(5) Diamandis, E. P. Mass spectrometry as a diagnostic and a cancer biomarker discovery tool opportunities and potential limitations. *Molecular & Cellular Proteomics* **2004**, *3*, 367–378.

(6) McDonnell, L. A.; Corthals, G. L.; Willems, S. M.; van Remoortere, A.; van Zeijl, R. J.; Deelder, A. M. Peptide and protein imaging mass spectrometry in cancer research. *Journal of proteomics* **2010**, *73*, 1921–1944.

(7) Eberlin, L. S.; Dill, A. L.; Golby, A. J.; Ligon, K. L.; Wiseman, J. M.; Cooks, R. G.; Agar, N. Y. Discrimination of human astrocytoma subtypes by lipid analysis using desorption electrospray ionization imaging mass spectrometry. *Angewandte Chemie International Edition* **2010**, *49*, 5953–5956.

(8) Golf, O.; Strittmatter, N.; Karancsi, T.; Pringle, S. D.; Speller, A. V.; Mroz, A.; Kinross, J. M.; Abbassi-Ghadi, N.; Jones, E. A.; Takats, Z. Rapid evaporative ionization mass spectrometry imaging platform for direct mapping from bulk tissue and bacterial growth media. *Analytical chemistry* **2015**, *87*, 2527–2534.

(9) Smith, C. A.; O'Maille, G.; Want, E. J.; Qin, C.; Trauger, S. A.; Brandon, T. R.; Custodio, D. E.; Abagyan, R.; Siuzdak, G. METLIN: a metabolite mass spectral database. *Therapeutic drug monitoring* **2005**, *27*, 747–751.

(10) Wishart, D. S.; Jewison, T.; Guo, A. C.; Wilson, M.; Knox, C.; Liu, Y.; Djoumbou, Y.; Mandal, R.; Aziat, F.; Dong, E. HMDB 3.0âĂŤthe human metabolome database in 2013. *Nucleic acids research* **2012**, *41*, D801–D807.

(11) Fournier, I.; Marinach, C.; Tabet, J.; Bolbach, G. Irradiation effects in MALDI, ablation, ion production, and surface modifications. Part II: 2, 5-dihydroxybenzoic acid monocrystals. *Journal of the American Society for Mass Spectrometry* **2003**, *14*, 893–899.

(12) Wortmann, A.; Pimenova, T.; Alves, S.; Zenobi, R. Investigation of the first shot phenomenon in MALDI mass spectrometry of protein complexes. *Analyst* **2007**, *132*, 199–207.

(13) Park, S.-G.; Murray, K. K. Infrared laser ablation sample transfer for MALDI imaging. *Analytical chemistry* **2012**, *84*, 3240–3245.

(14) Chaurand, P.; Schriver, K. E.; Caprioli, R. M. Instrument design and characterization for high resolution MALDI-MS imaging of tissue sections. *Journal of Mass Spectrometry* **2007**, *42*, 476–489.

(15) Gilmore, I. S. SIMS of organicsâĂŤAdvances in 2D and 3D imaging and future outlook. *Journal of Vacuum Science & Technology A: Vacuum, Surfaces, and Films* **2013**, *31*, 050819.

(16) Dreisewerd, K.; Schürenberg, M.; Karas, M.; Hillenkamp, F. Influence of the laser intensity and spot size on the desorption of molecules and ions in matrix-assisted laser desorption/ionization with a uniform beam profile. *International journal of mass spectrometry and ion processes* **1995**, *141*, 127–148.

(17) Corthals, G. L.; Wasinger, V. C.; Hochstrasser, D. F.; Sanchez, J.-C. The dynamic range of protein expression: a challenge for proteomic research. *Electrophoresis* **2000**, *21*, 1104–1115.

(18) Lu, Y.; Pieterse, C. L.; Robertson, W. D.; Miller, R. D. Soft Picosecond Infrared Laser Extraction of Highly Charged Proteins and Peptides from Bulk Liquid Water for Mass Spectrometry. *Analytical chemistry* **2018**,

(19) Skilling, J. *Maximum Entropy and Bayesian Methods: Cambridge, England, 1988*; Springer Science & Business Media, 2013; Vol. 36.

(20) Narayan, R.; Nityananda, R. Maximum entropy image restoration in astronomy. *Annual review of astronomy and astrophysics* **1986**, *24*, 127–170.

(21) Puetter, R.; Gosnell, T.; Yahil, A. Digital image reconstruction: Deblurring and denoising. *Annual Review of Astronomy and Astrophysics* **2005**, *43*.

(22) Karas, M.; Hillenkamp, F. Laser desorption ionization of proteins with molecular masses exceeding 10,000 daltons. *Analytical chemistry* **1988**, *60*, 2299–2301.

(23) Dreisewerd, K. The desorption process in MALDI. *Chemical reviews* **2003**, *103*, 395–426.

(24) Knochenmuss, R. The Coupled Chemical and Physical Dynamics Model of MALDI. *Annual Review of Analytical Chemistry* **2016**, *9*, 365–385.

(25) Bae, Y. J.; Kim, M. S. A thermal mechanism of ion formation in MALDI. *Annual Review of Analytical Chemistry* **2015**, *8*, 41–60.

(26) Luo, G.; Marginean, I.; Vertes, A. Internal energy of ions generated by matrix-assisted laser desorption/ionization. *Analytical chemistry* **2002**, *74*, 6185–6190.

(27) Luo, G.; Marginean, I.; Ye, L.; Vertes, A. Competing ion decomposition channels in matrix-assisted laser desorption ionization. *The Journal of Physical Chemistry B* **2008**, *112*, 6952–6956.

(28) Chen, Y.; Vertes, A. Pumping rate and surface morphology dependence of ionization processes in matrix-assisted laser desorption ionization. *The Journal of Physical Chemistry A* **2003**, *107*, 9754–9761.

(29) Brown, R. S.; Lennon, J. J. Mass resolution improvement by incorporation of pulsed ion extraction in a matrix-assisted laser desorption/ionization linear time-of-flight mass spectrometer. *Analytical chemistry* **1995**, *67*, 1998–2003.

(30) Vestal, M.; Juhasz, P.; Martin, S. Delayed extraction matrix-assisted laser desorption time-of-flight mass spectrometry. *Rapid Communications in Mass Spectrometry* **1995**, *9*, 1044–1050.

(31) Pieterse, C. L.; Busse, F.; Robertson, W. D.; Tellkamp, F.; Miller, R. J. D. Femtosecond Pumping Rate Dependence of Fragmentation Pathways in Matrix-Assisted Laser Desorption Ionization. *The Journal of Physical Chemistry Letters (to be submitted)* **00**, *00*.

(32) Strupat, K.; Karas, M.; Hillenkamp, F. 2, 5-Dihydroxybenzoic acid: a new matrix for laser desorptionâĂŤionization mass spectrometry. *International Journal of Mass Spectrometry and Ion Processes* **1991**, *111*, 89–102.

(33) Lucy, L. B. An iterative technique for the rectification of observed distributions. *The Astronomical Journal* **1974**, *79*, 745.

(34) Richardson, W. H. Bayesian-based iterative method of image restoration. *JOSA* **1972**, *62*, 55–59.

(35) Bernardo, J. M.; Smith, A. F. *Bayesian theory*; IOP Publishing, 2001.

(36) Shepp, L. A.; Vardi, Y. Maximum likelihood reconstruction for emission tomography. *IEEE Transactions on Medical Imaging* **1982**, *1*, 113–122.

(37) Geman, S.; Geman, D. Stochastic relaxation, Gibbs distributions, and the Bayesian restoration of images. *IEEE Transactions on Pattern Analysis and Machine Intelligence* **1984**, 721–741.

(38) Bertero, M.; Boccacci, P.; Desiderà, G.; Vicidomini, G. Image deblurring with Poisson data: from cells to galaxies. *Inverse Problems* **2009**, *25*, 123006.

(39) Starck, J.-L.; Pantin, E.; Murtagh, F. Deconvolution in astronomy: A review. *Publications of the Astronomical Society of the Pacific* **2002**, *114*, 1051.

(40) Hansen, P. C.; Nagy, J. G.; O'leary, D. P. *Deblurring images: matrices, spectra, and filtering*; Siam, 2006; Vol. 3.

(41) Jansson, P. A. *Deconvolution of images and spectra*; Courier Corporation, 2014.

(42) Young, S.; Driggers, R.; Jacobs, E. Image Deblurring. 2008.

(43) Csiszar, I. Why least squares and maximum entropy? An axiomatic approach to inference for linear inverse problems. *The Annals of Statistics* **1991**, 2032–2066.

(44) Natterer, F.; Wübbeling, F. *Mathematical methods in image reconstruction*; Siam, 2001; Vol. 5.

(45) Barrett, H. H.; Myers, K. J. *Foundations of image science*; John Wiley & Sons, 2013.

(46) Press, W. H.; Teukolsky, S. A.; Vetterling, W. T.; Flannery, B. P. *Numerical Recipes in C*; Cambridge University Press, Cambridge, 1996; Vol. 2.

(47) Dempster, A. P.; Laird, N. M.; Rubin, D. B. Maximum likelihood from incomplete data via the EM algorithm. *Journal of the Royal Statistical Society. Series B (methodological)* **1977**, 1–38.

(48) Dempster, A. P.; Laird, N. M.; Rubin, D. B. Maximum likelihood from incomplete data via the EM algorithm. *Journal of the Royal Statistical Society. Series B (methodological)* **1977**, 1–38.

(49) Lantéri, H.; Roche, M.; Cuevas, O.; Aime, C. A general method to devise maximum-likelihood signal restoration multiplicative algorithms with non-negativity constraints. *Signal Processing* **2001**, *81*, 945–974.

(50) Lanteri, H.; Roche, M.; Aime, C. Penalized maximum likelihood image restoration with positivity constraints: multiplicative algorithms. *Inverse problems* **2002**, *18*, 1397.

(51) Daube-Witherspoon, M. E.; Muehllehner, G. An iterative image space reconstruction algorthm suitable for volume ECT. *IEEE Transactions on Medical Imaging* **1986**, *5*, 61–66.

(52) De Pierro, A. R. On the convergence of the iterative image space reconstruction algorithm for volume ECT. *IEEE Transactions on Medical Imaging* **1987**, *6*, 174–175.

(53) Titterington, D. On the iterative image space reconstruction algorthm for ECT. *IEEE Transactions on Medical Imaging* **1987**, *6*, 52–56.

(54) Gobeli, D.; El-Sayed, M. Change in the mechanism of laser multiphoton ionization-dissociation in benzaldehyde by changing the laser pulse width. *The Journal of Physical Chemistry* **1985**, *89*, 3426–3429.

(55) Smith, D.; Ledingham, K.; Kilic, H.; McCanny, T.; Peng, W.; Singhal, R.; Langley, A.; Taday, P.; Kosmidis, C. Ionization and dissociation of benzaldehyde using short intense laser pulses. *The Journal of Physical Chemistry A* **1998**, *102*, 2519–2526.

(56) Weinkauf, R.; Aicher, P.; Wesley, G.; Grotemeyer, J.; Schlag, E. Femtosecond versus nanosecond multiphoton ionization and dissociation of large molecules. *The Journal of Physical Chemistry* **1994**, *98*, 8381–8391.

(57) Claereboudt, J.; Claeys, M.; Geise, H.; Gijbels, R.; Vertes, A. Laser microprobe mass spectrometry of quaternary phosphonium salts: direct versus matrix-assisted laser desorption. *Journal of the American Society for Mass Spectrometry* **1993**, *4*, 798–812.

(58) Claereboudt, J.; Baeten, W.; Geise, H.; Claeys, M. Structural characterization of mono- and bisphosphonium salts by fast atom bombardment mass spectrometry and tandem mass spectrometry. *Journal of Mass Spectrometry* **1993**, *28*, 71–82.

(59) Morháč, Miroslav, Deconvolution methods and their applications in the analysis of γ-ray spectra. *Nuclear Instruments and Methods in Physics Research Section A: Accelerators, Spectrometers, Detectors and Associated Equipment* **2006**, *559*, 119–123.

(60) Tikhonov, A. N.; Arsenin, V.; John, F. *Solutions of ill-posed problems*; Winston Washington, DC, 1977; Vol. 14.